Characterization and Classification of Seafloor by Acoustic Method Using Model-Based and Model-Free Techniques

THESIS SUBMITTED FOR THE DEGREE OF

DOCTOR OF PHILOSOPHY

IN THE FACULTY OF NATURAL SCIENCE

GOA UNIVERSITY

GOA

By

CHANCHAL DE

DEPARTMENT OF PHYSICS
GOA UNIVERSITY
GOA - 403 206

Examined
A. Kumar
(ARUN KUMAR)
Professor,
CARE, IIT Delhi

AUGUST 2010

All the corrections recommended by the examiners have been duly incorporated

A. Kumar
(Examiner)

R. Chakraborty
(Guide)

DECLARATION

The author hereby declares that the work presented in this thesis has not been submitted to any other University or Institution for the award of Degree, Diploma or any other such title.

Place: Goa University, Goa

Date: 12th August, 2010

Chanchal De

Chanchal De

CERTIFICATE

We hereby certify that the above Declaration of the candidate Shri Chanchal De is true and this thesis represents his independent work.

B. Chakraborty

Dr. Bishwajit Chakraborty
Scientist 'G'
National Institute of Oceanography
Dona Paula, Goa
Goa - 403 004

Dr. K. R. Priolkar
Assistant Professor
Department of Physics
Goa University, Goa
Goa - 403 206

Dedicated

To

My Father

Abstract

Seafloor sediments characteristics play a significant role in several field of research such as marine geology, hydrographic, marine engineering, fisheries sciences, environmental science, and defence. Traditional approach requires collection of sediment samples and analyzing them in a laboratory for obtaining qualitative and quantitative information on the seafloor sediments. However, remote acoustic techniques are regarded as the most efficient, cost effective and rapid methods for acquiring such information over large areas. This study focuses on acoustic characterization and classification of seafloor sediments using backscatter echo data obtained from normal-incidence, single-beam echo sounder at two conventional frequencies (33 and 210 kHz) in the central part of the western continental shelf of India in the Arabian Sea.

Remote acoustic characterization of seafloor sediments focuses on the applicability of a temporal acoustic backscatter model by estimating the values of seafloor sediment parameters through inversion. The studies on the applicability of this temporal backscatter model revealed that the estimated values of mean grain size of sediment are more consistent with the ground-truth at 33 kHz as compared to 210 kHz. Moreover, a combined two-frequency inversion scheme is explored in this work to investigate the combined use of two sets of backscatter data for improved characterization. In this inversion scheme, the backscatter echo data collected at two frequencies are jointly inverted to estimate a single set of seafloor sediment parameters. The results on the seafloor roughness spectrum parameters estimated from this combined two-frequency inversion approach show more consistency with the available

published information compared to those estimated from the single-frequency inversions.

The study on model-free methods of classification utilizing seafloor echo features aims at developing a hybrid scheme to improve the success of classification. Model-free techniques for seafloor classification usually require a-priori information on the number of sediment classes available in a dataset. However, this information could be obtained only from ground-truth data. An unsupervised method, based on Kohonen's self-organizing feature map, is demonstrated here to estimate the plausible number of sediment classes available in a given dataset in the absence of any a-priori information. Selection of echo features for achieving improved success is another important aspect in seafloor sediment classification. Two supervised methods, based on neural networks and fuzzy cluster algorithm, are demonstrated in this dissertation for the selection of an optimum subset of echo features. In these methods, the successes of classification with different subset of echo features are analyzed to select the optimum one. The results from fuzzy algorithm based method show that backscatter strength and time-spread when used in combination with statistical skewness and Hausdroff dimension provide improved classifications at 33 and 210 kHz respectively, whereas the results from neural networks based method reveal that the maximum success is achieved using all the above-mentioned four features together at both the frequencies. In addition, this study reveals that the use of 210 kHz is advantageous for seafloor classification.

It is demonstrated that the hybrid scheme consisting of the proposed unsupervised method along with either of the methods based on neural networks or fuzzy cluster algorithm provides improved seafloor classification.

Acknowledgements

I would like to take this opportunity to thank everybody who has helped me, directly or indirectly, during the period of my research.

First of all, I would like to express my sincere gratitude to my guide, Dr. Bishwajit Chakraborty, Scientist 'G' of National Institute of Oceanography (NIO), Goa for his guidance, thoughtful suggestions, constant encouragement during the course of this research, and his invaluable help for providing me with the experimental data.

I am also grateful to my co-guide, Dr. K.R. Priolkar, Assistant Professor, Department of Physics, Goa University, Goa for his persistent help, supervision, and encouragement during the work.

I would like to thank Shri S. Anathanarayanan, Director, Naval Physical & Oceanographic Laboratory (NPOL), Kochi for his support and encouragement. I am also thankful to Shri V. Chander, Director (Retd.), NPOL for granting me the permission to carry out this research. I also acknowledge R&D HQ, DRDO, Delhi for granting me the permission to pursue this degree.

I acknowledge and express my thanks to Dr. S.R. Shetye, Director, NIO, Goa for granting me the permission to utilize the experimental data collected by NIO.

I would also like to express my deep gratitude to Shri Manik Mukherjee, Director, Group for Forecasting and Analysis of Systems & Technologies (G-FAST), Delhi for his support and encouragement.

I wish to thank Shri Vasanth Sastry, Senior Scientist, G-FAST for his precious time to proofread this dissertation and providing me with his constructive comments.

I would like to place on record my acknowledgement for the support and encouragement received from Dean of Goa University, Faculties of Natural Science and Head, Department of Physics, Goa University.

I am indeed grateful to Professor P.R. Sarode, Department of Physics, Goa University for his wholehearted support and guidance during the period of my research.

I appreciate the assistance received from all the technical and administrative staff of the Department of Physics, Goa University, especially from Shri Ramachandra Naik.

I take this opportunity to thank Dr. Antony Joseph, Senior Scientist, NIO and a member of Faculty Research Committee, for his proactive suggestions.

I acknowledge and highly appreciate the effort of Shri R.G. Prabhudesai and Shri G.S. Navelkar, Senior Scientists of NIO during data acquisition activities. Also, I wish to thank Shri William Fernandes of NIO for his help in sorting out the field data.

Dr. J. Swain, Senior Scientist, NPOL has been a constant source of encouragement and without his full-fledged support this work would not have been possible. I take this opportunity to express my heartfelt gratitude to him.

Many interactions with Dr. N. Mohan Kumar, Senior Scientist, NPOL on various mathematical aspects have been very helpful. I gratefully acknowledge his help.

I would like to extend my sincere thanks to Shri K.A.A. Salam, Senior Technical Officer, NPOL for fruitful discussion on the technical aspects of acoustic data acquisition.

Above all, this work would have been impossible without my mother's love and inspiration and my mere expression of thanks is not sufficient for this. I am deeply grateful to my wife, Manideepa for her selfless support, encouragement, and efficient management of day-to-day household matters. I highly appreciate the tolerance of my loving children, Spandan and Manaswini, for a long period during which I could not spend much time with them. Also I am extremely thankful to my brother Dr. Sajal De for his encouragement to pursue this degree.

This work would not have been a reality without the divine blessings of my beloved father (Late) Dr. Sasadhar De. He was a scientist per excellence and a great human being. His dedicated struggle to continue academic research till his last breathe, in spite of all adversaries, is an example to me. I miss him every day. I am dedicating this thesis in the memory of my father.

Contents

List of Tables

List of Figures

List of Symbols

A	Area insonified by an acoustic beam
$a_{m,n}$	Orthogonal eigenvectors of a variance-covariance matrix
b	Bias term in neural networks
$b(\theta_i, \psi)$	Transducer beam pattern
BS	Backscatter strength
CS	Clayey silt sediment
C_h	Structure constant
c_i	i^{th} centroid or cluster center
$c_i^{(p)}$	i^{th} centroid or cluster center at the p^{th} iteration
dA	Elementary area on seafloor
d_{ij}	Euclidian distance between the i^{th} centroid and the j^{th} data point x_j
d_j	Euclidean distance between input and the j^{th} output
d_g	Grain size diameter of sediment in mm
d_{min}	Minimum Euclidean distance during the training of a neural network
$D(r_f)$	Structure function at a distance r_f
D_m	Delay in aligning the temporal feature for the m^{th} echo
dl	Elemental distance along the propagated distance
E_c	Total energy of an echo envelope
E_m	Error for the m^{th} vector
E/S	Error-to-signal ratio (also the objective function in inversion process)
f	Acoustic frequency
$f(p)$	Objective function after adding a penalty component
$f(x)$	Analytical function f with a variable x
$f(a), f(b), f(c)$	Function $f(x)$ evaluated at points a, b, and c
$F(NET)$	Activation function applied to a neural network

G_{tot}	Total gain, which includes the system gain plus operator gain
h	Root mean square relief of a rough surface from its mean value
h_0	Reference length; $h_0 = 1$ cm used to express w_2 in cm^4
h_s	Root mean square relief of a small-scale surface
H	Seafloor depth
HD	Hausdroff dimension - an echo feature
H_{ref}	Reference seafloor depth
i, j	Integer values
I	Identity matrix
$I(t)$	Echo intensity at a time t
I_0	Incident intensity
I_1	Intensity of acoustic energy at a radial distance R_1
I_2	Intensity of acoustic energy at a radial distance R_2
$I_i(t)$	Intensity of backscatter from the water-sediment interface at a time t
I_s	Scattered intensity
$I_v(t)$	Intensity of backscatter from the sediment volume at a time t
I_x	Transmitted intensity
$I_x(t)$	Transmitted intensity at a time t with magnitude I_x
J	Jacobian matrix for a system
J_m	Alignment index of the echo temporal feature for the m^{th} echo
J_{mean}	Mean alignment index
J_F	Objective function in a fuzzy cluster algorithm
$\mathbf{k}$	2D Spatial wave vector
k	Magnitude of 2D spatial wave vector $\mathbf{k}$
K	Pre-defined total number of iterations
k_a	Acoustic wave number ($= 2\pi/\lambda$)
k_c	Cutoff spatial wave number
$l_1(t)$	Propagation length of the trailing edge of a pulse with respect to entry point in sediment at a time t

$l_2(t)$	Propagation length of the leading edge of a pulse with respect to entry point in sediment at a time t
$L(t)$	Attenuation length at a time t
m, n	Integer values
M, N	Integer values
$MaxX$	Maximum value of input data X
$MinX$	Minimum value of input data X
m_n	Spectral moment of the order n, where $n = 0, 1, 2, 3$, and 4
M_ϕ	Mean grain size of sediments in phi unit
$N(r_0)$	Smallest number of open balls of radius r_0 needed to cover an object
$N_{j*}(p)$	Neighborhood size around the output neuron $j*$ at the p^{th} iteration
N_c	Cumulative number of iterations already carried out
nc	Total number of cluster centers
NET	Summation of the products of input and its weight, $NET = \sum_i x_i w_i$
O_{mj}	Actual output from the j^{th} output neuron for the m^{th} training vector
O_{mi}	Output from the i^{th} neuron for the m^{th} training vector
p	Integer value
P	Acoustic roughness
pH	pH value of seawater
p_a	rms pressure sequence of the observed averaged echo envelope
p_m	rms pressure sequence of the temporal modeled echo envelope
q	Weighting exponent in a fuzzy cluster algorithm
r	Correlation coefficient
$r(t)$	Radius of the insonified disc at a time t
r_f	The length of the footprint
$r_{ext}(\tau)$	External radius of the insonified area at a time τ
$r_{\text{int}}(\tau)$	Internal radius of the insonified area at a time τ
R	Radial distance of a point from acoustic source (i.e., Range)
R_1	Radial distance of a point 1 from acoustic source

R_2	Radial distance of a point 2 from acoustic source
$\Re$	Reflection coefficient
R_c	Radius of curvature of a large-scale surface
R_{xs}	Receiver sensitivity of the echo sounder receiver
$\Re(\theta_i)$	Reflection coefficient at an incidence angle θ_i
$\Re_\perp$	Reflection coefficient at normal-incidence i.e., $\Re_\perp = \Re(0)$
$R_{SS}(\tau_L)$	Autocorrelation function of $S(t)$ for a time lag τ_L
$R_{SS}(0)$	Autocorrelation function of $S(t)$ for zero time lag
$\overline{R}_{SS}(\tau_L)$	Normalized autocorrelation function
s	rms slope of a large-scale surface
S	Salinity of seawater in practical salinity units
$S(f)$	Power spectral density of an echo envelope in frequency domain
$S(t)$	Echo envelope in time domain
$S(t+\tau_L)$	Time lag version of the envelope $S(t)$ in time domain
Sa	Sand sediment
Si	Silt sediment
$S_i(\theta_i)$	Seafloor interface backscattering coefficient at an angle θ_i
SL	Source level of the echo sounder transmitted energy
S/E	Signal-to-error ratio
SpKurt	Spectral kurtosis - an echo feature
SpSkew	Spectral skewness - an echo feature
SpWidth	Spectral width - an echo feature
SS	Silty sand sediment
StatSkew	Statistical skewness - an echo feature
$\Im$	Transmission coefficient
T	Desired or target output in a neural network analysis
t	Time
t_0	Initial time
t_{bd}	Starting time of an echo envelope or time of bottom detect
t_c	Center of gravity of an echo envelope

t_{peak}	Time at which echo amplitude attains its peak value
T_s	Temperature of seawater in °C
T_0	Initial value of a control parameter in an annealing system (initial temperature)
T_i	The value of the control parameter at the i^{th} iteration during annealing
T_1	Time duration of an echo envelope for the calculation of echo features
T_{mj}	Desired value of the j^{th} output for the m^{th} training vector
TL	Transmission loss (in dB)
TS	Statistical time-spread - an echo feature
U	Membership matrix in cluster analysis
u_{ij}	i^{th} membership function of the j^{th} data point in U
$u_{ij}^{(p)}$	Value of the membership function u_{ij} at the p^{th} iteration
v_b	Speed of sound in sediment
v_w	Speed of sound in water
$V[n]$	Voltage sequence of an average echo with n number of samples
$V[m,n]$	Two-dimensional voltage array for the m^{th} echo with n number of samples
$V[m,(n-D_m)]$	Aligned two-dimensional voltage array
$V_l(\theta_i)$	Two-way transmission loss at a large-scale interface roughness for θ_i
$V_f(\theta_i)$	Two-way transmission loss at a flat interface for an angle θ_i
w_2	Seafloor roughness spectrum strength
$W(\mathbf{k})$	Energy of the power-law relief spectrum
w_i	Weight associated with the i^{th} input neuron
w_j	Weight associated with the j^{th} input neuron
w_{ji}	Weight connecting the i^{th} input neuron to the j^{th} output neuron
Δw_{ji}	Change in the weight w_{ji}
$\Delta w_{ji}(p)$	Change in the weight Δw_{ji} at the p^{th} iteration
x_i	i^{th} input data

x_a	Value of abscissa computed with inverse parabolic interpolation scheme
X	Input dataset (= $\{x_1,\ldots, x_n\}$) containing n variables
x_j	j^{th} input data
Xs	Scaled output of the input data X in neural network analysis
y	Total net output signal, $y = F(NET)$ (i.e., actual output)
Z_m	m^{th} orthogonal component (Principal Component)
1-D	One-dimentional
2-D	Two-dimensional
3-D	Three-dimensional
4-D	Four-dimensional
2F	Combined two-frequency Inversion (Inversion of a pair of echo envelopes at 33 and 210 kHz jointly)
α	A parameter expressed in terms of γ_2 as $\alpha = (\gamma_2 / 2) - 1$
α_w	Attenuation coefficient in seawater
α_s	Attenuation coefficient in sediment
β	Lipschitz exponent, used in Lipschitz-Hölder condition
β_e	Exponential attenuation rate
δ	Difference between the actual and the target output (the error term)
δ_{mj}	Error signal at the j^{th} neuron for the m^{th} training vector
δx_i	Error associated with the input data x_i
ε	Small positive constant in FCM computation
ϕ	Phi units to express the mean grain size diameter of sediments
ϕ_{16}	Representative grain size (phi value) within the interval 0-ϕ_{30}
ϕ_{50}	Representative grain size (phi value) within the interval ϕ_{30}-ϕ_{70}
ϕ_{84}	Representative grain size (phi value) within the interval ϕ_{70}-ϕ_{100}
φ	Scattered angle
γ_2	Seafloor roughness spectrum exponent
η	Learning rate parameter used in a neural network training
$\eta(p)$	Learning rate parameter at the p^{th} iteration

κ_p	Attenuation constant in sediment expressed in dB/m/kHz
λ	Acoustic wavelength
μ	Lambert's constant
μ_L	Levenberg's damping factor in Levenberg-Marquardt algorithm
ν	Ratio of speed of sound in sediment to speed of sound in water
θ	Echo sounder beam width
θ_c	Critical angle of incidence
θ_g	Grazing angle of incidence
θ_i	Angle of incidence relative to the vertical axis
θ_t	Transmission angle relative to the vertical axis
θ_{th}	Threshold value for calculating the net output
θ_1	Angle of the trailing edge of an acoustic pulse with the normal
θ_2	Angle of the leading edge of an acoustic pulse with the normal
ϑ	Local slope of a large-scale roughness
ρ	Ratio of bulk density of sediment to mass density of water
ρ_b	Density of seafloor sediment
ρ_w	Density of water
σ_2	Sediment volume scattering parameter
σ_v	Sediment volume scattering coefficient
τ	Time from the initial time ($=t-t_0$)
τ_d	Time scaling for echo compensation
τ_L	A small time lag to compute *HD* from an echo envelope
τ_p	Transmission pulse duration
ψ	Azimuthal angle
ψ_s	Solid angle of the echo sounder directivity pattern
ς	Constant used in the annealing scheme

Chapter 1

Introduction

1.1 BACKGROUND

Acoustic interaction with the seafloor and the properties of seafloor sediments are extensively researched over the past few decades, both experimentally and theoretically. Characteristics of seafloor sediments have wide range of applications in several fields such as economic, scientific, and defence. This has become an important subject for providing essential inputs to efficient management, monitoring, and exploitation of offshore petroleum products as well as marine biological resources especially fisheries. These studies are also useful for differentiating various marine habitats. Though acoustic techniques do not provide direct information on marine habitats, acoustic seafloor characteristics are indirectly important to fisheries sciences (Padian et al., 2009). Mapping of marine habitats, relationships of seafloor sediment characteristics with the associated biomass and benthic communities are being studied extensively (Siwabessy, 2001; Kostylev et al., 2001; Quintino et al., 2010). Moreover, seafloor sediment properties are essential for dredging of harbors and shipping channels; and pipeline as well as cable laying operations. Geo-technical characteristics (shear strength, bulk properties etc.) and acoustical properties of seafloor sediments are the essential inputs for designing offshore engineering structures, marine archeology

studies, and various types of underwater mooring applications (Hamilton, 2001). Therefore, detail knowledge of the seafloor sediment characteristics and their mapping are indispensable for efficient management of all these socio-economic activities.

Several defence applications such as submarine surveillances, navigations of submarines as well as surface vessels (Hamilton, 2001), acoustic homing torpedoes (Jackson and Richardson, 2007), and efficient use of a sonar for underwater target detection require an extensive knowledge on the interaction of sound energies with seafloor sediments. Interference of the scattering of acoustic energies from the seafloor degrades the capability of a sonar to detect and classify underwater targets such as submarines, buried mines etc. On the contrary, scattered acoustic energy (recorded by a sonar) provides useful information on the characteristics of seafloor sediments. In either case, detail knowledge on acoustic scattering from the seafloor, reverberation, seafloor roughness characteristics, and attenuation coefficients of seafloor sediments is essential for improving the performances of a sonar.

Characterization of seafloor sediment is a process to determine or to estimate various physical, chemical, geological, and biological characteristics of sediments. In other words, direct or indirect assessment of the seafloor sediment properties is called characterization of seafloor sediments. There are two basic approaches for characterization - empirical approach and model-based approach. Empirical approaches commonly utilize an experimental or observational dataset. Experimental data are calibrated in these methods to predict the properties of seafloor sediments in the vicinity of ground-truth sample locations. Several empirical approaches are available in literature (McKinney and Anderson, 1964; Stanton, 1985; Stanic et al., 1988) for seafloor sediment characterization. On the contrary, model-based approaches utilize physics-based theoretical models for characterization of the seafloor sediments.

Theoretical models are used to predict the characteristics of sediments for a given environmental condition. Once these theoretical models are validated against ground-truth, these model-based approaches essentially eliminate the need for collecting a large number of seafloor sediment samples and analyzing them in a laboratory. A number of acoustic models exist for predicting the interaction of acoustic energy with the seafloor (Ivakin and Lysanov, 1981a, 1981b; Boehme et al., 1985; Hines, 1990). In addition, various frequency dependent backscatter models have been developed utilizing the sediment geo-acoustic parameters, seafloor roughness characteristics, water-sediment interface scattering, and volume scattering coefficients as a function of grazing or incidence angles (Jackson et al., 1986a; de Moustier and Alexandrou, 1991; Sternlicht and de Moustier, 2003a). It is established from various field experiments (Jackson et al., 1986a, 1986b; Stanic et al., 1988, 1989; Jackson and Briggs, 1992; Williams et al., 2002, 2009) that acoustic backscatter energies contain information on the characteristics of surficial seafloor sediments such as seafloor roughness, volume in-homogeneity, mean grain size of sediment, etc. Therefore, scientific interests on the characterization of seafloor sediment either by direct measurements of backscatter energies or by indirect estimation of the sediment properties utilizing theoretical models have been increasing.

Classification of seafloor sediment is a process of segmenting or qualitative grouping of surficial sediments based on their properties (such as sand, silt, clay, and their mixtures). This means that classification is a process of segmenting different sedimentary regions on the seafloor with distinct physical entities (but similar properties within a segment or cluster) based on their characteristic features. Therefore, this process is complex in nature. In general, it would be easy to classify the seafloor sediments after the characterization has been done. However, only qualitative

assessment of the seafloor characteristics could be possible after the seafloor has been classified. Acoustic classification techniques have now become standard tools for classification and mapping of the seafloor sediments. Many approaches have been evolved in the recent years for classification of seafloor such as statistical analysis (Legendre et al., 2002), cluster analysis (Preston and Kirlin, 2003; Legendre, 2003), discriminant analysis (Hutin et al., 2005), neural network analysis (Dung and Stepnowski, 2000; Moszynski et al., 2000; Stepnowski et al., 2003), wavelet analysis (Atallah et al., 2002), and Fractal analysis (Lubniewski and Stepnowski, 1998; Chakraborty et al., 2007b).

Qualitative and quantitative information on the sediment characteristics, when obtained from the measurements in a laboratory or *in-situ* (in the field) analysis of seafloor sediment samples, is called ground-truth. Grabs and corers are the widely used instruments for obtaining sediment samples from the seafloor. Visual observations (video or still photography) of seafloor also provide supportive evidence on the seafloor roughness characteristics. Laboratory analyses of sediment samples from grab or corer provide the most reliable information on the characteristics of sediment. Though laboratory analyses of seafloor sediment samples provide an accurate assessment of the properties of sediment; collection and analyses of large number of samples over a wide area is time consuming and expensive job. Moreover, most of these methods fail to collect undisturbed sediment samples in the field and these methods can provide information on the sediment characteristics only at selected discrete locations. In addition, it is known that the seafloor is not a static environment over a long time period, because of the natural phenomena. Therefore, labeling (i.e., classification) of the seafloor sediments (as sand, silt, clay, and their mixtures) over a wide area, based on the quantitative analysis of a small portion of sediment at discrete locations, is inadequate

as well as inaccurate. Other methods such as optical methods (stereo photogrammetry) and laser scanning systems have also been developed for precision mapping and assessment of the characteristics of seafloor sediments (Richardson et al., 2001; Moore and Jaffe, 2002; Briggs et al., 2002; Lyons et al., 2002; Wang et al., 2009, Wang and Tang, 2009). However, the applications of these high precision methods are again restricted at discrete locations due to the operational limitations.

Hence, in analogy with Satellite Remote Sensing, which senses certain properties on the earth's surface, underwater acoustic remote sensing has become one of the most widely investigated subjects in the recent years for rapid assessment of the sediment properties over a large area as well as for its easy operations and cost effective nature. Characterization and classification of seafloor sediments based on the properties of surficial sediments (Orlowski, 1984; Chivers et al., 1990; Chakraborty and Pathak, 1999; Chakraborty et al., 2000; Briggs et al., 2002) and habitat characteristics (Kostylev et al., 2001; Anderson et al., 2002) are being investigated extensively.

Various complex dynamic processes affect the interaction and scattering mechanism of acoustic energies from the seafloor. Understanding of these mechanisms at different levels led to the development of numerous theoretical models to describe the seafloor scattering processes. Every theoretical model is based on certain understanding of sound scattering mechanism from the seafloor. Therefore, it is important and essential to appreciate the limitations of various acoustic models for effective characterization of the seafloor. In addition, studies on the validation and applicability of these theoretical models over a wide range of acoustic frequencies are indispensable.

The choice of instrumentation to characterize seafloor sediments primarily depends on the purpose of operations such as classification of sediments, surface and sub-surface object detection, searching for mineral deposits etc. Four types of

instruments are generally used in the field namely, single-beam normal-incidence echo sounder, side-scan sonar, multi-beam echo sounder, and sub-bottom profiler. Single-beam echo sounder utilizes backscatter data for the characterization of seafloor (Stanton and Clay, 1986; Pouliquen and Lurton, 1992; Lurton, 2002). Side-scan sonar exploits the information on texture analysis of acoustic images for describing the seafloor sediments. The use of spectral analysis for classification of seafloor with side-scan sonar data is also demonstrated (Pace and Gao, 1988). Many other investigations also demonstrate the characterization of seafloor using side-scan sonar images (Stewart et al., 1992, 1994; Zerr et al., 1994). Mapping of seafloor bathymetry and characterization of sediments using multi-beam echo sounder are most common (de Moustier and Matsumoto, 1993; Chakraborty et al., 2000, 2004; Collins and Preston, 2002; Zhou and Chen, 2005). Acoustic sub-bottom profilers, which include seismic system, parametric sonar, and chirp sonar are also used for seafloor sediment characterization (LeBlanc et al., 1992; Schock, 2004a, 2004b).

Though several instruments could be used for the purpose of characterization and classification of seafloor sediments, emphasis is given only on the normal-incidence, single-beam echo sounder in this work. Studies on the acoustic seafloor sediment classification have gained momentum after the development of few systems in 1990s. The advantages of these systems are that these can be attached to any existing echo sounder available on a research vessel for classification purposes. Most of these available systems use certain proprietary signal processing algorithms, which are not fully revealed to the users. Once these systems are calibrated properly in a known sedimentary environment, these systems or devices are capable of providing a real-time classification of the seafloor sediments. Therefore, these classifications are not absolute and highly dependent on the training (or calibration) dataset as well as on the

sedimentary environment in the experimental area, where the calibrations are carried out. In addition, the success of classification is a function of the sediment characteristics as well as echo sounder characteristics such as frequency of operation, pulse length, and beam width. Moreover, calibrations of these systems in a given sedimentary environment are not always very easy and unambiguous tasks. Therefore, there is a need for an extensive research in the field of classification of seafloor sediment utilizing various techniques such as principal component analysis, cluster analysis, and neural network analysis. These methods mostly based on the empirical approaches for classification of seafloor sediments and are often called model-free techniques. There is no quantitative physics-based theory behind the inferred relationships between the acoustical parameters and the sediment characteristics.

It is already mentioned that there are several acoustic systems for the classification of seafloor. An overview of the few existing available systems and their practical issues are briefed in the following sections to understand the need for further research on this subject.

1.2 SYSTEMS FOR SEAFLOOR CLASSIFICATION

There are several systems for acoustic classification of seafloor sediments. These systems provide automatic classification of seafloor along survey tracks, when attached to an echo sounder. Sediment classification systems were first developed for normal-incidence, single-beam echo sounder. Thus, single-beam echo sounders are often called as Acoustic Ground Discrimination Systems (ADGS). Classification systems for side-scan sonar, multi-beam, and sub-bottom profilers have also been developed

subsequently. However, in this section, the classification systems that are generally used with normal-incidence, single-beam echo sounder are briefed. RoxAnn, ECHOplus, QTC View, and VBT Bottom Classifier are the few widely used systems. The comparisons on the performances of different classification systems (such as RoxAnn and QTC View) are also investigated in detail (Hamilton et al., 1999).

RoxAnn system is designed and manufactured by M/s Stenmar Marine Micro Systems Ltd., UK. This system was probably the first system used for the classification of seafloor sediments. The RoxAnn system utilizes two parameters called E1 and E2. These parameters are derived from the first and the second acoustic returns from the seafloor. The first acoustic return is a direct reflection from the seafloor, whereas the second return suffers reflection twice at the seafloor and once at the sea surface. The second return follows an acoustic path: transducer-to-seafloor-to-sea surface-to-seafloor-to-receiver. The parameter, E1 is a measure of the total energy in the trail portion of the first acoustic return from the seafloor and it provides an index of roughness of the seafloor. Since the second acoustic return reflected twice at the seafloor, the energy within the second return is strongly affected by the hardness of the seafloor. Therefore, the parameter, E2 provides an index of hardness of the seafloor. E2 is derived from the total energy of the complete second acoustic return from the seafloor. Roughness and hardness characteristics are different for different seafloor materials. Scatter plots between E1 and E2 (roughness vs. hardness) are used for the classification of seafloor sediment. The total region of a plot is divided into a number of areas, called RoxAnn squares, where each square represents a particular seafloor sediment type or substrate. Seafloor sediment samplings are required to identify and correlate the sediment types associated with the clustering of each E1-E2 space. The lesser values of E1-E2 pair are generally associated with softer sediments, and rocky

seafloors have higher values of E1-E2 pair. Orlowski (1984) first reported this method of classification and later Chivers et al. (1990) refined this methodology.

The ECHOplus system (of M/s SEA Ltd., UK) comprises of hardware as well as software. It uses a patented technique for analyzing an echo trace to derive the integrals of the first and the second echo of the acoustic returns. Ground-truth data from sediment samples are initially used to associate each hardness-roughness space with the sediment type. Subsequently, different unknown seabed sediment types are identified in this hardness-roughness space. Essentially, the working principle of RoxAnn and ECHOplus are similar (Bates and Whitehead, 2001).

Quester Tangent Corporation, Canada developed QTC view system. It utilizes different characteristics of the first acoustic returns from the seafloor (Prager et al., 1995; Collins, 1996; Tsemahman et al., 1997). This system extracts 166 "echo features" from raw digital echo envelopes of the first bottom echo. These 166 features are called full feature vectors (FFV). The QTC system utilizes its built-in software based on Principal Component Analysis (PCA) to reduce the dimensionality of 166 echo features. PCA is used to identify the dominant FFVs, which explain at least 90% of the total variability of acoustic diversity. Finally, three parameters, called Q-values (Q1, Q2, and Q3) are derived. The clusters of these Q-values in three-dimensional space are used to differentiate different seafloor sediment type (Prager et al., 1995; Collins and McConnaughey, 1998; Legendre et al., 2002; Freitas et al., 2008). Later, an improved version of the software called QTC Impact was introduced. This software processes raw waveforms and automatically provides the clusters using an unsupervised mode of operations (Collins et al., 1996; Anderson et al., 2002) for seafloor discrimination. In the supervised mode of operation, the software uses a catalogue of Q-space clusters with reference to the data of known seafloor sediment types.

The VBT (Visual Bottom Typing) sediment classifier (from M/s BioSonics Inc., USA) is a post-processing software package (Burczynski, 1999; Hamilton, 2001) to analyze the acoustic returns from seafloor. It does not have any hardware components. This system uses four different methods for the classification of seafloor sediments. One of the methods of VBT software uses roughness and hardness features (same as RoxAnn and ECHOplus). Another method of VBT software utilizes hardness of sediments as the basis for classification. The hardness of sediment is assessed from the cumulative energy in the first echo. This method is based on a concept that hard seafloor sediments tend to have a sharp increase in the cumulative energy curves, while soft sediments tend to have a gradual increase in the cumulative energy curves. The next method of VBT software utilizes scatter plots between the energy of the first part of the first echo and the energy of the second part of the same first echo to differentiate sediment types. The last method of VBT software utilizes scatter plots between the roughness signature of sediments derived from the first echo and the fractal dimensions of echo envelopes (Burczynski, 1999).

1.3 LIMITATIONS OF AVAILABLE SYSTEMS

The afore-mentioned classification systems utilize empirical approaches. Hence, it becomes a prerequisite to establish an essential database before using these systems.

Studies on the performance of RoxAnn system indicate that the parameter E2 is inversely related to vessel speed (Hamilton et al., 1999). The system could produce optimal results only at a constant vessel speed during the operations and a prior knowledge on the maximum depth to be surveyed was necessary for selecting a suitable

depth range of the echo sounder for the entire survey area (Schlagentweit, 1993). This imposes constraints in operating RoxAnn in a coastal area. Moreover, the result obtained from RoxAnn system changes with the variation of seafloor depth, even if the sediment type remains unchanged (Kloser et al., 2001; Greenstreet et al., 1997).

Limited studies on the use of ECHOplus system restrict a comprehensive assessment on the performance of the system in discriminating seafloor sediments (Penrose et al., 2005).

QTC view system uses echo features for classification of sediments. However, physical and mathematical expressions for extracting these features are not revealed to the users (Hamilton, 2001). Information on the various stages of data processing (or the processing algorithms) of QTC system is also not revealed, thereby imposing difficulties in carrying out further research on the improvement of the processing algorithm.

It is reported (Hamilton, 2001) that VBT software for the classification of seafloor sediments does not use depth normalization and the method for selection of echo envelopes from raw data is not very robust in this software. This software is suitable for the classification of sediments, if seafloor depth is constant over the entire survey area.

All these qualitative systems could be used to achieve average to good results for the classification of sediments and these results depend on the accuracies of training in a known seafloor sedimentary environment. The main limitation of these seafloor classification systems is that the raw acoustic echo data are not available to the users for further studies. Hence, there is a need for an extensive research on the theoretical model-based characterization and model-free classification of the seafloor sediments.

1.4 RESEARCH OBJECTIVES

The main objective of the research is model-based characterization and model-free classification of seafloor sediments by acoustic means in the central part of the western continental shelf of India in the Arabian Sea. The studies on the characterization of seafloor sediments aim at investigating the applicability of a temporal backscatter model, utilizing the echo data obtained from normal-incidence, single-beam echo sounder at two conventional frequencies. Furthermore, the studies on model-free techniques for the classification of seafloor sediments aim at developing a hybrid scheme, which combines unsupervised and supervised approaches for achieving improved success in the classification.

It is understood that backscatter echo from the seafloor contains information on the characteristics of seafloor sediments such as mean grain size, seafloor roughness spectrum parameters, sediment volume scattering parameter, density of sediments, sound speed, etc. (Holliday, 2007). Thus, a temporal acoustic backscatter model (Sternlicht and de Moustier, 2003a) has been employed here for estimating the seafloor sediment parameters namely, mean grain size, roughness spectrum strength, roughness spectrum exponent, and volume scattering parameter through inversions. The applicability of this temporal model is investigated by comparing the estimated values of sediment parameters with the ground-truth in the study area. Moreover, it is reported (van Walree et al., 2006; Anderson et al., 2008) that the use of multiple frequencies enhances the ability to characterize the seafloor sediments considerably, because the interface roughness spectrum and the sediment volume backscattering strength may vary with acoustic frequencies. Lower acoustic frequencies penetrate the seabed to

greater depths, whereas higher frequencies will have improved resolving capability. Therefore, it is expected that the use of two conventional frequencies of a single-beam echo sounder will provide improved understanding on the interaction of acoustic energy with the seafloor sediments. Therefore, a combined two-frequency inversion scheme has been explored for obtaining the improved estimation on the various seafloor sediment parameters. In this combined two-frequency inversion approach, the backscatter echo data collected at two conventional frequencies (33 and 210 kHz) of a single-beam echo sounder are jointly inverted for estimating a single set of seafloor sediment parameters applicable to echo data at both of the frequencies.

Seafloor sediment classifications using model-free techniques are generally based on a-priori information on the number of sediment classes (or cluster centers), which specifies different sedimentary environments available in a given dataset. However, this information could be obtained only from the ground-truth. Hence, in the absence of any prior information, the decision on the plausible number of sediment classes is very important for achieving a significant success in classifying the seafloor sediments. An unsupervised approach, based on Kohonen's self-organizing feature map (Kohonen, 1989, 1990), is developed to estimate the plausible number of sediment classes available in a given dataset without any a-priori information. The effectiveness of this proposed method is also assessed with the simulated data at two different frequencies.

Moreover, selection of an optimum subset of features with dominant discriminatory characteristics is another important aspect for achieving the improved success in the classification of seafloor sediments. Therefore, two methods are developed to address this feature selection issue utilizing neural networks and fuzzy

cluster algorithm. The successes of classification with different subsets of echo features are analyzed in these two methods to select an optimum subset.

Therefore, the unsupervised scheme (for estimating the plausible number of sediment classes) in combination with any one of the methods, based on either neural networks or fuzzy cluster algorithm, provides an efficient hybrid scheme for the classification of seafloor sediments.

1.5 OUTLINE OF THE THESIS

The work has been divided into eight chapters. This chapter discusses the importance of this study. In addition, four widely used seafloor classification systems along with the practical issues are discussed to understand the need for further research on this subject.

Chapter 2 describes the study area, acoustic data collection, and methodology for pre-processing the backscatter echo data obtained from a normal-incidence, single-beam echo sounder. The details of sediment ground-truth based on the percentage compositions of sand, silt, and clay obtained from the laboratory analysis are presented.

Chapter 3 introduces the basic theoretical concepts of acoustic interactions with the seafloor sediments. Subsequently, a concise review on the relevant acoustic models for interpreting the backscatter echo data is presented.

Chapter 4 discusses the theory of a temporal backscatter model. This theoretical model is used for indirect estimation of the values of seafloor sediment parameters. The sensitivity analyses of this model with reference to various model parameters are discussed. The procedures adopted for estimating the values of seafloor sediment parameters using the backscatter echo envelopes collected at two conventional

frequencies of a single-beam echo sounder and a combined two-frequency inversion scheme are discussed in this chapter. Finally, comparisons of the inversion results with the ground-truth and other published information are presented.

Chapter 5 reviews several existing model-free approaches for the classification of seafloor sediments. Following this, the background for computing seafloor echo features and two model-free techniques namely principal component analysis and fuzzy cluster algorithms are presented. This chapter discusses the results obtained from the cluster analysis using the first three principal components along with the comparisons with ground-truth.

Chapter 6 introduces the basics of artificial neural networks relevant to the present study. Following this, a neural network based supervised method is presented for the selection of an optimal subset of echo features to achieve a significant success in the classification of seafloor sediments.

In Chapter 7, a hybrid scheme is proposed for the classification of seafloor sediments utilizing an unsupervised neural network and fuzzy cluster analysis. The unsupervised approach, based on Kohonen's self-organizing feature map, is discussed for estimating the plausible number of sediment classes in a given dataset without any a-priori information. This proposed method is also demonstrated with the simulated data. A fuzzy cluster algorithm based features selection method (in addition to the neural network based method, as mentioned in Chapter 6) is discussed in this chapter. Subsequently, the comparison of results obtained from the proposed hybrid scheme (consisting of the unsupervised approach and the fuzzy cluster algorithm based method) with that of another existing hybrid scheme is discussed. In addition, the results of two proposed features selection methods are compared.

Chapter 8 summarizes the results from this study. The practical utilities and future work are also presented in this chapter.

Chapter 2

Pre-Processing Methodology

2.1 EXPERIMENTAL AREA

Characteristics of seafloor sediment in the continental shelf of India are becoming crucial for civilian as well as defence applications. Efficient management of marine resources (e.g., marine fishes, mineral, and petroleum resources) requires detail understanding of the characteristics of seafloor sediments in this area. In addition, realistic characteristic map of seafloor sediments has significant importance for the successful operations of underwater surveillance and detection systems in coastal areas.

The study area is selected in the central part of the western continental shelf of India in the Arabian Sea (Fig. 2.1). Acoustic data were collected with a normal-incidence, single-beam echo sounder using two conventional acoustic frequencies (33 and 210 kHz) at 20 experimental sites. Ground-truth sediment samples were collected from the same 20 spots. Out of the 20 identified sites, 7 are located towards south of Mormugao Port (labeled with serial no. 1 to 7 in Fig. 2.1), 5 are off Bethul coast (serial no. 8 to 12), and the rest 8 are towards North of Mormugao Port (serial no. 13 to 20). Seafloor depths vary between 21-109m in the study area. The experiments were conducted in calm weather conditions (Chakraborty et al., 2005; Navelkar and Mahale, 2005). Seafloor sediments in the coastal area of the western continental shelf of India

consist of different types of sediments (such as sand, silt, clay, and their mixtures). Gravels are generally not observed in the selected study area.

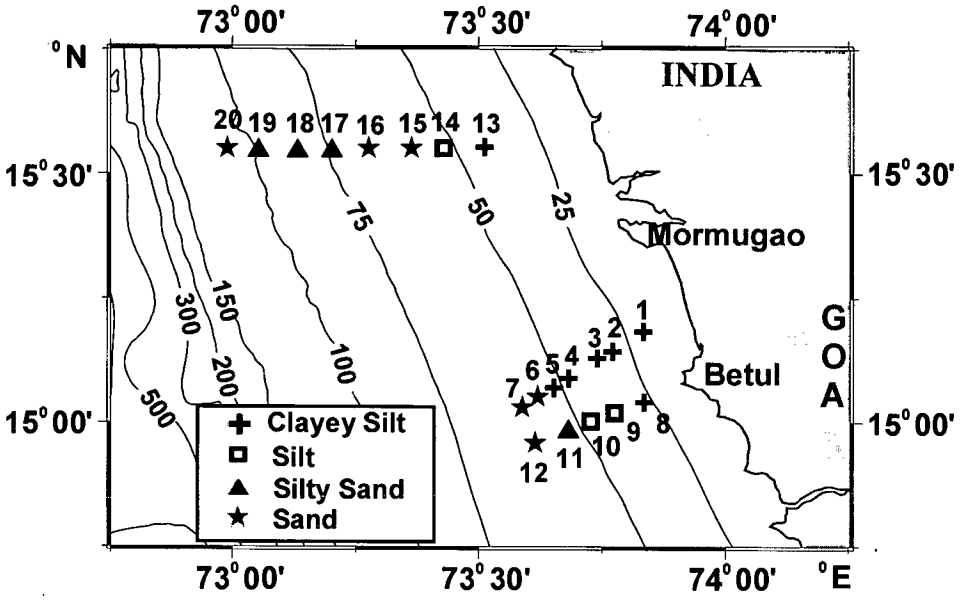

Fig. 2.1 Seafloor sediment types at 20 spot locations in the study area (in the western continental shelf of India) are shown with different symbols

2.2 ACOUSTIC DATA

National Institute of Oceanography, Goa had collected the acoustic backscatter echo data at 20 locations in the study area under a project granted by Department of Information Technology, Government of India (Chakraborty et al., 2005; Navelkar and Mahale, 2005). National Institute of Ocean Technology, Chennai had provided the necessary logistics and ship facilities to National Institute of Oceanography, Goa for collection of data. Acoustic backscatter data were acquired using a hull-mounted dual-frequency (33 and 210 kHz) normal-incidence Reson Navitronics NS-420 single-beam echo sounder (Anonymous, 1999) from all the identified sites.

A brief description of the characteristics of the single-beam echo sounder (Reson Navitronics NS-420) along with the methodology adopted for data acquisition and pre-processing is given below.

2.2.1 Characteristics of Reson Navitronics NS-420

This echo sounder has the following characteristics. Transmitter sensitivities of Reson Navitronics NS-420 single-beam echo sounder are 167 dB and 170 dB re 1μPa/V at 1m for 33 and 210 kHz respectively. Receiver sensitivities of the same echo sounder are -178 and -190 dB re 1V/μPa for 33 and 210 kHz respectively (Anonymous, 1999). Beam shape of the echo sounder is conical and -3dB beam widths (width of the main lobe measured between the -3dB points on either side of the beam pattern) are 20^0 and 9^0 at 33 and 210 kHz respectively. Pulse widths of the echo sounder were selected as 0.97ms and 0.61ms respectively for the two acoustic frequencies.

2.2.2 Data Acquisition

Single-beam echo sounder, one of the most common sonar systems, is designed to measure seafloor depths. An acoustic pulse, transmitted by the transceiver of an echo sounder, travels through the water column and reflected back (from the seafloor) to the transceiver. Echo sounder system processes this received echo to calculate the seafloor depth from the measured two-way travel time of the pulse through the water column. Reson Navitronic NS 420 echo sounders do not provide any digital outputs of the raw echo data. Therefore, a system, developed by National Institute of Oceanography, Goa (Navelkar et al., 2005), was attached to Reson Navitronics NS-420 for acquiring the raw

acoustic echo data in the study area. The block diagram of the echo data acquisition system is shown in Fig. 2.2. A 12-bit A/D card (PCL-1712L) with 1 MHz sampling rate is used in the system to acquire the raw digital acoustic echo data at 33 and 210 kHz. The variations of echo amplitude are recorded within a voltage range of ± 5V.

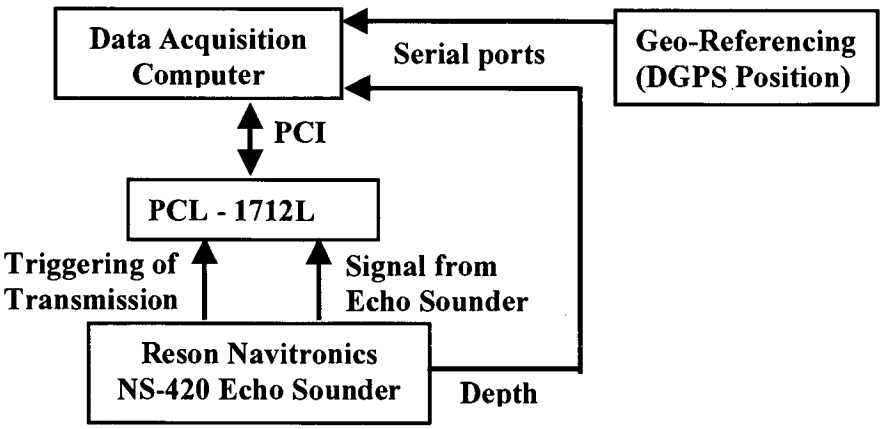

Fig. 2.2 A Block diagram of the data acquisition system (Navelkar et al., 2005)

A typical echo record (basically a voltage trace) obtained from the echo sounder for one transmission cycle is shown in Fig. 2.3. A typical echo record consists of the transmission pulse, the reflections from water column, and the reflections from seafloor. The voltage fluctuations at the starting point (on the extreme left side of the echo trace) represent the transmission pulse. The next fluctuation represents a direct reflection from the seafloor. The direct reflection has two distinct parts, the initial part and the trail part. The initial part of the echo trace is the reflection from the water-seafloor interface. The trail portion of the echo represents the energy backscattered from the sediment volume.

About 1500 echo data were acquired using two acoustic frequencies (33 and 210 kHz) at each of the 20 locations in the study area. Echo traces with saturated voltages are first removed from the stack in the initial stage of the pre-processing. Remaining echo traces are subjected to Hilbert Transform to obtain the echo envelopes (or echo

waveforms). These echo envelopes are used for further study. A typical echo envelope is shown in Fig. 2.4.

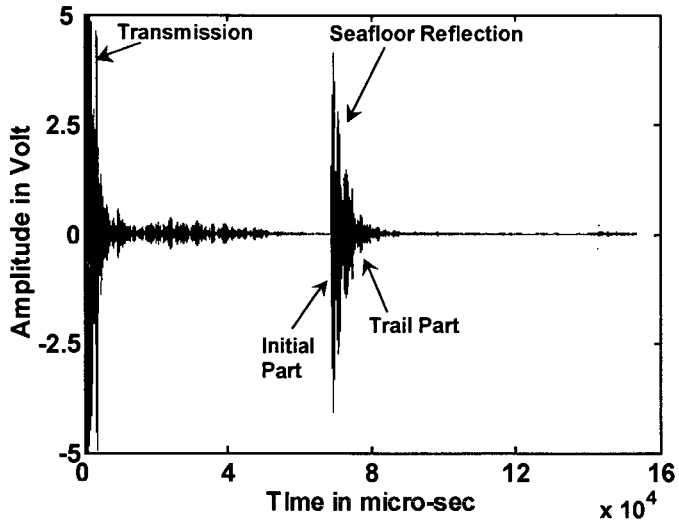

Fig. 2.3 A typical echo record from the single-beam echo sounder

2.2.3 Pre-Processing of Echo Envelopes

The shape of an echo envelope depends on various factors such as natural variability of seafloor, transducer heave, noise due to the echo-sounder instability, etc. A variety of biologic (e.g., fishes) concentrations and other suspensions in the water column also cause distortions in echo shapes. Therefore, several steps such as bottom detection, echo alignment, and echo averaging are essential for obtaining good averaged echo envelopes for further utilization.

2.2.3.1 Bottom Detection

Bottom detection is the estimation of the starting time of an echo envelope, which corresponds to the seafloor depth (Hamilton, 2001; Sternlicht and de Moustier,

2003a). Bottom detection is essential for obtaining a reference point to align all the echo envelopes correctly.

Selection of echo envelopes (without or less distortion) is the first step to achieve the improved bottom detection. This is achieved by carefully selecting the echo envelopes, characterized by a well-defined initial rise and peak amplitude followed by a slow decay, through visual checks (Sternlicht and de Moustier, 2003a; Klusek et al., 1994). First, echoes with inconsistent depth (compared to the depth recorded by the echo sounder) are eliminated from the stack. Subsequently, echo envelopes are selected by checking the initial rise times of the envelopes. Echoes with initial rise time shorter than or equal to a fixed duration of time (based on the pulse duration of an echo sounder) are selected for further analysis. However, this method is not suitable for slanting seafloor. It is important to mention that the spot locations were not selected over any slanting region of the seafloor. It is noticed from the present analysis that approximately 20-45% of the total number of echoes at each location are only qualified for further analysis.

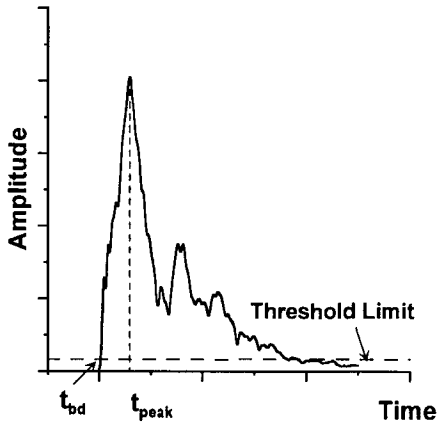

Fig. 2.4 Illustrating sea bottom detection method

The next step is the estimation of the seafloor depth from an echo envelope. This is carried out based on a certain threshold level with respect to the peak amplitude of the

echo envelope, as illustrated in Fig. 2.4. However, there is no specific rule for deciding this threshold level and it depends on the distortion of echo shapes. In this study, -20dB of the peak amplitude (t_{peak}) (i.e., 10% of the peak amplitude) is chosen as the threshold level (or threshold limit). The starting time (t_{bd}) of the echo envelope is decided based on this threshold limit (Fig. 2.4). This time t_{bd} is utilized for estimating the seafloor depth of that particular echo envelope.

Subsequently, leading and trailing edges of the envelope are truncated (based on the threshold limit) and these truncated envelopes are finally used for echo alignment and averaging. This threshold detection method is not suitable for a rough interface of the seafloor. In such cases, the position of peak amplitude (t_{peak}) is first determined and then a time window of fixed width is used to scan and estimate the seafloor depth in that echo trace. Time window widths of 1.1 ms for 33 kHz and 0.85 ms for 210 kHz are found suitable for obtaining reasonable seafloor depths.

2.2.3.2 Echo Alignment

Due to the up and down movement of transducer and small depth variations over the consecutive pings, arrival times of all the echo envelopes are not same. Hence, it is essential to align all echo envelopes before further processing. The alignment is based on identifying and indexing a temporal feature on an echo envelope. The initial rise time (t_{bd}), and time of peak amplitude (t_{peak}) are considered as important temporal features of an echo. After identifying this temporal feature, all echoes within the ensemble are shifted in time to align up with that (selected) feature. The following procedure is adopted for alignment. First, an alignment index J_m ($1 \le J_m \le N$) is found, where J_m

is the matching time of the m^{th} echo with respect to the selected temporal feature (i.e., J_m is an integer value) and N is the number of samples in the echo envelope. A mean alignment index J_{mean} is then calculated as (Sternlicht and de Moustier, 2003a),

$$J_{mean} = \frac{1}{M} \sum_{m=1}^{M} J_m, \tag{2.1}$$

Here, M is the total number of echoes. This leads to a delay in time of $D_m = J_m - J_{mean}$ in the alignment for the m^{th} echo. This delay time is utilized to get an aligned array of echoes. Fig. 2.5 and Fig. 2.6 illustrate the echo alignment process in two sediment environments (with 300 number of echoes) at 33 and 210 kHz using the initial rise time as a temporal feature. This alignment method is called threshold minimum alignment (Sternlicht and de Moustier, 2003a) or bottom pick alignment (Preston et al., 1999).

Alignments based on other techniques (e.g., cross-correlation or matched filters) induce vertical disproportions (i.e., exaggerated peak amplitude) in the averaged echo (obtained after alignment) (Sternlicht and de Moustier, 2003a), which is not suitable for the echo envelope shape matching technique (employed here for the characterization of seafloor). Excessive peak amplitude may lead to the inconsistent estimation in the value of mean grain size of sediments (in comparison with ground-truth). Thus, alignment based on the threshold minimum method is used in the characterization of seafloor sediments that preserves the integrity of the rising shape as well as the rising time of an echo envelope (Sternlicht and de Moustier, 2003a).

2.2.3.3 Echo Average

Echo averaging is carried out on the aligned echoes. To reduce the effects of transducer heave and variations of depth over consecutive pings, it is essential to use

averaged echo envelope for further analysis. The averaging gives a smooth and stable acoustic signal, which is useful for comparison with theoretical models. The voltage sequence $V[n]$ of an average echo is calculated from an ensemble of M contiguous echo using aligned two-dimensional voltage array $V[m,(n-D_m)]$,

$$V[n]=\frac{1}{M}\sum_{m=1}^{M}V[m,(n-D_m)], \tag{2.2}$$

where m = 1, ..., M is the number of echoes (or pings), and n = 1, ..., N is the number of samples per echo, and $V[m,(n-D_m)]$ is the aligned two-dimensional voltage array created from two-dimensional unaligned voltage array $V[m, n]$ for the m^{th} echo envelope.

2.2.3.4 Echo Compensation

The shape and the power of backscatter signals change significantly with the variations in seafloor depth even if the seafloor sediment remains unchanged. This is due to the spreading loss, absorption loss, and the variation in footprint size of the beam. Therefore, it is essential to compensate the backscatter echo data at a reference seafloor depth. The requirement of time adjustment (i.e., depth compensation) and power compensation of echo envelopes are investigated earlier (Clarke and Hamilton, 1999; Pouliquen, 2004; Lubniewski and Pouliquen, 2004) to achieve correct classification of sediment with the data collected at different seafloor depth. Therefore, echo envelopes acquired over the seafloor with varying depth are compensated at a reference depth. These compensated echo envelopes are used for the classification of seafloor sediments using various model-free techniques. However, it is important to note that the depth of seafloor from echo sounder transducer is used as one of the input parameters in most of

the physics-based scattering models. Hence, time and power adjustments of the echo envelopes are not required for theoretical model-based characterization of the seafloor.

An echo recorded at a greater depth (compared to the reference depth) is expanded in time and an echo recorded at a lesser depth (compared to the reference depth) is compressed in time. If H is the actual seafloor depth and H_{ref} is the reference seafloor depth, then the time scaling (τ_d) is expressed as (Caughey and Kirlin, 1996; Pouliquen, 2004),

$$\tau_d = t\left(H_{ref} / H\right) \tag{2.3}$$

where t is the actual recorded time of the echo obtained from the true seafloor depth.

The loss of intensity of an echo increases with the increase in seafloor depth. This loss of intensity increases due to the loss in spherical spreading, loss in attenuation, and larger beam insonified area (footprint). The amount of absorption depends on the propagation distance and the attenuation coefficient in seawater (α_w). The compensated power of the acoustic return at a reference seafloor depth (H_{ref}) is computed using a correction factor and the power of the time scaled echo (Clarke and Hamilton, 1999; Pouliquen, 2004). This power compensation corresponds to a correction close to $30\log_{10}(H / H_{ref})$ in addition to the attenuation losses of an echo envelope.

Even after converting an echo envelope to a reference depth, a small amount of geometric error is always associated with the compensated (depth as well as power) envelope (Clarke and Hamilton, 1999; Pouliquen, 2004). This error can only be removed by adjusting the active pulse length while acquiring the experimental data in the field (Pouliquen, 2004). This means that echo sounder returns could be transformed precisely to a specific reference seafloor depth if sampling rate, pulse duration, and intensity of transmission are tuned (based on the seafloor depth) during field experiments. If this method is not adapted during data acquisition, compensations of echo envelopes are required.

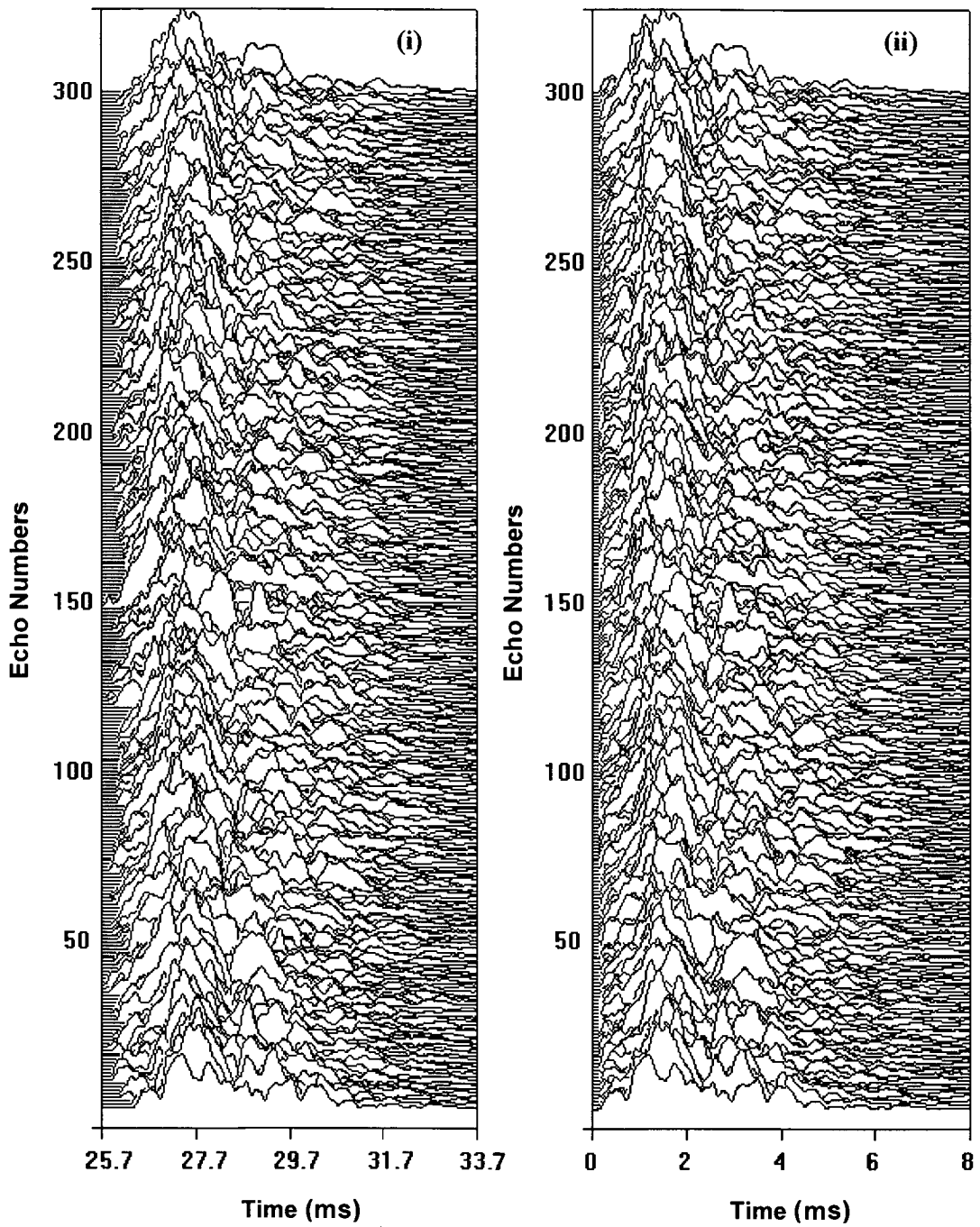

Fig. 2.5 Illustrating the effect of echo alignment process for a clayey silt region (Station No. 1) at 33 kHz **(i)** without alignment, and **(ii)** with alignment

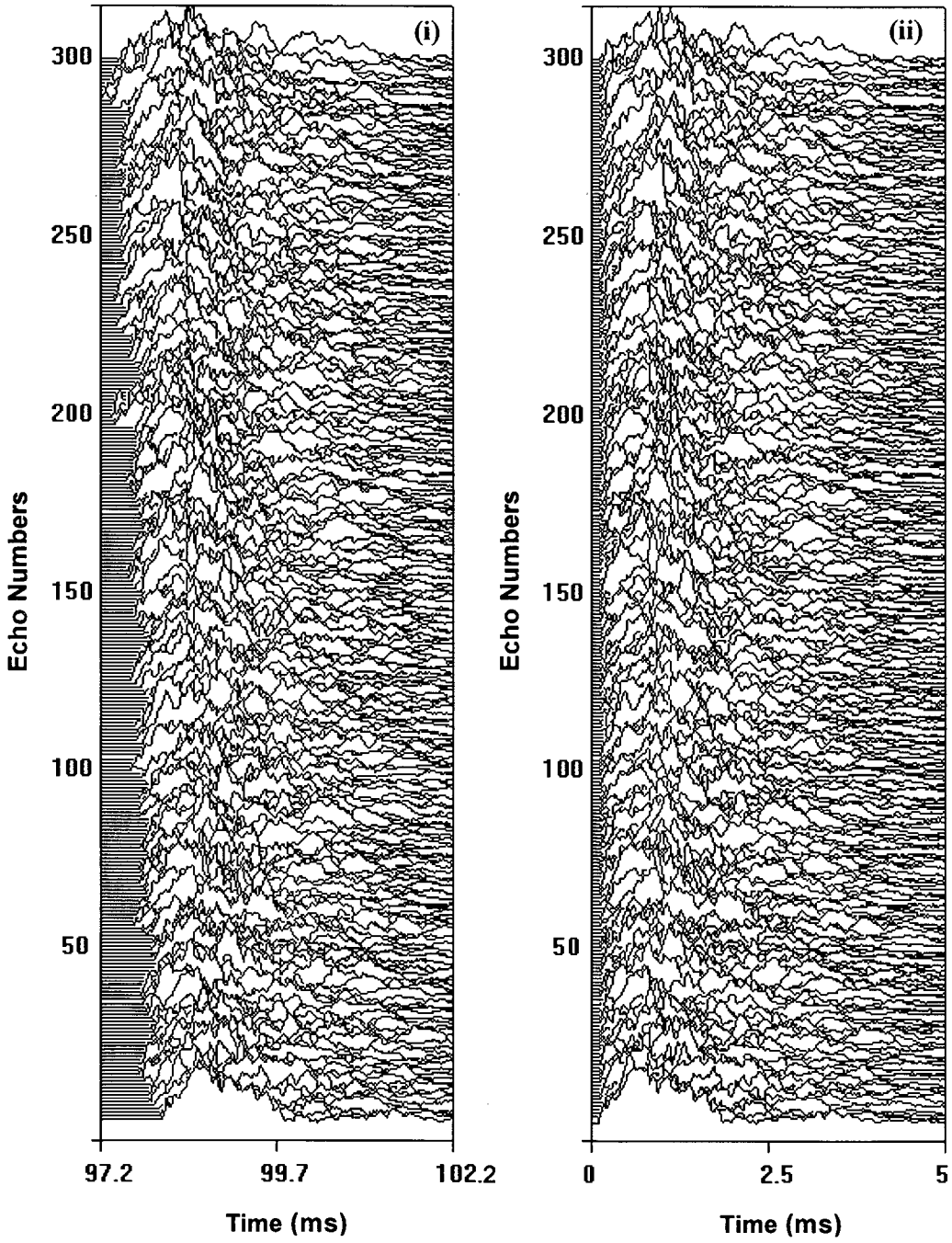

Fig. 2.6 Illustrating the effect of echo alignment process for a silty sand region (Station No. 17) at 210 kHz **(i)** without alignment, and **(ii)** with alignment

2.3 GROUND-TRUTH

Sediment samples were collected using a Van Veen grab at the same 20 locations in the study area, where the acoustic data were collected, for obtaining ground-truth information on the seafloor sediments (Fig. 2.1). The acoustic backscattering from the seafloor is primarily influenced by the contributions of the energy scattered at the water-sediment interface and from the sediment volume. Interface scattering can be described by the interface roughness coupled with acoustic impedance. Volume scattering depends on the water-sediment interface characteristics for transmission of the energies and then absorption inside the sediment volume. A significant contribution, due to volume scattering (in addition to interface scattering) from various scatterers (e.g., shells, pebbles, gas bubbles, living organisms, sediment layering etc.), is expected at 33 kHz due to greater penetration of energies. However, the effect of volume scattering is expected to decrease (in contrast with the interface scattering) with the increase in the acoustic frequency because of enhanced absorption. The absorption in seafloor sediments typically varies in the range 0.1 dB to 1.0 dB/wavelength (Hamilton, 1972). In this study, the acoustic wavelengths for 33 and 210 kHz are 4.5 and 0.7 cm respectively. Thus, surficial sediments collected by a grab sampler can be considered as the property representative of the portion of sediment probed by the echo sounder, providing quantitative information on seafloor sediment grain size distribution. Grain sizes of seafloor sediment samples are analyzed in the laboratory (at National Institute of Oceanography, Goa) using Malvern Mastersizer 2000 Laser Particle Size Analyzer (manufactured by M/s Malvern Instruments Ltd.). In laser diffraction granulometry, when a laser beam falls on dispersed particles, information on the particle sizes is obtained from the light diffraction pattern (Storti and Balsamo, 2009). Information on the fractions of sand, silt, and clay portion in sediments is obtained from a cumulative

particle grain size distribution curve. These percentage compositions of sand, silt, and clay in surficial sediment samples are given in Table 2.1.

The graphic mean size of sediment is calculated from the cumulative particle size distribution vs. grain size diameter (in phi units) curve. A common unit based on logarithmic scale is generally used to express the graphic mean grain size of sediments. This unit (ϕ) is called phi-unit and is expressed as (Jackson and Richardson, 2007),

$$\phi = -\log_2(d_g), \tag{2.4}$$

where d_g is the grain size diameter of sediments in mm. The graphic mean grain size (M_ϕ) in phi unit is calculated as (Jackson and Richardson, 2007),

$$M_\phi = \frac{\phi_{16} + \phi_{50} + \phi_{84}}{3} \tag{2.5}$$

where ϕ_{16} is assumed as the representative grain size within interval 0-ϕ_{30} and is computed from the cumulative particle size distribution vs. grain diameter (phi units) curve. Similarly, ϕ_{50} and ϕ_{84} are assumed as the representative grain sizes within the interval ϕ_{30}-ϕ_{70} and ϕ_{70}-ϕ_{100} respectively. This graphic mean grain size is one of the most important characteristics of the seafloor sediment and will be simply (hereafter) referred to as the mean grain size of sediment in the following text. The computed values of mean grain size of sediments (using the equation (2.5)) at all locations are also listed in Table 2.1. Folk's inclusive graphic standard deviation values (or the sorting coefficients) indicate that sediments in this experimental area are mainly poorly to very poorly sorted. The sorting coefficients for clayey silt and silt samples vary within a range of 1.32ϕ to 1.96ϕ, whereas, for silty sand and sand samples the sorting coefficients vary within 0.99ϕ to 2.24ϕ.

Since mean grain size is the most basic attribute of seafloor sediments, the nomenclature describing the size distribution is very important. Initially, geologists divided sediments into four groups based on grain sizes, which are gravel, sand, silt, and

clay. The logarithmic Wentworth grade scale (Wentworth, 1922) was the most commonly used scale, where the boundaries between the successive grain sizes differ by a factor of two. At present, two main classification schemes are available based on the relative proportions of grain sizes in sediments. The classification scheme, devised by Folk (1954, 1974), is based on a triangle divided into 15 partitions. This scheme groups the mixtures of gravel, sand, and mud to map sediments ranging from 'sandy mud' to 'sandy gravel'. Another classification scheme is devised by Shepard (1954), which utilizes a ternary diagram to classify sediments based on the proportions of sand, silt, and clay in the sediment samples. Sand, silt, and clay are placed at the corners of a ternary diagram to show the relative proportions among these three types within the sediment sample. Since sediment samples in the western continental shelf of India do not contain any gravel fraction, Shepard's scheme (1954) is used to classify seafloor sediments (Fig. 2.7) in the present study.

Table 2.1 Ground-truth data

Station no.	% Sand	% Silt	% Clay	Laboratory measured M_ϕ	Sediment type
1	1.49	65.28	33.23	6.71	Clayey Silt
2	0.41	71.59	27.99	6.68	Clayey Silt
3	1.78	70.06	28.16	6.67	Clayey Silt
4	3.17	71.93	24.90	6.32	Clayey Silt
5	8.03	71.52	20.45	5.83	Clayey Silt
8	0.78	70.95	28.27	6.66	Clayey Silt
13	0.13	70.66	29.21	6.79	Clayey Silt
9	0.54	75.86	23.60	6.42	Silt
10	0.64	75.91	23.45	6.50	Silt
14	0.92	79.05	20.03	6.20	Silt
11	57.42	32.30	10.28	4.02	Silty Sand
17	70.31	24.45	5.24	2.40	Silty Sand
18	73.64	22.29	4.07	1.99	Silty Sand
19	54.58	38.52	6.90	3.32	Silty Sand
6	95.33	3.08	1.59	1.69	Sand
7	91.26	6.13	2.61	2.31	Sand
12	91.26	6.87	1.87	2.03	Sand
15	80.90	14.24	4.86	2.42	Sand
16	89.05	8.65	2.30	1.16	Sand
20	83.77	14.01	2.23	2.07	Sand

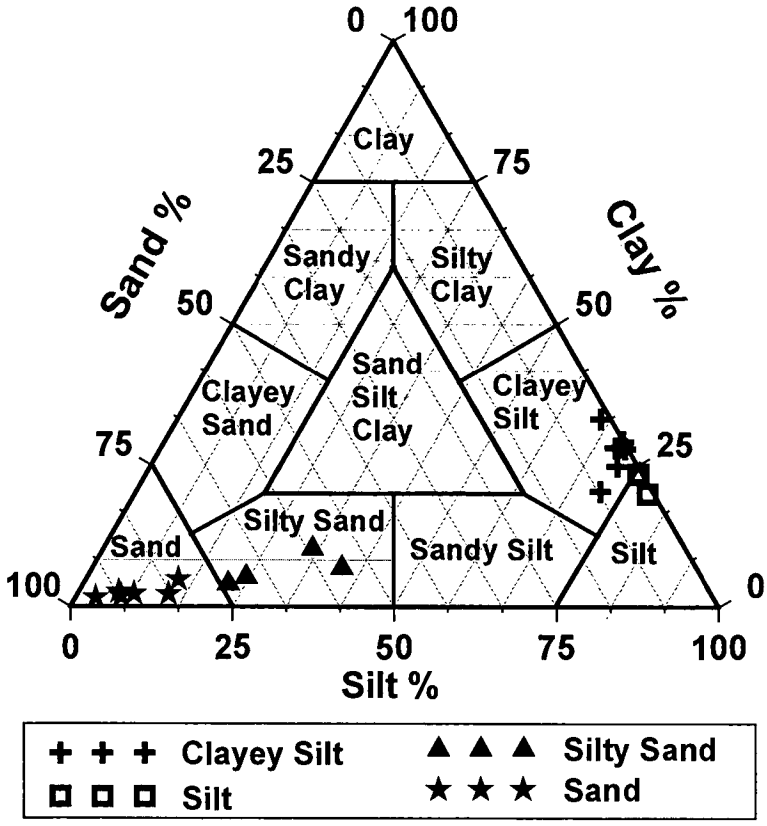

Fig. 2.7 Ternary diagram for the classification of seafloor sediment

Shepard's ternary diagram reveals that four types of sediments are available in the study area. These sediment types namely clayey-silt, silt, silty sand, and sand are shown in Fig. 2.7 (and also in Fig. 2.1) with different symbols. These four sediment types are also referred to as CS (clayey silt), Si (silt), SS (silty sand) and Sa (sand) in the following text. The data in Table 2.1 are sorted based on the types of sediment available in the experimental area (i.e., not sorted according to the station number).

This chapter has dealt with the acoustic data collection and their pre-processing methodology. The next chapter will focus on the review of literature available on acoustic models relevant to the seafloor characterization.

Chapter 3

A Concise Review on Acoustic Models

3.1 THEORETICAL BACKGROUND

Several processes are involved in the recording of seafloor backscatter energy using a single-beam echo sounder. These are (a) transmission of acoustic signal from the transmitter, (b) propagation of acoustic signal in the water column (towards the seafloor), (c) reflection, refraction, and scattering of acoustic energies from the water-seafloor interface, (d) scattering of acoustic energies from the sediment volume inhomogeneities, (e) propagation of acoustic signal from the seafloor towards the receiver through water column, and (f) reception of the return signal by the echo sounder receiver. Transmission of acoustic signal is mainly controlled by the characteristics of transmitter such as source level, pulse duration, and beam pattern. After transmission, the acoustic signal suffers various losses in the water medium during propagation towards the seafloor and back propagation towards the receiver. Spreading loss, absorption loss, scattering from the in-homogeneities (e.g., suspended particles, fishes, plankton etc.), and bending of sound rays are few important processes during the propagation of acoustic energy in the water medium. The phenomena namely reflection, refraction, and scattering take place as the acoustic energy interacts with the seafloor. The factors involved in these processes are - angle of incidence, ratio of speed

of sound in sediment to speed of sound in water, ratio of density in sediments to water density, attenuation in sediments, seafloor roughness characteristics, sediment layering, sediment volume inhomogeneities, and various objects (with different shapes) embedded in sediment volume. The reception of backscatter signal also depends on the characteristics of receiver (such as receiver sensitivity), noises from other sources, and relative movements of the receiver (such as, heave, roll, and pitch).

Literature on acoustic backscatter from seafloor is unlimited. Detail descriptions on various theoretical topics and related literature are available in several books (Urick, 1983; Medwin and Clay, 1998; Lurton, 2002; Brekhovskikh and Lysanov, 2003; Jackson and Richardson, 2007). However, basic concepts related to acoustic interactions with the seafloor sediments are introduced and the relevant literature on acoustic models for characterization of the seafloor is reviewed concisely in this chapter.

3.1.1 Reflection and Transmission

When a plane acoustic wave impinges upon seafloor (an interface between water and sediment with different acoustic impedances), a part of the energy is reflected back (Fig. 3.1) in the water medium with an angle equal to the angle of incidence (θ_i). This is called reflection and it occurs at a flat or plane interface. The incident energy is reflected in a direction symmetrical to the direction of arrival (like a mirror, and hence this is also called specular reflection). However, there is a loss of amplitude in this process. Reflection depends on the angle of incidence, density contrast, and sound speed contrast at the two mediums of reflecting interface. Part of the energy is transmitted into

the sediment volume with an angle (θ_t) and it is often called transmitted or refracted wave.

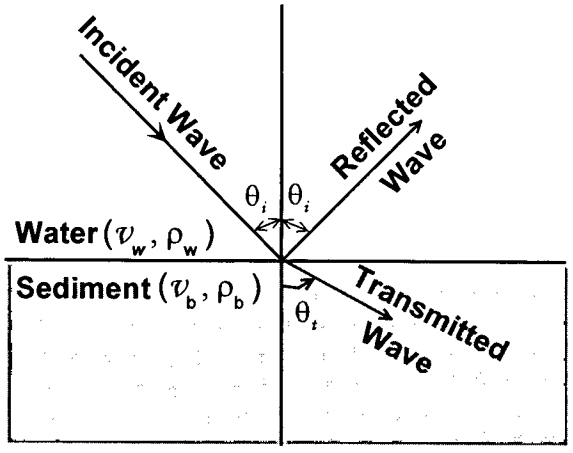

Fig. 3.1 Reflection and transmission at a flat interface

This angle θ_t is called transmission angle and it follows Snell's law of refraction (Lurton, 2002),

$$\frac{\sin(\theta_i)}{v_w} = \frac{\sin(\theta_t)}{v_b}, \tag{3.1}$$

where v_w and v_b are the speeds of sound in water and seafloor sediment respectively. The amplitudes of reflected and transmitted waves are determined by reflection and transmission coefficients. The reflection coefficient ($\Re$) and transmission coefficient ($\Im$) for the geometry given in Fig. 3.1 are given by (Lurton, 2002),

$$\Re = \frac{\rho_b v_b \cos\theta_i - \rho_w v_w \cos\theta_t}{\rho_b v_b \cos\theta_i + \rho_w v_w \cos\theta_t} \tag{3.2}$$

$$\Im = \frac{2\rho_b v_b \cos\theta_i}{\rho_b v_b \cos\theta_i + \rho_w v_w \cos\theta_t}, \tag{3.3}$$

where ρ_w and ρ_b are the densities of water and seafloor sediment respectively.

For normal angle of incidence ($\theta_i = 0$), the equation (3.2) reduces to:

$$\Re = \frac{\rho_b v_b - \rho_w v_w}{\rho_b v_b + \rho_w v_w} \tag{3.4}$$

Transmission of acoustic energy in seafloor sediments is not possible beyond a certain angle, called critical angle (θ_c) and this critical angle (when $v_b > v_w$) is given by,

$$\theta_c = \sin^{-1}\left(\frac{v_w}{v_b}\right) \tag{3.5}$$

At this critical angle, the total reflection occurs (i.e., $\theta_t = 90^0$). As the angle of incidence (θ_i) decreases from a very high value and crosses the critical angle; the reflection coefficient decreases very suddenly and then subsequently varies smoothly with the angle of incidence.

3.1.2 Acoustic Scattering

Scattering is an important phenomenon to describe the interaction of acoustic energy with seafloor. The roughness of water-seafloor interface and the in-homogeneities in sediment volume cause the acoustic energies to scatter in all directions. The scattering of energy towards the transmitter of a sonar is called backscattering. Backscatter energies are generally used in mono-static sonar systems (e.g., single-beam echo sounder, where transmitter and receiver are located at the same position) (Lurton, 2002). The backscatter of energies from objects other than the echo of desired target is called reverberation. However, the definitions of target echo and reverberation are relative (and arbitrary) and depend on the objectives of study. Acoustic backscattering from the boundaries of propagation medium (sea surface and seafloor) are called surface and bottom reverberations. Similarly, backscatter of energies

from various objects in water medium such as fish, plankton, suspended particle or a bubble is called volume reverberation in the water medium.

Seafloor is not the ideal plane surface for acoustic waves. Therefore, interpretation of backscatter data from the seafloor is very complex in nature and depends mainly on the interface roughness as well as the volume scattering. If micro-scale roughness of an interface is comparable in magnitude with the acoustic wavelength, the interface may be considered as locally plane surface for that acoustic frequency. Interface irregularities will scatter acoustic energies in all the possible directions. This scattering of energy depends on the frequency of incident acoustic wave, incidence angle, and local characteristics of the interface relief (i.e., the ratio of the mean amplitude of interface roughness to the acoustic wavelength). The scattered energy is segregated into two parts: coherent and incoherent. The coherent part of the energy contains specular reflections, where a part of the incident wave is reflected in a specular direction without any deformations other than the loss in amplitude. The rest of the energy is scattered in the entire medium, including the backscatter energy towards the source. This scattered energy represents the incoherent part (Lurton, 2002).

Fig. 3.2a and Fig. 3.2b illustrate the effect of reflection, transmission, and scattering from a smooth and a rough surface for hard as well as soft seafloor interface. Low interface roughness produces relatively larger specular component and smaller scattered component around the specular direction. In such cases, the seafloor appears as acoustically smooth surface (Fig. 3.2a). Similarly, high interface roughness reduces the specular component and increases the scattered component in all directions. For such cases, the seafloor appears as an acoustically rough surface (Fig. 3.2b). Acoustic roughness of seafloor is essentially a measure of the variability in acoustic impedance (of the interface). However, the physical roughness of seafloor mainly depends on the

surface topography. Therefore, the acoustic roughness of seafloor may not always be identical with the physical roughness (Holliday, 2007).

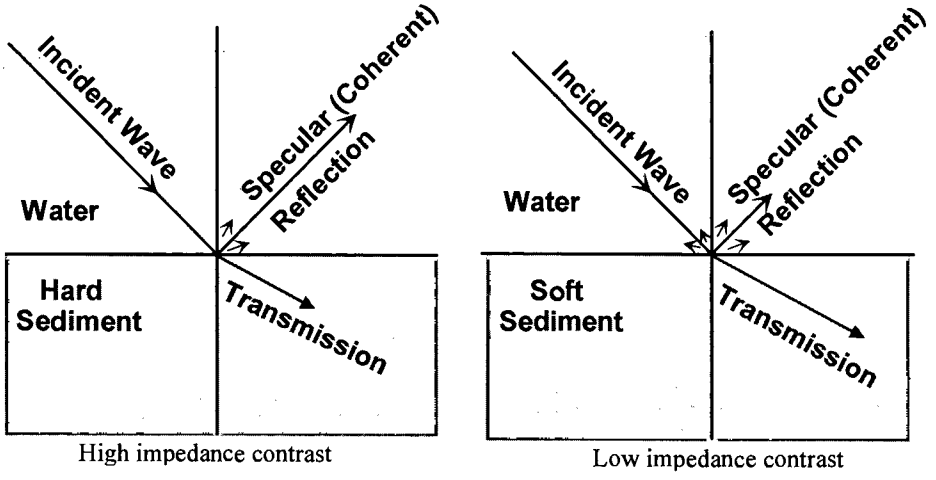

Fig. 3.2a Scattering from a smooth and flat seafloor

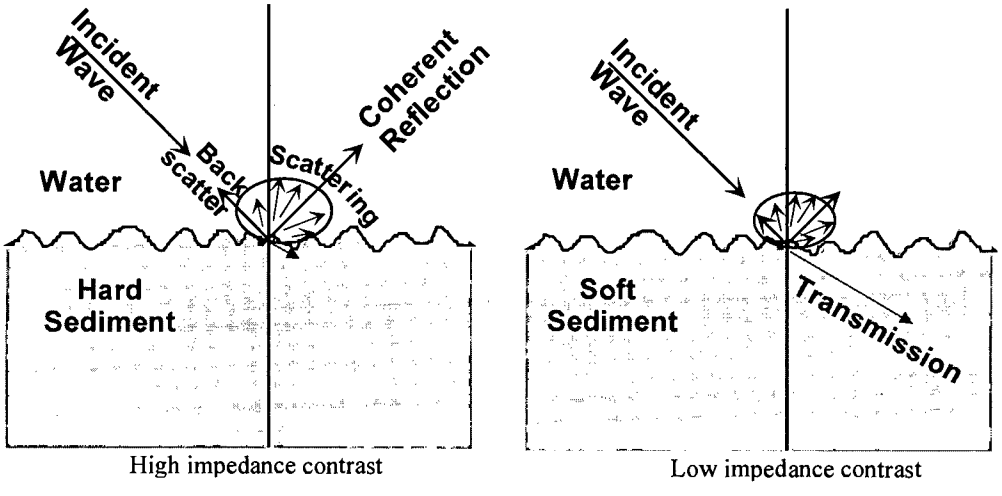

Fig. 3.2b Scattering from a rough seafloor

The micro-scale roughness of seafloor depends on several aspects such as sedimentary compositions, ripples on the seafloor (due to tide and current), and the presence of gas as well as living bio-organisms. The amplitude of micro-scale roughness

ranges between a millimeter and few meters depending on the frequency of operation of a sonar. Several micro-scale roughness scales corresponding to different physical processes may coexist on the seafloor. Seafloor interface roughness is quantified by a parameter called Rayleigh Parameter. The Rayleigh parameter is expressed as $P = 2k_a h \cos\theta_i$, where $k_a = 2\pi/\lambda$ is the acoustic wave number, θ_i is the angle of incidence, h is the root-mean square relief of the rough surface from its mean value, and λ is the acoustic wavelength. For $P << 1$, the roughness of the surface is small and most of the sound energy propagates in a specular direction as a coherent wave. Whereas $P >> 1$ corresponds to large roughness, which causes considerable amount of energy to scatter (Brekhovskikh and Lysanov, 2003).

3.1.3 Interaction of Acoustic Waves with Seafloor

Interaction of acoustic waves with the seafloor mainly depends on the frequency. At high frequency, interaction is limited within surficial sediments due to less penetration. The complications in scattering processes at high frequencies arise due to the seafloor interface irregularities as well as the nature of sediments (Lurton, 2002). A significant part of the incident energy penetrates in seafloor sediments at low frequencies. The characteristics of seafloor sediments play a major role as compared to the interface relief irregularities, at these low frequencies. Thus, reflection and refraction at various interface layers within the sediment volume are very significant at low frequencies. Moreover, the presence of bio-organisms in the seafloor sediments and their effects on the scattering processes complicates the situation further (Holliay,

2007). Therefore, the interpretation of echo obtained from the scattering of acoustic energy from the seafloor sediments is a challenging task.

3.1.4 Transmission Losses

Transmission loss quantitatively describes the weakening of acoustic energy between a point 1m from the source and a point at a distance in the sea. Transmission loss is considered as the sum of a loss due to geometrical spreading and a loss due to the attenuation (Urick, 1983).

Acoustic energy spreads in all directions from a source during the propagation (Fig. 3.3). The decrease in acoustic intensity is inversely proportional to the surface area of a sphere. This phenomenon is called geometric spreading loss (Lurton, 2002). Since intensity decreases inversely with the square of the radius of a sphere, the decrease in acoustic intensity between points 1 and 2 (in Fig. 3.3) can be written as,

$$\frac{I_2}{I_1} = \left(\frac{4\pi R_1^2}{4\pi R_2^2}\right) = \left(\frac{R_1}{R_2}\right)^2 \tag{3.6}$$

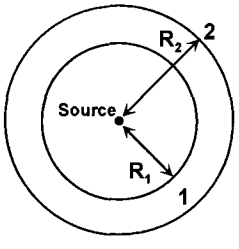

Fig. 3.3 Acoustic intensity decreases inversely with the surface area of a sphere

Here R_1 and R_2 are the radial distances from the source located at the center of a sphere. The transmission loss (TL in dB) due to spreading at a distance R is expressed as (with reference to unit distance)

$$TL = 20\log_{10} R \tag{3.7}$$

In addition, there is another type of loss, called attenuation loss in water medium. Since seawater is a dissipative propagation medium, part of the acoustic energy is absorbed due to various chemical processes (Medwin and Clay, 1998). The amount of loss depends on the characteristics of a propagation medium and the frequency of operation. The model developed by Francois and Garrison (1982a, 1982b) is the most widely used attenuation model, which uses temperature, salinity, hydrostatic pressure, and acoustic frequency as inputs. This model has three terms corresponding to the contributions of boric acid, magnesium sulphate, and pure water. The attenuation, α_w in dB/km is given by,

$$\alpha_w = \underbrace{A_1 P_1 \frac{f_1 f^2}{f_1^2 + f^2}}_{B(OH)_3\ Contribution} + \underbrace{A_2 P_2 \frac{f_2 f^2}{f_2^2 + f^2}}_{MgSO_4\ Contribution} + \underbrace{A_3 P_3 f^2}_{Pure\ Water\ Viscosity} \tag{3.8}$$

The parameters for Boric acid contribution are:

$$\begin{aligned} A_1 &= \frac{8.86}{v_w} 10^{(0.78pH-5)}, \quad dBkm^{-1}kHz^{-1} \\ P_1 &= 1, \\ f_1 &= 2.8\sqrt{\frac{S}{35}} 10^{\left(4-\frac{1234}{T_s+273}\right)}, \quad kHz \\ v_w &= 1412 + 3.12T_s + 1.19S + 0.0167H, \quad m/s \end{aligned} \tag{3.9}$$

where H is the water depth in meters; S is the salinity in practical salinity units; T_s is the temperature of seawater in °C; pH is the pH value of seawater, f is the frequency in kHz; and v_w is the sound speed in m/s. The parameters for magnesium sulphate contribution are (Francois and Garrison, 1982a, 1982b):

$$A_2 = 21.44\frac{S}{v_w}(1+0.025T_s),\ \ dBkm^{-1}kHz^{-1}$$
$$P_2 = 1-1.37x10^{-4}H+6.2x10^{-9}H^2, \tag{3.10}$$
$$f_2 = \frac{8.17x10^{\left(8-\frac{1990}{T_s+273}\right)}}{1+0.0018(S-35)},\ \ kHz$$

The parameters for pure water viscosity are:

$$P_3 = 1-3.83x10^{-5}H+4.9x10^{-10}H^2,$$
$$A_3 = 4.937x10^{-4}-2.59x10^{-5}T_s+9.11x10^{-7}T_s^2-1.5x10^{-8}T_s^3,$$
$$for\ \ T_s < 20^oC,\ \ dBkm^{-1}kHz^{-2} \tag{3.11}$$
$$A_3 = 3.964x10^{-4}-1.146x10^{-5}T_s+1.45x10^{-7}T_s^2-6.5x10^{-10}T_s^3,$$
$$for\ \ T_s > 20^oC,\ \ dBkm^{-1}kHz^{-2}$$

The equation (3.8) shows that the total attenuation increases rapidly with the frequency. The total transmission loss (in dB) is expressed as (Lurton, 2002; Urick, 1983),

$$2TL = 2(20\log_{10}R+\alpha_w R) \tag{3.12}$$

The factor two in equation (3.12) is multiplied to account the losses for outgoing and return signals. Here the range R is expressed in meters and the attenuation α_w is expressed in dB/km. Therefore, the unit of either R or α_w has to be converted appropriately for the calculation of TL.

3.1.5 Echo Formation

The insonified area on seafloor (by an incident acoustic energy) changes gradually with time. The formation of echo from a flat water-sediment interface has few distinct phases. A description on the formation of echo is given in this section with an

assumption that the seafloor surface is horizontal, smooth, and the echo sounder beam has a conical directivity pattern (Lurton, 2002; Burczynski, 1999; Kloser, 2007).

The major distinct phases in the formation of echo (Fig. 3.4) are as follows:

(a) At initial instant $t_0 = 2H / v_w$, the insonified area is just a point and it is called an impact point.

(b) As time (t) increases, the impact point becomes a disc. The radius $r(t)$ of the disc increases with time and the instantaneous radius at time t is expressed as $r(t) \approx \sqrt{Hv_w(t-t_0)} = \sqrt{Hv_w\tau}$, where $\tau = t - t_0$. Therefore, the active area (A) increases linearly with time and is expressed as $A \cong \pi Hv_w\tau$.

(c) At time $\tau = \tau_p$ (τ_p is the pulse duration), the insonified area does not increase with time (i.e., growth of the disc stops) and the maximum area of insonification at this time is $\pi Hv_w\tau_p$. The duration from the beginning of the pulse emission to pulse duration (τ_p) of the signal is called attacking phase. In this phase, the peak amplitude of the return signal mainly depends on the impedance contrast at the water-sediment interface.

(d) At time beyond the pulse duration ($\tau > \tau_p$), the insonified area takes a shape of annular form and the signal footprint becomes a crown of the internal radius. The internal (r_{int}) and external (r_{ext}) radiuses are expressed as $r_{\text{int}}(\tau) \approx \sqrt{Hv_w\tau}$ and $r_{ext}(\tau) \approx \sqrt{Hv_w(\tau+\tau_p)}$ respectively. During this phase, the active area does not increase with time and remains constant at $\pi(r_{ext}^2 - r_{\text{int}}^2) \cong \pi Hv_w\tau_p$.

(e) As time further increases, the (annular form of) insonified area finally disappears when the crown grows out of the beam's footprint limits. The maximum possible

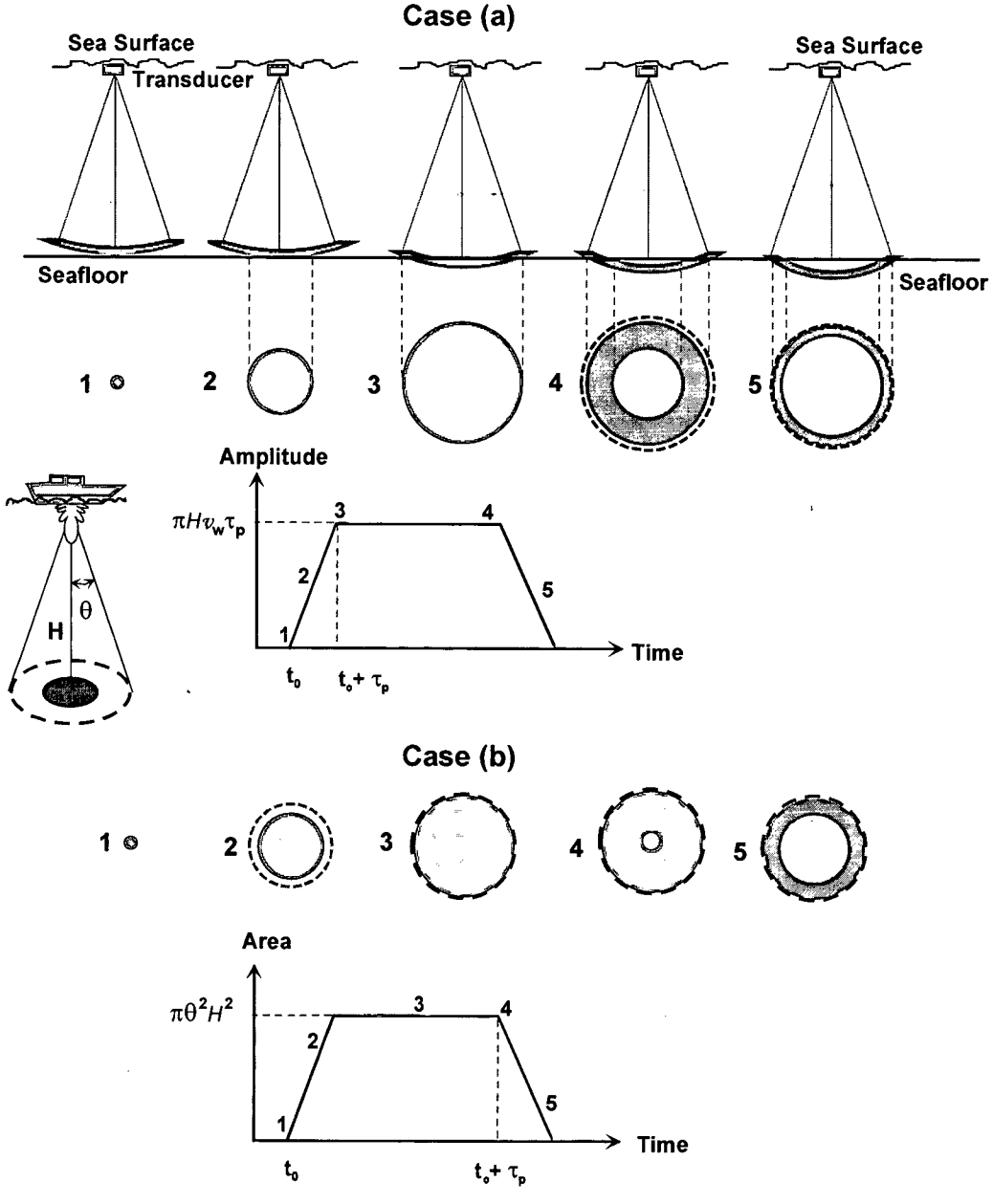

Fig. 3.4 Schematic diagram of echo formation: **Case (a)** with short pulse length, and **Case (b)** with long pulse length. The echo sounder beam width is θ, water depth below the transducer is H, v_w is the sound speed in water, t_0 is the starting time, and τ_p is the signal duration (Lurton, 2002; Kloser, 2007).

radius, r_{max} (depends on the beam width θ of an echo sounder) is given by $r_{max} = \theta H$. During this period, the insonified area decreases and is given by $\pi(r_{max}^2 - r_{int}^2) = \pi(\theta^2 H^2 - H v_w \tau_p)$.

Two types of echo formations are possible based on the beam width and the pulse duration of an echo sounder. If the beam width is sufficiently wide for the footprint to reach its full extent, then the maximum area of the footprint is limited by the pulse duration. This is called pulse-limited (or short pulse) regime. Again, if the pulse length is sufficiently long, then the maximum limit of the beam footprint reaches before $\tau = \tau_p$ and this is called beam-limited (or long pulse) regime. At this moment, the full beam footprint may be simultaneously insonified for a conical beam and the maximum backscattering area reaches to $\psi_s H^2 = \pi\theta^2 H^2$ (where ψ_s is the equivalent solid angle of the directivity pattern). This long-pulse regime happens at short ranges (less depth) and the transition range (between short and long pulse regimes) is roughly given by $\psi_s H^2 \approx \pi H v_w \tau_p$ (or $H \approx \pi v_w \tau_p / \psi_s$). Long signal is required to insonify a target completely at a given time. On the contrary, the short signals are required to differentiate two closely spaced targets. For a narrow beam and moderate depth, the illuminated volume increases linearly with time till the whole pulse penetrates within the sediment volume (Lurton, 2002).

The duration of acoustic signal transmitted from an echo sounder strongly influences the shape and the peak amplitude of the received signal. At any instant of time, the amplitude of returned signal depends on the instantaneous insonified area (by the signal), backscatter strength, and beam directivity pattern. The backscatter strength has a maximum value in the vicinity of normal-incidence and decreases (significant

decrease occurs especially for soft sediments) as the incidence angle increases. As time increases (i.e., as the incident angle increases), the backscatter strength as well as the directivity pattern decreases while the footprint size increases. Therefore, the amplitude of an echo envelope first increases to a maximum value and then starts decreasing due to the combined effect of backscatter strength, directivity pattern, and footprint size (Lurton, 2002). The trailing edge of the echo envelope depends on the seafloor backscatter strength at oblique incidence (due to the side lobes of the directivity pattern).

3.2 MODELS FOR CHARACTERIZATION OF SEAFLOOR

It is mentioned earlier that characterization of seafloor is a process to differentiate or to recognize different regions based on physical, chemical, geological, and biological characteristics of the sediments. This is possible by measuring the properties of seafloor sediments directly in a field or in a laboratory. However, the more cost effective and rapid method is the remote acoustic characterization using backscatter models.

A number of acoustic models have been developed to describe the interaction of acoustic waves with seafloor sediments. Initially, simple mathematical models were developed from a very limited measurement of field data. One such simple model is to distinguish sediment types from the reflectivity measurements (Srinivasan et al., 1982). If the acoustic reflection from seafloor at normal-incidence is correlated with the ground-truth, it is possible to differentiate sediment types based on the reflectivity. Such a simple model is not always sufficient to describe seafloor sediments. Reflectivity could be different (for the same sediment type) due to volume heterogeneity, slope of a

surface, presence of gas and bio-organisms etc. Thus, there is a need for systematic and quantitative approach to develop theoretical models, which include all the possible variability. Backscatter models generally estimate the surface scattering and the volume scattering coefficients as a function of frequency, angle of incidence, seafloor geo-acoustic parameters, surface roughness, and sediment volume in-homogeneities.

The advent of increased computational capabilities gave a thrust for the development of new and more realistic complex models to explain the acoustic scattering from seafloor. Predictions of backscatter echo characteristics from the physical processes of seafloor scattering are generally called forward problems. Whereas, the quantitative estimation of seafloor characteristics based on the information embedded in the scattered echo is called inverse problem (Holliday, 2007). For an inverse problem, the first step is to decide a forward theoretical model, which describes or relates various physical processes of acoustic interaction with the seafloor sediments. Inversion approaches are commonly used for the estimation of seafloor characteristic parameters (Gott and Martinez, 1993; Sternlicht and de Moustier, 2003b; Chakraborty and De, 2008; Tolstoy, 2010; Ballard et al., 2010; Jiang et al., 2010).

Models for seafloor characterization are broadly grouped into two categories - empirical and theoretical. A concise review on the relevant acoustic models is presented in the following sections.

3.2.1 Empirical Models

Empirical models are the simplest models to describe the acoustic scattering from seafloor. These models attempt to correlate the backscatter strength to a general seafloor sediment descriptor such as particle size and type of sediment. McKinny and

Anderson (1964) collected scattering data from depths less than 61m in the frequency range 12.5 to 290 kHz at 16 coastal sites of the US. Their model dealt with the dependence of seafloor backscatter strength on acoustic frequency, sediment type, and grazing angle. However, this empirical model has limited validity outside the frequency range 12.5-290 kHz. Hamilton carried out extensive researches for formulating the empirical relationships between several seafloor properties (few of them are - Hamilton, 1971a, 1971b, 1972, 1980; Hamilton and Bachman, 1982). Though these relationships do not directly describe the mechanism of acoustic scattering from the seafloor, these are very useful for the development of theoretical models. Urick (1983) reported that there are large variances associated with the seafloor scattering strengths obtained from different seafloor sediments in the frequency range 24-100 kHz and he reported that it is difficult to assign a single value of backscatter strength to a particular sediment type.

Since simple geological descriptions of sediments are insufficient to describe the scattering from a rough seafloor, the Lambert's rule is used to explain the backscatter strengths (Lurton, 2002; Holliday, 2007). According to the Lambert's rule (Lurton, 2002; Jackson and Richardson, 2007), the scattered intensity (I_s) from a small seafloor area (dA) is related to the incident intensity (I_0) at a grazing angle θ_g, and the scattering angle φ by (in analogy with optics, where angle of incidence is used instead of grazing angle),

$$I_s = \mu I_0 \sin\theta_g \sin\varphi \; dA \tag{3.13}$$

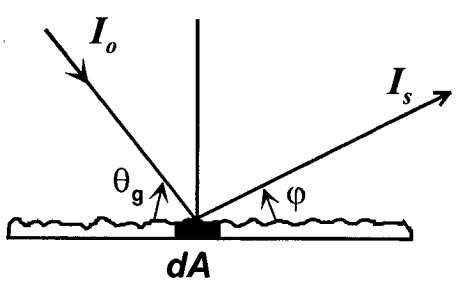

Fig. 3.5 Scattering geometry for Lambert's Rule

where μ is called Lambert's constant and is numerically equal to the backscatter strength at normal-incidence. For a perfectly reflective seafloor, the total incident energy redistributes into water medium (with a result $\mu = 1/\pi$) and the normal-incidence backscatter strength would be $10\log_{10}(1/\pi)$= -5 dB (Urick, 1983). At a grazing angle $\varphi = \pi - \theta_g$, the energy is backscattered towards the source and the total backscatter strength (in logarithmic form) is given by, $10\log_{10}\mu + 10\log_{10}(\sin^2\theta_g)$ (Urick, 1983). This is the simplest of all models to interpret the acoustic backscattering from seafloor. The Lambert's Law is frequency independent and it needs a single empirical coefficient called Lambert's constant. The value of μ depends on the sediment type. Mackenzie (1961) found that a value of $10\log_{10}\mu$ = -27dB is needed to fit well his observation at the frequencies 530 and 1030 Hz. Mackenzie (1961) proposed the generalized version of Lambert's rule (without any physical basis). This rule is often called as Lambert-Mackenzie rule and the backscatter strength is expressed as $\mu\sin^m\theta_g$, where the integer constant m varies within 1 and 2 depending on the sediment type (Mackenzie, 1961). Lambert's rule is valid for very rough surfaces i.e., it is valid for totally diffuse scattering, where the seafloor roughness is large compared to the acoustic wavelength. For specular scattering, the validity of the model is limited. For grazing angles exceeding 40^0, the observed backscatter strengths exhibit a strong rise with the increase in angle, which is in accordance with the perturbation theory but not with the Lambert's rule (Essen, 1994). However, at grazing angles below 45^0, Lambert's rule reasonably agrees with the field data for many deep-water seafloor sediments (Urick, 1983). Many researchers investigated the applicability of Lambert's rule by comparing the predictions (from the rule) with the experimental results

(McKinney and Anderson, 1964; Boehme and Chotiros, 1988; Stanic et al., 1988, 1989).

Roughness is another important descriptor of the seafloor. The roughness is expressed as the root mean square (rms) amplitude of seafloor topography. Seafloor roughness varies with the physical and the biological activities along with the type of sediments. Initially, many researchers investigated the scattering of acoustic energy from a rough seafloor (Eckart, 1953; Clay et al., 1973; Clay and Leong, 1974). Eckart (1953) first showed that spatial wave number spectrum is an important factor in the scattering of sound from a randomly rough surface. Stanton (1984, 1985) studied the correlation between statistical Rice probability distribution function from the echo envelopes and stochastic scattering from a rough seafloor. The analyses revealed that the shape of PDF obtained from the backscatter echo envelope could be estimated from the products of rms roughness amplitude and two orthogonal correlation lengths (Stanton 1984, 1985). The shape of PDF was also very sensitive to small changes in micro-topography or roughness. In addition, it was stated that the shape of PDF of an echo envelope could be estimated from the integral of the correlation function (even if the echo is obtained from an un-calibrated conventional echo sounder). Discrimination between seafloor sediments with same roughness but different properties is possible using the orthogonal correlation length and the roughness with this method (Chakraborty, 1989).

The disadvantages of empirical models are that these are not developed based on the physical processes of acoustic scattering from the seafloor. As mentioned earlier that the study on the scattering of acoustic energy from the seafloor has gained importance in the recent years because of its applications in several fields ranging from the target detection to the management of marine environment. Hence, physics-based theoretical

models are being developed to interpret the acoustic scattering from seafloor at different acoustic frequencies.

3.2.2 Theoretical Models

In a typical echo sounding system, the arrival time of the reflected echo provides a measure of seafloor depth. The characteristic shape and energy of the received signal are considerably different from the original pulse and this backscattered signal provides information on the seafloor roughness characteristics and the geo-acoustic properties of sediment. Seafloor scattering models, which use physics-based theory to describe the interaction of acoustic waves with sediments, are usually termed as theoretical models.

There are three broad categories of acoustic scattering: sea surface scattering, water column scattering, and seafloor scattering. Out of these three categories, only seafloor scattering is of main interest for the present study and relevant theoretical investigations on the seafloor scattering are reviewed in this section.

Scattering from the seafloor has two main components: (a) scattering from the interface between water and seafloor sediment, and (b) scattering from the sediment volume. Scattering from the interface mainly depends on the nature of roughness of seafloor coupled with the impedance contrast. The interface roughness can be large topographic features such as undersea ridges or small features such as sand ripples. On the other hand, buried rocks, shells, and boundaries of sediment layers with lateral variability are the primary sources for the sediment volume scattering.

Acoustic scattering from a rough surface are computed using two theoretical methods namely the Rayleigh-Rice method and the Kirchhoff method. The Rayleigh-Rice method is based on small perturbation approach. If rms relief is comparatively

smaller than that of the acoustic wavelength, the perturbations theory is applicable to the seafloor scattering (Thorsos and Jackson, 1989). Therefore, the rough surface can be treated as a perturbed smooth surface. If h_s is the rms relief of the small-scale surface, and k_a is the acoustic wave number then the condition for small-scale surface (the Rayleigh-Rice approximation) is expressed as (Jackson et al., 1986a),

$$2k_a h_s < 1 \tag{3.14}$$

The small-scale rms relief h_s in the Rayleigh-Rice criteria can be calculated (Jackson et al., 1986a) in terms of the relief spectrum $W(\mathbf{k})$ as,

$$h_s^2 = 2\pi \int_{k_c}^{\infty} W(\mathbf{k}) k dk = \frac{2\pi w_2 k_c^{2-\gamma_2}}{\gamma_2 - 2}, \tag{3.15}$$

where $\mathbf{k}$ is 2D spatial wave vector with magnitude k and k_c is the cutoff spatial wave number, which separates the band-limited power-law relief spectrum into large and small-scale roughness components. The parameter w_2 is called roughness spectrum strength and γ_2 is called roughness spectrum exponent (unit less parameter). The relief spectrum $W(\mathbf{k})$ is given by,

$$W(\mathbf{k}) = w_2 k^{-\gamma_2} \tag{3.16}$$

The parameter w_2 is expressed in units of length to the power $(4-\gamma_2)$. For a reference length h_0, the spectrum $W(\mathbf{k})$ is expressed as, $W(\mathbf{k}) = w_2 (h_0 k)^{-\gamma_2}$. This in turn gives the dimension of w_2 as h_0^4. For $h_0 = 1$ cm, w_2 is expressed in cm^4 (Sternlicht and de Moustier, 2003a).

The cutoff wave number k_c is expressed as,

$$k_c = \left(\frac{\gamma_2 - 2}{8\pi w_2 k_a^2 \cos^2 \theta_i} \right)^{1/(2-\gamma_2)} \tag{3.17}$$

where θ_i is the angle of incidence. Within this band-limited power law spectrum, the rms slope (s) of the large-scale surface is used to compute the transmission of acoustic energy into the sediment. This rms slope s is expressed as,

$$s^2 = 2\pi \int_0^{k_c} W(\mathbf{k}) k^3 dk = \frac{2\pi w_2 k_c^{4-\gamma_2}}{4-\gamma_2} \tag{3.18}$$

On the contrary, if the radii of curvature of a large-scale surface are comparable to or larger than the acoustic wavelengths, the Kirchhoff approximation is applicable (Jackson et al., 1986a; Thorsos, 1988; Chotiros, 1994). The large-scale surface must satisfy the Kirchhoff's criterion on the radius of curvature R_c and this criterion is expressed as (Jackson et al., 1986a),

$$\left(\frac{2}{k_a R_c \cos^3 \theta_i} \right) < 1, \tag{3.19}$$

where the mean-square radius of curvature is expressed as,

$$R_c^{-2} = 2\pi \int_0^{k_c} W(\mathbf{k}) k^5 dk = \frac{2\pi w_2 k_c^{6-\gamma_2}}{6-\gamma_2} \tag{3.20}$$

In reality, there exist many scales of the seafloor surface roughness. For these surfaces, both the perturbation (Rayleigh-Rice theory) and the Kirchhoff's theory are not valid. Therefore, a composite (two-scale) model that combines both the approximations in a single model is developed (Jackson et al., 1986a). However, composite model fails in a region, where multiple scattering and shadowing are important phenomena. As mentioned earlier, a significant amount of acoustic energy penetrates the sediment volume at low frequencies. The volume scattering can be dominant (compared to the interface scattering) for a soft sedimentary environment at low frequencies. Therefore, the modeling of seafloor backscatter is a very complicated process and more understanding on the scattering mechanisms are required to predict

the total backscatter strength through a model-based approach. To explain the mechanisms of scattering phenomena, several backscatter models are developed.

Ewing et al. (1957) first gave the expressions for reflection and transmission coefficients describing the amplitudes of compressional and shear waves that penetrate the seafloor. Many investigators studied the scattering of acoustic energy from smooth and soft sediments. Stockhausen (1963) derived an expression for calculating volumetric backscatter strength from the seafloor. The derivation of Stockhausen is based on two assumptions. First, the water-sediment interface is assumed as a flat surface. Second, a set of uniform solid spherical particles are embedded in a homogeneous sediment volume, which cause the acoustic energies to scatter. The small spheres are considered as uncorrelated point scatterers in the model. Stockhausen (1963) derived his expression using Morse's expression (Morse, 1948), which is valid for the scattering from spheres with diameters much smaller than the acoustic wavelength. At the same time, Nolle et al. (1963) developed a scattering model based on the mean value of scattering strength, where the scattering strength was randomly distributed around the mean value. In their model (Nolle et al., 1963), the scattering autocorrelation function was considered as decaying exponentially and the autocorrelation length was proportional to the particle size in the sediment volume. Nolle et al. (1963) also studied the acoustic scattering from a smooth sand surface in a laboratory and compared their model with the experimental data. The results indicated that the model was unable to explain the scattering mechanism fully at the sub-critical angles. During this time, Kuo (1964) derived a theoretical expression for the backscattering from a rough interface with an assumption that two homogeneous fluids were separated by an interface. Later, Crowther (1983) developed an acoustic scattering model by combining the Kuo's model (Kuo, 1964) for roughness scattering and the effects of volume inhomogeneities. Crowther's model (1983) also failed to explain the problems with the scattering at sub-

critical angles (penetration of sound into the seafloor for grazing angles below a 'critical angle'), when compared with the laboratory measured backscatter data by Nolle et al. (1963). Other researchers also investigated this aspect (Chotiros, 1989, 1995; Boyle and Chotiros, 1992, 1995b; Greenlaw et al., 2004). The classical theory suggests that sound cannot penetrate into the seafloor below a certain grazing angle, called 'critical angle', and all the acoustic energy would be reflected into the seawater. Since the penetration of acoustic energy below a sub-critical angle is difficult to explain with the classical theories, new theoretical models have been developing. These models are tested with the recent field experiments as well as with the laboratory measurements (Richardson et al., 2001; Thorsos et al., 2001; Briggs et al., 2002; Williams et al., 2002).

To study the dependency of backscatter data with the frequency, Ivakin and Lysanov (1981a) developed a statistical backscatter model using the Born approximation. The effect of interface was not taken into account as the model assumed that the changes in sound speed as well as density from seawater to sediments were negligible (i.e., water saturated). Later, Ivakin and Lysanov (1981b) revised their model to include the refraction at a randomly rough interface. Subsequently, Ivakin (1986) again extended his earlier model by taking into account the volume scattering from the stratified sediments. This model (Ivakin, 1986) incorporates the linear changes in sediment sound speed and density with the seafloor depth.

At the same time, Jackson et al. (1986a) proposed a composite approximation approach dealing with the scattering from interface roughness in the frequency range 10-100 kHz. Jackson et al. (1986a) used Stockhausen's formulation (Stockhausen, 1963) and the ideas of Ivakin and Lysanov (1981b) to take into account the contributions from the sediment volume. This approach assumed that there is no correlation between the scattering due to the interface roughness and the sediment volume inhomogeneities (Ivakin and Lysanov (1981a) used some correlation function).

Multiple scattering was not considered in Jackson's model (Jackson et al., 1986a). This model used one free parameter, called sediment volume scattering parameter (σ_2), to fit the model predicted data with the experimental data. The experiments indicated that the sediment volume scattering was comparatively more important than the interface scattering in soft sediments. For a rough sandy bottom, the interface scattering is relatively prominent. The geo-acoustic parameters, which are used in this model as inputs, are not always readily available in any experimental area. These input parameters could be obtained from direct measurements, however this is difficult. Due to these practical issues, subsequently, Mourad and Jackson (1989) generalized the model (of Jackson et al., 1986a) using the empirical relationships (Hamilton, 1972) for estimating the geo-acoustic parameters of the surficial sediments based on the mean grain size. However, this model did not take into account the gradients of sound speed and density in sediments.

Hines (1990) developed a backscatter model incorporating the fluctuations of sound speed and density in the seafloor sediment. This model (Hines, 1990) agrees well with various published data. Many other authors also investigated the effects of sound speed and density fluctuations (Yamamoto, 1995, 1996) as well as the density gradients in sediments (Lyons and Orsi, 1998) on the scattering of acoustic waves. Mourad and Jackson (1993) developed a low frequency (100-1000Hz) backscatter model incorporating the gradient of sound speed in sediments. The model was based on the assumption that the backscatter of acoustic energy is due to the presence of uncorrelated omni-directional discrete point scatterers in the sediment. Novarini and Caruthers (1998) also developed a simple backscatter model with an assumption that the scatterers inside the sediment volume are uniformly distributed. Lyons et al. (1994) extended the composite roughness model (developed by Jackson et al., 1986a) by incorporating the

compressibility and density variations in the sediments. The anisotropy in sediment volume was modeled with the different correlation lengths in horizontal as well as in vertical planes. The volume backscattering cross section was modeled using the Born approximation (which was a free parameter in the model by Jackson et al., 1986a). The authors (Lyons et al., 1994) showed that the comparison between model and data (observation) was satisfactory. Moreover, Jackson and Briggs (1992) investigated the relative importance of the water-sediment interface roughness and the volume scattering.

Tang and Frisk (1991, 1992, and 1995) discussed the scattering from half-space, where the sound speed is assumed as constant with a small random component. These models take into account the anisotropy of the scatterers. Holland and Neumann (1998) proposed a model dealing with the scattering from inhomogeneities within the sediment and the sub-bottom layers. They demonstrated the success of their model against the measured data, particularly at low grazing angles. Several other approaches have also been developed to address the acoustic scattering from rough and corrugated surfaces (Biot, 1957, 1968; Tolstoy, 1982).

Another important field of research is related to the acoustic scattering due to the presence of gas in sediments. As the presence of gas bubbles significantly alters the physical properties of sediments, acoustic models are being developed to predict the scattering of acoustic energy from gassy sediments (Anderson and Hampton 1980a, 1980b; Boyle and Chotiros, 1995a, 1995b; Richardson and Davis, 1998; Fonseca et al., 2002). Though the present studies do not aim to address another important aspect related to the acoustic scattering due to biological activities in sediments, it is mentioned here for completeness of review. The acoustic scattering due to the biological activities (Smith et al., 2001; Reid, 2007 and the references therein) as well as the models for

detection and mapping of benthic, epibenthic flora and fauna (Stanton et al., 2000; Stanton and Chu, 2004; Orlowski, 2007) are being extensively investigated.

All the acoustic models discussed in the above paragraphs are not directly used for comparing the backscatter echo waveforms obtained from the field experiments. Sternlicht and de Moustier (1997, 2003a) developed a physics-based temporal backscatter model for a finite duration of signal. This temporal backscatter model generates an echo waveform for a given sediment properties. Sternlicht and de Moustier (2003a) implemented the Helmholtz diffraction integral and the Kirchhoff approximation to model the interface scattering component using mean grain size of sediment, coherent reflection coefficient, and roughness spectrum parameters. The sediment volume scattering component utilizes the composite roughness approach (with a modification of the approach proposed by Jackson et al., 1986a) for a finite duration of the transmitted signal. This model computes the acoustic backscattering from the water-sediment interface as well as from the sediment volume independently, and finally sums up to compute the total backscatter intensity. This model was also validated (Sternlicht and de Moustier, 2003b) using the backscatter echo data collected at 33 and 93 kHz over three sites in San Diego Bay, USA.

After a concise review on the relevant acoustic models applicable for interpreting the backscatter data, the next chapter describes the procedure for estimating the seafloor sediment parameters using a temporal backscatter model (Sternlicht and de Moustier, 2003a, 2003b) mentioned above and the comparison of results with the ground-truth.

Chapter 4

Model-Based Estimation of Seafloor Sediment Parameters

4.1 INTRODUCTION

Estimations of seafloor sediment parameters by acoustic methods are usually obtained from the comparisons of theoretical prediction and field measurements. A number of investigations (with different acoustic instrumentation) have been carried out to characterize seafloor sediments utilizing different theoretical models (Schock et al., 1989; LeBlanc et al., 1992; de Moustier and Matsumoto, 1993; Michalopoulou et al., 1994; Michalopoulou and Alexandrou, 1996; Sternlicht and de Moustier, 2003b; Schock, 2004a, 2004b; Chakraborty and De, 2008; Jiang et al., 2010). Validations of theoretical models over different experimental area are essential for the efficient use of these models in real scenario. In this study, the applicability of a physics-based temporal backscatter model (developed by Sternlicht and de Moustier, 2003a) is investigated to estimate the seafloor sediment parameters at two conventional frequencies (33 and 210 kHz) of a single-beam echo sounder through inversions.

In general, the use of multiple acoustic frequencies increases the ability to characterize the seafloor sediment because the roughness spectrum and the volume backscattering strength may vary with acoustic frequency (van Walree et al., 2006;

Anderson et al., 2008; Korneliussen et al., 2008; Cuff et al., 2009). Lower acoustic frequencies penetrate the seafloor to greater depths, whereas higher frequencies have greater resolving capability. Therefore, it is expected that two or more frequencies of a single-beam echo sounder will improve the understanding of acoustic backscatter from different seafloor sediments. In this study, a single set of seafloor sediment parameters is estimated through the inversion using a pair of echo envelopes (obtained with two conventional frequencies of the echo sounder at a particular site) jointly. This inversion process is referred here as combined two-frequency inversion approach. The applicability of this combined two-frequency inversion approach is also discussed here.

4.2 TEMPORAL BACKSCATTER MODEL

The temporal backscatter model developed by Sternlicht and de Moustier (2003a) is described in this section.

4.2.1 Mathematical Background

Utilizing the approaches of Jackson et al. (1986a) and de Moustier and Alexandrou (1991), the total backscatter intensity $I(t)$ is modeled by summing the intensity of backscatter, $I_i(t)$ from the water-sediment interface and the intensity of backscatter, $I_v(t)$ from the sediment volume. Therefore, $I(t)$ is expressed as,

$$I(t) = I_i(t) + I_v(t) \tag{4.1}$$

The model incorporates various environmental factors such as spherical spreading and absorption losses in the water column; acoustic energies scattered from the water-

sediment interface and inhomogeneities in the sediment volume. The transducer characteristics and the geometry of an echo sounder such as transducer beam pattern, altitude, tilt angle, and characteristics of the transmitted signal are also incorporated in this model. The model considers the case of a normal-incidence echo sounder with mono-static transducer (where transmitter and receiver are located at the same place) emitting acoustic pulses with pulse duration τ_p and intensity $I_x(t)$, $0 \le t \le \tau_p$. As the normal-incidence acoustic backscatter is only considered in this model, the effects of shadowing and multiple scattering are neglected (Sternlicht and de Moustier, 2003a). In this temporal backscatter model, single scattering phenomenon is assumed. The acoustic energy propagates as a spherical shell with a sound speed v_w. This shell initially interacts with the seafloor in the form of a disk and then gradually changes to an annular ring (as explained in Chapter 3). The length of the pulse in water is $\tau_p v_w$. The schematic diagram of the seafloor at a certain time $t > H/v_w + \tau_p$ is shown in Fig. 4.1, where H is the altitude of the transducer from the seafloor. The leading and the trailing edge of the pulse have angles θ_2 and θ_1 respectively with the normal at any instant t. In Fig. 4.1, θ_i represents the angle of incidence and ψ represents the azimuthal angle. The transducer starts receiving backscattered signal from the seafloor at a time $t_{bd} = 2H/v_w$. The quantity t_{bd} is called the time of bottom detect (as discussed in Chapter 2).

At an instant t, the acoustic intensity $I_i(t)$ backscattered from the seafloor interface and received at the transducer over the angular sectors $\theta_1 \le \theta_i \le \theta_2$ and $0 \le \psi < 2\pi$ (in Fig. 4.1) is given by (Sternlicht and de Moustier, 2003a),

$$I_i(t) = \int_{\psi=0}^{2\pi} \int_{\theta_i=\theta_1(t)}^{\theta_2(t)} I_x\left(t - \frac{2R}{v_w}\right) \frac{S_i(\theta_i) b^4(\theta_i, \psi)}{R^4 10^{\alpha_w R/5}} dA, \tag{4.2}$$

$$\text{where } \theta_1 = \begin{cases} \cos^{-1}\left(\dfrac{2H}{v_w(t-\tau_p)}\right), & (t-\tau_p) \geq t_{bd} \\ 0, & (t-\tau_p) < t_{bd} \end{cases}$$

$$\theta_2 = \begin{cases} \cos^{-1}\left(\dfrac{2H}{v_w t}\right), & t \geq t_{bd} \\ 0, & t < t_{bd} \end{cases} \tag{4.3}$$

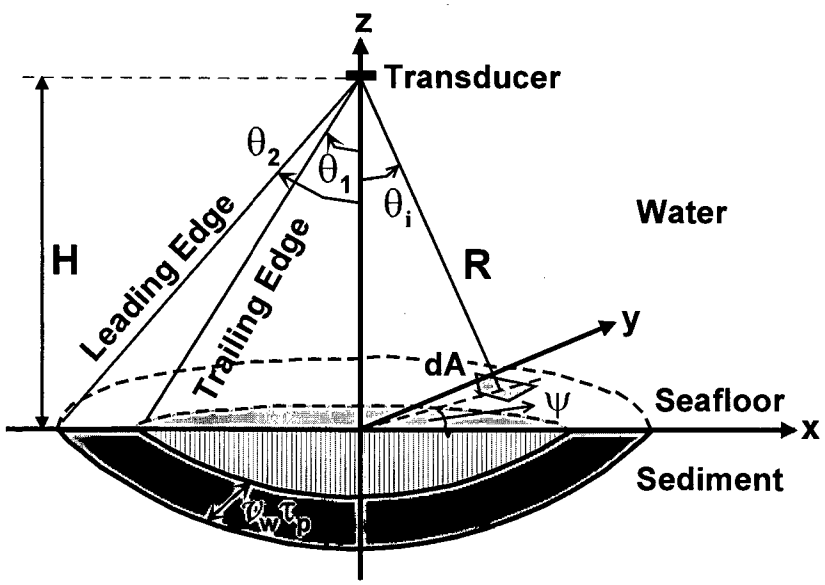

Fig. 4.1 Schematic diagram of the insonified area on seafloor surface and sediment volume to model a temporal echo envelope (Sternlicht and de Moustier, 2003a)

The elemental area dA is given by $dA = R^2 \sin(\theta_i) d\theta_i d\psi$, where $R = H/\cos(\theta_i)$ is the range, α_w is the frequency dependent absorption coefficient in water, and $b(\theta_i, \psi)$ is the transducer beam pattern. For a perfectly rectangular pulse, the quantity $I_x(t - 2R/v_w)$ is considered as constant (I_x). The parameter $S_i(\theta_i)$ is called seafloor interface

backscattering coefficient. This interface scattering coefficient $S_i(\theta_i)$ is calculated from the Kirchhoff's approximation with a power-law spectrum and is given by (Jackson et al., 1986a),

$$S_i(\theta_i) = \begin{cases} \Re_\perp^2 [8\pi \cos^2(\theta_i)\sin^2(\theta_i)]^{-1} \int_0^\infty \exp(-qu^{2\alpha}) J_0(u) u du, & \theta_i > 0 \\ \Re_\perp^2 [8\pi\alpha]^{-1} C_h^{-2/\alpha} (2k_a^2)^{(\alpha-1)/\alpha} \Gamma(\frac{1}{\alpha}), & \theta_i = 0 \end{cases} \tag{4.4}$$

$$\text{with } q = \cos^2(\theta_i)\sin^{-2\alpha}(\theta_i) C_h^2 2^{1-2\alpha} k_a^{2(1-\alpha)} \tag{4.5}$$

where J_0 is the zeroth-order Bessel function of the first kind, C_h is the structure constant, k_a is the acoustic wave number, $\Re_\perp$ is the normal-incidence ($\theta_i = 0^0$) reflection coefficient (i.e., $\Re_\perp = \Re(0)$), and $\alpha = (\gamma_2 / 2) - 1$. The value of structure constant (C_h) depends on the seafloor roughness spectrum parameters namely spectrum strength (w_2) and spectrum exponent (γ_2). The reflection coefficient $\Re(\theta_i)$ at an incidence angle θ_i is assumed as a constant at each point on the interface (between two acoustic half-spaces) and is expressed as (from equation (3.1) and (3.2)),

$$\Re(\theta_i) = \frac{\rho\nu\cos(\theta_i) - [1 - (\nu\sin(\theta_i))^2]^{1/2}}{\rho\nu\cos(\theta_i) + [1 - (\nu\sin(\theta_i))^2]^{1/2}} \tag{4.6}$$

where ρ is the density ratio (the ratio of the bulk density of sediment to the density of water) and ν is the sound speed ratio (the ratio of the speed of sound in sediment to the speed of sound in water).

The statistics governing sub-bottom inhomogeneities are assumed as isotropic and homogeneous in the model (Sternlicht and de Moustier, 2003a). Furthermore, the model assumed single scattering phenomenon. This indicates that the sediment volume scattering coefficient (σ_v) is constant and is expressed as (Jackson et al., 1986a),

$$\sigma_v = \sigma_2 \alpha_s \tag{4.7}$$

where the term σ_2 is called the sediment volume scattering parameter; the term α_s is called the attenuation coefficient in sediment and is expressed in dB/m. The attenuation coefficient α_s is assumed as proportional to the first power of frequency (based on the observations of Hamilton, 1972) and is expressed as,

$$\alpha_s = \kappa_p f \tag{4.8}$$

where κ_p is an attenuation constant in sediments and is expressed in dB/m/kHz, and f is the acoustic frequency in kHz. The regression equations relating κ_p and the mean grain size (M_ϕ) of sediments (Hamilton, 1972) are utilized to estimate the value of κ_p from the value of M_ϕ.

As discussed in Chapter 3, Jackson et al. (1986a) proposed a composite scale roughness model utilizing the ideas of Ivakin and Lysanov (1981b) and Stockhausen (1963) formulations. Later, Sternlicht and de Moustier (2003a) modified the composite roughness approach of Jackson et al. (1986a) to take into account a finite duration of the transmitted signal for computing the intensity of sediment volume backscatter. This sediment volume backscatter model is discussed in the following paragraphs.

The total sediment volume backscattering $I_v(t)$ is considered as a sum of all the contributions from the volume tubes of elemental cross section dA at the receiver (Sternlicht and de Moustier, 2003a). In the angular intervals $0 \le \theta_i \le \theta_2$, and $0 \le \psi < 2\pi$, the term $I_v(t)$ can be expressed as,

$$I_v(t) = \int_{\psi=0}^{2\pi} \int_{\theta_i=0}^{\theta_2(t)} \frac{\sigma_2 \alpha_s b^4(\theta_i, \psi)}{R^4 10^{\alpha_w R/5}} V_l(\theta_i) \left\{ \int_{l_1(t)}^{l_2(t)} I_x \left(\tau_p - \frac{l - l_1(t)}{v_b} \right) e^{-2\beta_e l} dl \right\} dA, \tag{4.9}$$

Here β_e is the round-trip attenuation between the scattering center and the water-sediment interface and is called the exponential attenuation rate. At an instant $t > (R/v_w) + \tau_p$, a portion of the incident energy penetrates the sediment volume. The angle $\theta_2(t)$ is given in equation (4.3). The edges of the transmitted pulse have the propagation distances l_1 and l_2 with respect to the point of entry into the sediment and at an instant t, $l_1(t)$ and $l_2(t)$ are given by (Sternlicht and de Moustier, 2003a),

$$l_1(t) = \begin{cases} \left[\frac{t}{2} - \tau_p - \frac{R}{v_w}\right] v_b, & t \geq 2\left(\frac{R}{v_w} + \tau_p\right) \\ 0, & t < 2\left(\frac{R}{v_w} + \tau_p\right) \end{cases}, \tag{4.10}$$

$$\text{and} \quad l_2(t) = \begin{cases} \left[\frac{t}{2} - \frac{R}{v_w}\right] v_b, & t \geq 2R/v_w, \\ 0, & t < 2R/v_w, \end{cases} \tag{4.11}$$

The equation (4.9) is valid from normal-incidence to a critical angle. In addition, the spherical spreading within the elemental tubes is considered negligible. For a perfectly rectangular pulse, the intensity is a constant term and then the remaining expression inside the integral (of equation (4.9)) gives an attenuation length $L(t)$, which is expressed as,

$$L(t) \equiv \int_{l_1(t)}^{l_2(t)} e^{-2\beta_e l}\, dl = \frac{1}{2\beta_e}\left(e^{-2\beta_e l_1(t)} - e^{-2\beta_e l_2(t)}\right) \tag{4.12}$$

The term $V_l(\theta_i)$ in equation (4.9) accounts for the two-way transmission losses at the water-sediment interface with a large-scale roughness. This is computed from the distribution of incidence angles expected for a large-scale roughness. If the large-scale roughness has a local slope ϑ, then the angle of incidence with respect to the local

surface is $(\theta_i - \vartheta)$. If all the slopes are Gaussian distributed about a horizontal plane with small rms slopes ($s < 0.1$), then the transmission term for the large-scale interface roughness ($V_l(\theta_i)$) is the average of coherent reflection coefficients from the flat surfaces at each plane part of the slope on the rough surface (Sternlicht and de Moustier, 2003a). This term $V_l(\theta_i)$ is expressed as,

$$V_l(\theta_i) = \frac{1}{\sqrt{\pi}s} \int_{-(\pi/2-\theta_i)}^{\infty} V_f(\theta_i - \vartheta) \exp\left(-\frac{\vartheta^2}{s^2}\right) d\vartheta \tag{4.13}$$

Here, the term $V_f(\theta_i)$ is the angle-dependent two-way transmission through a flat water-sediment interface. $V_f(\theta_i)$ is expressed in terms of the plane-wave reflection coefficient $\Re(\theta_i)$ and the sound speed ratio (v) at the interface as (Stockhausen, 1963),

$$V_f(\theta_i) = [1 - \Re^2(\theta_i)]^2 \cos^2\theta_i \ [1 - (v\sin\theta_i)^2]^{-1/2} \tag{4.14}$$

The total intensity (using equation (4.1)) calculated from this temporal backscatter model is the average echo intensity envelope obtained for a normal-incidence, single-beam echo sounder. Here the interface scattering is modeled in two-dimension and the volume scattering is treated in three-dimension.

4.2.2 Geo-Acoustic Parameters

This temporal backscatter model requires few geo-acoustic parameters as inputs. In the absence of measured geo-acoustic parameters from the study area, these inputs are estimated in terms of the mean grain size (M_ϕ) (APL Handbook, 1994). These estimations provide approximate generic values of the geo-acoustic inputs. The

expressions for different geo-acoustic parameters and other input parameters in terms of M_ϕ are given in this section (APL Handbook, 1994).

(a) The density ratio (ρ) is defined as the ratio of mass density (ρ_b) of sediment to mass density (ρ_w) of water and is expressed in terms of M_ϕ as,

$$\begin{aligned}\rho &\equiv \frac{\rho_b}{\rho_w} \\ &= 0.007797M_\phi^2 - 0.17057M_\phi + 2.3139, && -1 \le M_\phi < 1 \\ &= -0.0165406M_\phi^3 + 0.2290201M_\phi^2 - 1.1069031M_\phi + 3.0455, && 1 \le M_\phi < 5.3 \\ &= -0.0012973M_\phi + 1.1565, && 5.3 \le M_\phi \le 9\end{aligned} \tag{4.15}$$

(b) The sound speed ratio (v) is the ratio of speed of sound in sediment (v_b) to speed of sound in water (v_w) and is expressed in terms of M_ϕ as,

$$\begin{aligned}v &\equiv \frac{v_b}{v_w} \\ &= 0.002709M_\phi^2 - 0.056452M_\phi + 1.2788, && -1 \le M_\phi < 1 \\ &= -0.0014881M_\phi^3 + 0.0213937M_\phi^2 - 0.1382798M_\phi + 1.3425, && 1 \le M_\phi < 5.3 \\ &= -0.0024324M_\phi + 1.0019, && 5.3 \le M_\phi \le 9\end{aligned} \tag{4.16}$$

(c) The strength of the seafloor relief spectrum (cm^4) at a wavelength of 1 cm^{-1} is called roughness spectrum strength (w_2) and is expressed in terms of M_ϕ as,

$$\begin{aligned}w_2 &= 0.00207\left(\frac{2.03846 - 0.26923M_\phi}{1.0 + 0.076923M_\phi}\right)^2, && -1 \le M_\phi < 5.0 \\ &= 0.0005175, && 5.0 \le M_\phi < 9.0\end{aligned} \tag{4.17}$$

(d) The sediment volume scattering parameter (σ_2) is defined as the ratio of the sediment volume scattering coefficient (σ_v) to the sediment attenuation coefficient (α_s) (equation (4.7)). The value of $\sigma_2 [= \sigma_v / \alpha_s]$ is assumed as 0.004 for the initial estimation of seafloor characteristics within a range of $-1 \le M_\phi \le 9$.

(e) The attenuation constant (κ_p) is the ratio of the attenuation coefficient in sediment to the frequency and is expressed as dB/m/kHz (equation (4.8)).

$$\begin{aligned}
\kappa_p &= 0.4556, && -1 \le M_\phi < 0 \\
&= 0.0245M_\phi + 0.4556, && 0 \le M_\phi < 2.6 \\
&= 0.1245M_\phi + 0.1978, && 2.6 \le M_\phi < 4.5 \\
&= 0.20098M_\phi^2 - 2.5228M_\phi + 8.0399, && 4.5 \le M_\phi < 6.0 \\
&= 0.0117M_\phi^2 - 0.2041M_\phi + 0.9431, && 6.0 \le M_\phi < 9.5 \\
&= 0.0601, && M_\phi \ge 9.5
\end{aligned} \tag{4.18}$$

4.3 SENSITIVITY ANALYSIS

The method for assessing the relative importance of various inputs to the output of a system is called sensitivity analysis. This is a very effective method to judge how "sensitive" a model is to the changes in the values of input parameters. The influences of the input parameters namely mean grain size (M_ϕ), roughness spectrum strength (w_2), roughness spectrum exponent (γ_2), sediment volume scattering parameter (σ_2), pulse duration (τ_p), and geo-acoustic parameters on modeled echo envelopes are discussed in this section.

4.3.1 Influence of Mean Grain Size

Mean grain size of sediment is related to the diameter of the grain size (d_g) in mm and the relationship is given by, $M_\phi = -\log_2 d_g$ (as discussed in Chapter 2). Fine-

grain sediments with high values of M_ϕ have less impedance contrasts (ρv) and hence, low backscatter strengths. Thus, an increase in the value of M_ϕ results in a decrease in the value of impedance contrast. A decrease in the impedance contrasts in turn decreases the peak amplitude of an echo envelope. On the contrary, a decrease in the value of M_ϕ means an increase in the impedance contrast with high backscatter strength. Also, the increase in impedance contrast indicates an increase in the peak amplitude of an echo envelope.

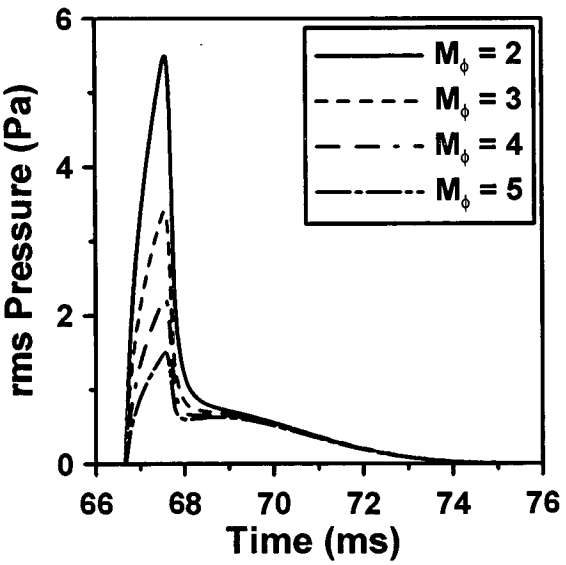

Fig. 4.2 Illustrating the effect of M_ϕ on modeled echo envelopes

The effect of M_ϕ on the total (interface and volume scattering component together) backscatter echo envelope is illustrated in Fig. 4.2 with simulated data. The simulation is carried out with the values of M_ϕ varying from 2ϕ to 5ϕ at 33 kHz. The other parameters such as altitude of the transducer from the seafloor (H = 50m), σ_2= 0.0015, γ_2= 3.25, w_2= 0.00112 cm^4, frequency (f = 33 kHz), and τ_p = 0.97 ms remain the same for all the cases in simulations. Fig. 4.2 shows that the echo peak amplitude

increases with the decrease in values of M_ϕ. In addition, the rise time of an echo envelope also decreases with the decrease in the values of M_ϕ.

4.3.2 Influence of Roughness Spectrum Parameters

Changes in the values of roughness spectrum strength as well as roughness spectrum exponent produce similar effect on the backscatter echo envelopes. A higher value of w_2 or γ_2 produces a less-steep slope in the response curves with the reduced amplitude of the seafloor echo. A decrease in the values of spectral exponent and spectral strength generates a sharp angular response near nadir. The response curves for this case are associated with a fast initial decay of the backscatter strength from normal to high incidence angles. The influence of w_2 on the total backscatter echo envelope is illustrated in Fig. 4.3.

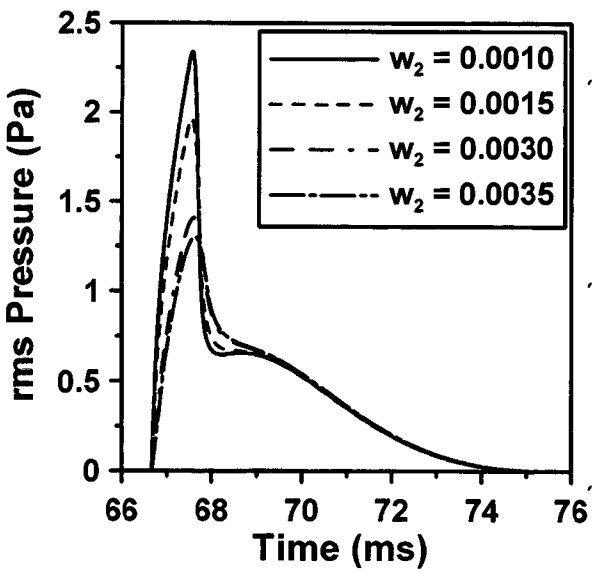

Fig. 4.3 Illustrating the influence of w_2 on modeled echo envelopes

The simulation is performed with the values of w_2 changing from 0.001 to 0.0035 cm^4 at 33 kHz. The other parameters such as H = 50m, M_ϕ= 4ϕ, σ_2= 0.0015, γ_2= 3.25, f= 33 kHz, and τ_p= 0.97 ms are kept unchanged for all the cases. Fig. 4.3 illustrates that the echo peak amplitude as well as the initial decay-time increases sharply with a decrease in the value of w_2. A change in the value of w_2 has significant effect on the interface component (of scattering) and marginal effect on the trail part (i.e., the sediment volume component of scattering) of the echo response curves.

Similarly the effect of γ_2 on a model output is illustrated in Fig. 4.4. The values of γ_2 vary from 3.0 to 3.4. Other input parameters such as H = 50m, M_ϕ= 4ϕ, σ_2= 0.0015, w_2 = 0.00112 cm^4, f= 33 kHz, and τ_p= 0.97 ms are kept unchanged for all the cases. Fig. 4.4 illustrates that the echo peak amplitude increases with a decrease in the value of γ_2.

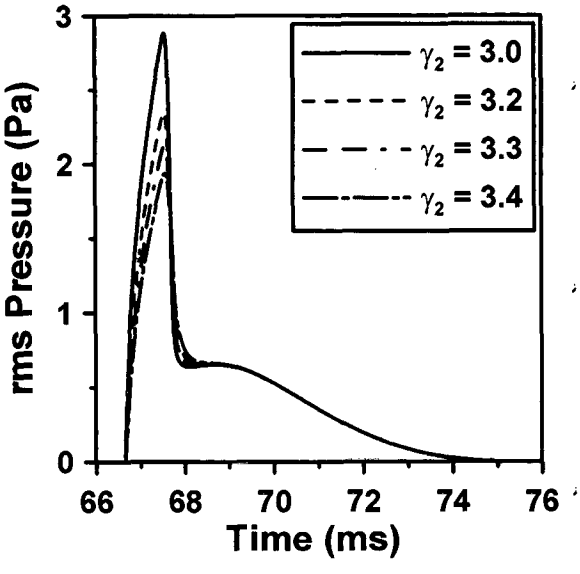

Fig. 4.4 Illustrating the effect of γ_2 on modeled echo envelopes

4.3.3 Influence of Sediment Volume Scattering Parameter

The sub-bottom scattering contribution is mainly controlled by the sediment volume scattering parameter (σ_2) or the sediment volume scattering coefficient (σ_v). The scattering from sediment volume generally affects the energy levels in the tail portion of the backscatter echo. The effect of σ_2 is illustrated in Fig. 4.5.

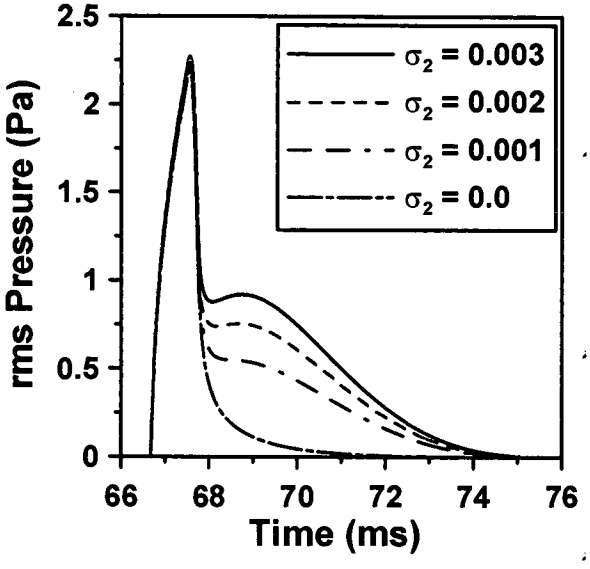

Fig. 4.5 Illustrating the effect of σ_2 on modeled echo envelopes

Here the value of σ_2 changes from 0 to 0.003. The other input parameters to the model such as $H = 50$m, $M_\phi = 4\phi$, $w_2 = 0.00112$ cm^4, $\gamma_2 = 3.25$, $f = 33$ kHz, and $\tau_p =$ 0.97 ms are kept unchanged for all the cases. Fig. 4.5 shows that the sediment volume component is completely absent for a case with $\sigma_2 = 0$. As σ_2 increases, the contribution of the sub-bottom scattering in the total echo envelope becomes prominent near the tail portion of the echo envelope. The peak amplitude of the total (interface plus volume scattering components) echo envelope changes marginally with an increase in

the value of σ_2. For soft sediments, penetration of the energy at low acoustic frequency increases significantly. Eventually, the sediment volume scattering component also increases in comparison with the interface scattering component for soft sediments.

4.3.4 Influence of Pulse Duration

The effect of pulse duration on a model output is illustrated in Fig. 4.6. The pulse duration is varied from 0.75 ms to 1.89 ms, while the values of other parameters are kept unchanged as H = 50m; $M_\phi = 4\phi$; w_2 = 0.00112 cm^4; γ_2 = 3.25; σ_2 = 0.0015; and f = 33 kHz.

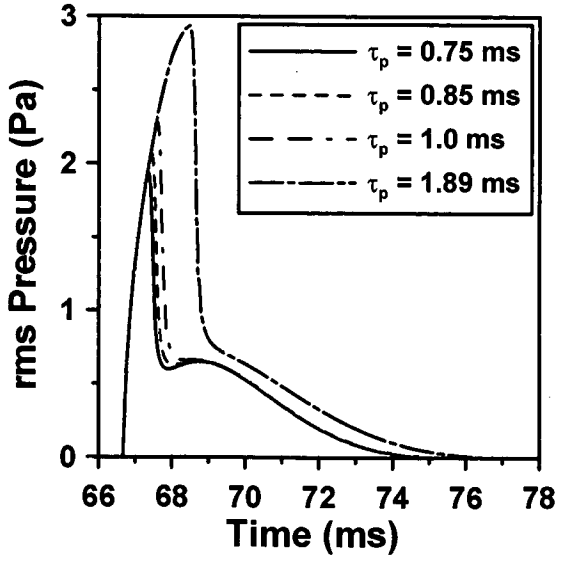

Fig. 4.6 Illustrating the effect of pulse duration on modeled echo envelope

Fig. 4.6 shows that the echo peak amplitude as well as the delay in rise time increases with the increase in pulse duration. The peak amplitude of the water-sediment interface component increases with the pulse duration. However, the peak amplitude remains the same even if the pulse duration is increased beyond a certain value (in this

case it is τ_p = 1.89 ms) (as explained in Chapter 3). Sediment volume component also increases with the increase in the value of pulse duration. However, the combined effect due to the interface and the volume scattering component on an echo envelope increases till the pulse duration reaches its limiting value. The shape of an echo envelope does not change beyond this limiting value of the pulse duration.

4.3.5 Influence of Geo-Acoustic Parameters

The temporal backscatter model also contains geo-acoustic parameters such as sound speed ratio, density ratio, and attenuation coefficient of sediment. Density ratio and sound speed ratio are used in the computation of reflection coefficient. The interface backscatter strength from the seafloor sediments is proportional to the reflection coefficient (equation (4.2) and (4.4)). Again, reflection coefficient depends on the impedance contrast between water and seafloor sediments. Though the relation between the reflection coefficient and the impedance contrast is non-linear (equation (4.6)), the interface backscatter strength usually increases with the increase in sound speed ratio and density ratio of sediments. Since coarse sediments have higher sound speed ratio as well as density ratio, the interface backscatter strength for coarser sediments is higher (i.e., higher peak of an echo envelope) than that of finer sediments (as shown in Fig. 4.2). However, some other factors such as presence of gas bubbles and biological organisms in sediments could influence the interface backscatter strength significantly.

The attenuation in sediments controls the penetration of acoustic energy in the sediment volume. As the attenuation increases, the penetration depth in the sediment

volume decreases. This in turn reduces the backscatter strength from the sediment volume. In addition, attenuation depends on the acoustic frequency. A higher acoustic frequency is more attenuated in sediments than a lower acoustic frequency. Hence, a higher acoustic frequency produces lower returns from the sediment volume.

4.4 ESTIMATION OF SEAFLOOR PARAMETERS

It is mentioned earlier that the temporal backscatter model developed by Sternlicht and de Moustier (2003a) is employed here for model-based characterization of seafloor sediments. The total backscatter intensity (measured at the transducer face) for a finite duration of transmitted signal is modeled by summing the intensities from the water-sediment interface and from the sediment volume inhomogeneities. This total backscatter intensity is a function of the sediment mean grain size (M_ϕ), roughness spectrum strength (w_2), roughness spectrum exponent (γ_2), and the sediment volume scattering parameter (σ_2) or the sediment volume scattering coefficient (σ_v). It is mentioned earlier that the computation of total backscatter intensity also takes into account various environmental factors such as spherical spreading, absorption losses in the water column, transducer characteristics, transmitting pulse duration, and the altitude of the transducer from the seafloor. In addition, various geoacoustic parameters (which are used in this model) are estimated from the sediment mean grain size using the published relationships (APL Handbook, 1994). Based upon the approach of Jackson et al. (1986a), the sedimcnt volume scattering parameter is assumed as a free parameter in this temporal backscatter model and is expressed as $\sigma_2 = \sigma_v / \alpha_s$, where α_s is the attenuation coefficient in sediment in dB/m (as mentioned earlier). Following

Hamilton (1972), the coefficient α_s is assumed as proportional to the first power of an acoustic frequency (equation (4.8)).

At first, the two-stage inversion approach using a one-dimensional search and a three-dimensional global optimization method (referred to as three-dimensional inversion scheme in this text), as implemented by Sternlicht and de Moustier (2003b), is described in section 4.4.1. In addition, the one-dimensional search technique and the simulated annealing with downhill simplex global optimization scheme are introduced. Subsequently, the two-stage inversion scheme using the one-dimensional search and a four-dimensional global optimization (here referred to as four-dimensional inversion approach) adopted in the study is discussed in section 4.4.4.

4.4.1 Three-Dimensional Inversion Scheme

As the solution from inversion of the acoustic backscatter model may not be unique, Sternlicht and de Moustier (2003b) proposed a well-constrained two-stage inversion approach to estimate the values of four sediment parameters (M_ϕ, w_2, σ_v, and γ_2) through an optimized echo matching method. To measure the match between the recorded field data and the model prediction, the signal-to-error (*S/E*) ratio is used as a merit function in this study (Sternlicht and de Moustier, 2003b). The *S/E* measures the energy discrepancy between the data and the model prediction. The inverse of *S/E* ratio (i.e., error-to-signal ratio, *E/S*) is used as the objective function in this study and is expressed as,

$$E/S = \sum_n (p_a[n] - p_m[n])^2 / \sum_n p_a^2[n] \tag{4.19}$$

where the terms $p_a[n]$ and $p_m[n]$ represent the rms pressure (in Pascal) sequences of the averaged echo (field observation) and the temporal modeled echo envelope respectively with n samples. The rms pressure sequence of the modeled echo intensity envelope (computed from the temporal model) is obtained using the equation (Sternlicht and de Moustier, 2003a),

$$p_m = \sqrt{\rho_w v_w I[n]} \tag{4.20}$$

where $I[n]$ is the intensity of the computed temporal echo envelope with n number of samples; ρ_w and v_w are the density and the speed of sound in seawater respectively. The voltage values of the measured echo envelope are also converted to pressure values for the calculation of *E/S*. The goal is to minimize the objective function *E/S* using a global optimization technique. Geo-acoustic parameters in the temporal backscatter model makes the process complicated due to the presence of numerous local minima in the search space. Therefore, a-priori knowledge is essential to constrain the solution space as well as to avoid unrealistic solutions.

In the first stage, a representative value of M_ϕ and the sediment type (fine- or coarse-grained sediment based on the value of M_ϕ) are first estimated from the echo envelope peak amplitude through a one-dimensional (1-D) iterative golden section search coupled with inverse parabolic interpolation. At every stage of iteration, the values of w_2 and other geo-acoustic parameters are estimated from the value of M_ϕ (using the relationships given in equations (4.15) to (4.18)). The value of γ_2 is set to 3.25 during this 1-D search, as this generic value of γ_2(= 3.25) (APL Handbook, 1994) falls within the overlapping regions of coarse and fine-grain sediments (as evident from various field measurements of Briggs, 1989 and Jackson and Briggs, 1992). In addition,

the sediment volume scattering parameter σ_2 is set to 0.004 and the value of σ_v is obtained by multiplying the attenuation coefficient (α_s) in sediments with σ_2 (equation (4.7)). Hence, the value of M_ϕ is only varied to get a match with the peak amplitude of echo envelope in the first stage, and all other parameters are either fixed or estimated using M_ϕ. A flow chart of this 1-D iterative search is shown later in Fig. 4.7a.

Based on the estimated sediment type, the value of γ_2 is fixed at either 3.3 (for fine-grain sediment with $M_\phi \geq 4\phi$) or 3.0 (for coarse-grain sediment with $M_\phi < 4\phi$) for the second stage of the inversion process. These specific values of γ_2 are chosen based on the observations from several other field experiments (Briggs, 1989; Jackson and Briggs, 1992) over different sedimentary environments. In the second stage, a three-dimensional (3-D) global optimization is performed to estimate the values of (M_ϕ, w_2, and σ_v) using simulated annealing and a downhill simplex algorithm (Sternlicht and de Moustier, 2003b). The mean grain size of sediment is varied within $M_\phi \pm 1.0\phi$ during the optimization process, where M_ϕ is the value of mean grain size obtained from the 1-D search. The search bounds $0.0002 \leq w_2 \leq 0.009$ are used for the estimation of w_2. The sediment volume scattering coefficient is assumed as non-negative values ($\sigma_v \geq 0$).

As normal-incidence, single-beam echo sounder backscatter data are used in the study, the interface scattering components are expected to have larger contributions than that of the volume scattering components. Occasionally, model-data match produces a very low value of E/S due to the unreasonably large contributions from sediment volume component in the total intensity of the temporal model. This unrealistically "very good" match does not represent a consistent solution in comparison with the

ground-truth data. Therefore, a penalty component is added to avoid such unrealistic solutions. The new objective function $f(p)$ after adding the penalty component is given by (Sternlicht and de Moustier, 2003b),

$$f(p) = [E/S].4[1 + 5((I_{v\max} / I_{i\max}) - 0.63)] \quad (4.21)$$

This equation states that if the maximum value of the volume intensity component ($I_{v\max}$) is more than 2dB of the maximum value of the interface intensity component ($I_{i\max}$), an empirical penalty component is added to the objective function *E/S* (when $(I_{v\max} / I_{i\max}) > 0.63$).

The 1-D golden section search algorithm coupled with inverse parabolic interpolation and the simulated annealing with downhill simplex scheme are introduced in the following sections for better understanding of the process.

4.4.2 One-Dimensional Search Algorithm

The roots of an analytical function $f(x)$ in 1-D could be obtained by bracketing the root in an interval (a,b) utilizing a bisection method (Press et al., 1992). A sequence of points is evaluated along a search direction to achieve this goal. The function is evaluated at an intermediate point x and a new bracketing interval, either (a,x) or (x,b) is obtained. The process continues till the bracketing interval is acceptably small. However, a root of the function is considered as bracketed within a pair of points a and b, when the function has the opposite signs at these two points. A minimum is bracketed only when there is a triplet of points, $a < b < c$ (or $c < b < a$), so that $f(b)$ is less than both $f(a)$ and $f(c)$. A new point x is to be chosen (with an analogy of bisection

method) either between a and b or between b and c. First the function $f(x)$ is evaluated at a point x and then tested against the value $f(b)$. If $f(b) < f(x)$, then a new bracketing triplet of points is obtained as (a,b,x). Otherwise if $f(b) > f(x)$, then the new bracketing triplet is (b, x, c). In all these cases, middle point of the new triplet forms the abscissa, and its ordinate is the best minimum achieved so far. The process of bracketing continues until a distance between the two outer points of the triplet is tolerably small. This tolerable limit is either the computer's floating-point precision or pre-defined by the user. While bracketing the triplet of points (a,b,c) at each stage of the search, the next point b is tried in such a way that it is at a fractional distance 0.38197 from one end (say a) and 0.61803 from the other end (say c). In this way, this search algorithm guarantees that evaluation of each new function will bracket the minimum to an interval of just 0.61803 times the size of the preceding interval (Press et al., 1992). These fractional distances 0.38197 and 0.61803 are called golden mean or golden section. This optimal bisection method for function minimization is called *golden section search* method in 1-D (Press et al., 1992).

If a parabola is fitted through three points containing the true minimum, then the minimum point can be reached with a single step. Since the abscissa rather than an ordinate is searched for locating a true minimum, this procedure is called *inverse parabolic interpolation.* The formula for the abscissa x_a, which is the minimum of a parabola through three points $f(a), f(b),$ and $f(c)$ is given by (Press et al., 1992),

$$x_a = b - \frac{1}{2}\frac{(b-a)^2[f(b)-f(c)]-(b-c)^2[f(b)-f(a)]}{(b-a)[f(b)-f(c)]-(b-c)[f(b)-f(a)]} \tag{4.22}$$

This formula fails if all the three points are collinear. Therefore, this 1-D search may be called the *golden section search* algorithm coupled with *inverse parabolic interpolation.*

4.4.3 Simulated Annealing with Downhill Simplex Method

Simulated annealing (SA) is one of the adaptive mathematical techniques for solving optimization problems. Metropolis et al. (1953) introduced a numerical algorithm to simulate the annealing process in solid. Metropolis algorithm is a Monte Carlo technique based simulation procedure. SA algorithm accepts those solutions, which gives improved results of the objective function or cost function. It also accepts solution (to a limited extent), which gives deteriorated results of the cost function. This feature of SA gives the capability of heuristic hill climbing in a search space, which in turn facilitates SA to escape from any local optimum and reach global optimum. In the initial stage, the probability of accepting incorrect solutions (with deteriorated results of cost function) is more. However, as the process advances, a very few incorrect solutions are accepted by the algorithm. Finally, a correct solution is obtained. This is called *adaptive hill climbing capability* of SA and it makes the algorithm very robust and effective. However, SA is a computationally intensive method (Press et al., 1992).

The global minimum of a function, which has more than one independent variable, is found through the use of downhill simplex method (Nelder and Mead, 1965) along with SA. This method requires an evaluation of a function and not the derivatives of the function. A simplex is a geometrical figure with N dimensions and N+1 vertices (or points). In two dimensions, a simplex is a triangle. In three dimensions, it is a tetrahedron. In four dimensions, it is a pentagon. If any point of this simplex is considered as an origin, the rest N points of the simplex define the vector directions that cover N-dimensional vector space. A downhill simplex method is started with N+1 points, called initial simplex. This method assumes a series of steps to move a point of the simplex, where the function has largest value ("highest point"), through the opposite

face of the simplex to a lower point. These steps are called reflections and movement of points happens in such a way that the volume of the simplex is conserved. Larger steps are possible when the simplex expands in one or more direction. When it reaches a minimum point (or "valley floor"), the method contracts itself in a transverse direction and tries to ooze down the valley (Press et al., 1992). It is also possible that the simplex contracts itself in all the directions. At the zero value of a controlling parameter (analogous to the temperature in an annealing process), the simplex is considered as reached in the vicinity of a global minimum point. Therefore, as the value of the controlling parameter or the temperature decreases from a high value to zero, SA converges asymptotically to an optimum solution.

The average of N+1 values of cost functions over the simplex vertices is generally set as the initial value of the controlling parameter T_0 of the annealing scheme. The annealing schedule is based on a hybrid linear-exponential cooling scheme. The number of iterations increases at each stage of temperature as the annealing process advances. After each temperature step or iteration, a set of parameters, which produces the least error, is used as the seed set for the succeeding annealing step. In the i^{th} iteration, the controlling parameter T_i decreases according to a cooling scheme $T_i = T_0(1 - N_c / K)^{\varsigma}$, where N_c is the cumulative number of iterations already carried out; K is the pre-defined total number of iterations, and ς is a constant (here it is set to ς = 2) (Press et al., 1992). During the annealing process, whenever the parameters (selected by a random process) fall outside a search range (i.e., constraints provided by user), a penalty factor is generally added to the value of the cost function. The penalty factors are computed from how much the value of each parameter exceeds the pre-specified search range.

This SA with downhill simplex method requires a continuous function. Though this temporal backscatter model lacks analytical derivatives, it is continuous in the sense that a small change in the parameter value is accompanied by a proportional change in the objective or cost function (Sternlicht and de Moustier, 2003b).

4.4.4 Four-Dimensional Inversion Approach

Following the two-stage inversion scheme as proposed by Sternlicht and de Moustier (2003b) (i.e., using the 3-D inversion scheme as discussed in section 4.4.1), initially an attempt was made to characterize the seafloor by estimating the values of sediment property parameters (M_ϕ, w_2, σ_v, and γ_2) with a limited data set collected from the present experimental area (Chakraborty and De, 2008). However, that study (Chakraborty and De, 2008) revealed that the estimated values of the roughness spectrum strength w_2 are different at 33 and 210 kHz. Because the interface roughness is modeled (based on the assumption of isotropic Gaussian distribution of surface relief) by a single power-law relief energy, the values of the roughness spectrum strength are not expected to vary with the acoustic frequency.

In view of the above observations, the two-stage 3-D inversion scheme has been slightly modified to compare the estimated values of seafloor sediment properties at different acoustic frequencies. The following modifications are made.

1. Because the aim is to investigate the applicability of the temporal backscatter model for characterizing the seafloor sediments at two different acoustic frequencies, the sediment volume scattering parameter (σ_2) is used for better comparison instead of sediment volume scattering coefficient (σ_v). Following

Jackson and Briggs (1992), the parameter σ_2 is assumed as a frequency-independent parameter in this study.

2. Following Sternlicht and de Moustier (2003b), the initial study (Chakraborty and De, 2008) assumed only one of the two values of γ_2 depending on the rough estimate (from the 1-D iterative search) of the sediment type (i.e., γ_2= 3.0 for coarse sediments and γ_2= 3.3 for fine sediments). However, if γ_2 is different from the assumed values, the error would be translated into the different values of w_2 at different acoustic frequencies. Thus, the values of γ_2 are not considered as constants in this modified inversion approach. In the second stage of the inversion process, the value of γ_2 is also inverted along with M_ϕ, w_2, and σ_2. Thus, the inversion approach changes from 3-D inversion to a four-dimensional (4-D) inversion scheme.
3. Furthermore, the two-frequency backscatter data are jointly utilized for improved characterization of the seafloor sediment (Jackson, 2009). Accordingly, a combined two-frequency inversion (hereafter referred to as 2F inversion) is performed to estimate the values of a single set of sediment property parameters (M_ϕ, w_2, γ_2, and σ_2) applicable to the backscatter data at both the acoustic frequencies (i.e., applicable in the frequency range 33-210 kHz). All the four sediment parameters are assumed as frequency independent in this study.

Average echo waveforms are utilized in this model-based characterization of seafloor sediments. The averaging is performed using 20 successive echoes with 50% overlap to obtain stable acoustic signals in the study area (i.e., the echoes are averaged in a moving average sense with sequences 1-20, 11-30, and so on till the end of the number of consistent echo envelopes available). The 1-D golden section search with

inverse parabolic interpolation is performed in the same way as discussed in section 4.4.1 to determine a broad sediment type based on the value of M_ϕ. The flow chart of this 1-D iterative search process is shown in Fig. 4.7a. The value of γ_2 is set to $\gamma_2 = 3.25$ in the 1-D search, as this generic value of γ_2 is normally assumed in the absence of field measurements (APL Handbook, 1994). The value of the free parameter σ_2 is set to 0.004 and the values of w_2 and other geo-acoustic parameters are estimated based on the value of M_ϕ in the 1-D search (using equations (4.15) to (4.18)).

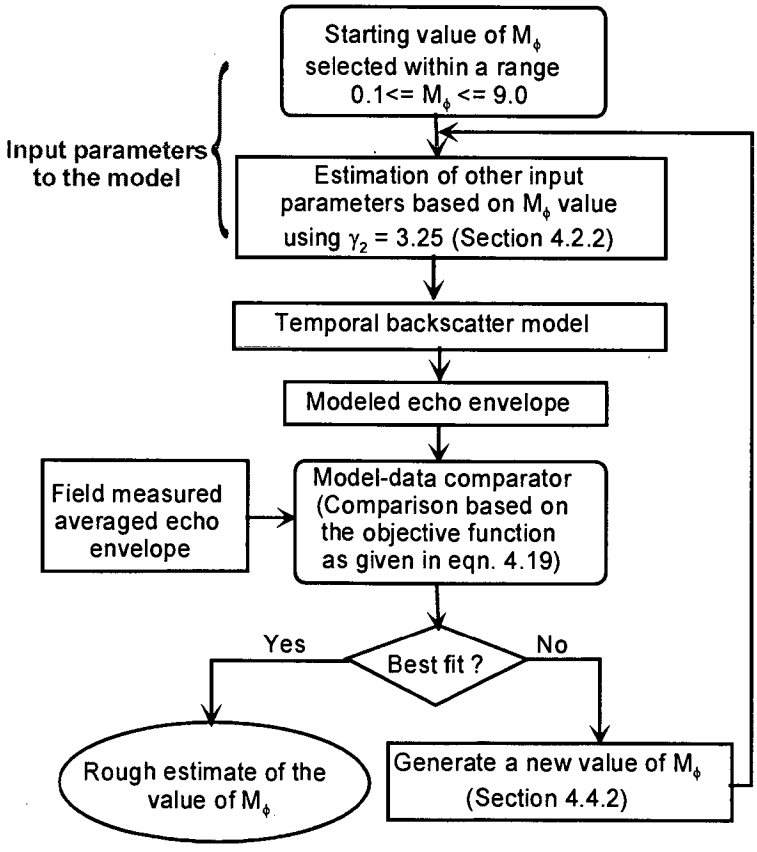

Fig. 4.7a Flow chart of the 1-D local search process for optimization of M_ϕ

The 4-D inversion is carried out using SA with the downhill simplex (SADS) algorithm (Press et al., 1992; Sternlicht and de Moustier, 2003b). The parameters

estimated through the inversion are essentially constrained over a limited search range in the solution space to avoid unrealistic solutions. Accordingly, the value of M_ϕ obtained from the echo envelope peak amplitude (using the 1-D search) is allowed to vary within $M_\phi \pm 1.0\phi$ in the 4-D inversion scheme to adjust the model-data matches for estimating the values of sediment parameters (M_ϕ, w_2, γ_2, and σ_2). In 4-D inversion, a broad search range $0.0002 \le w_2 \le 0.009$ is chosen for w_2 based on the published observations from various other field experiments (Jackson and Briggs, 1992; Briggs, 1989). The field experiments by Jackson and Briggs (1992) and Briggs (1989) over different sedimentary environments also revealed that a majority of the measured values of γ_2 lie within a range of 2.9 to 3.5. Thus, the values of γ_2 are varied within 2.9 to 3.5 in the 4-D inversion scheme. Moreover, the values of the free parameter σ_2 are varied in the range 0.0001 to 0.006. Though there is no hard upper limit in the search range for the parameter σ_2, the value 0.006 is chosen here to avoid the large contribution of volume scattering components. Stewart and Chotiros (1992) reported much higher values of σ_2 (>> 0.006) to obtain model-data fit with their scattering data, however the experiments by several other researchers (Jackson et al., 1986a; Mourad and Jackson, 1989; Jackson and Briggs, 1992; Stanic et al., 1989) revealed that in general the maximum values of this free parameter σ_2 in the range 0.004 to 0.006 give the best fit to the measured scattering data. In this temporal backscatter model, unrealistically high values of the volume scattering parameter ($\sigma_2 >$ 0.006) may exhibit very high values of *S/E* ratio (i.e., "good" model-data fit). Because only normal-incidence, single-beam echo sounder backscatter data are considered in this study, the interface

scattering components are expected to have larger contributions than that of the volume scattering components. To avoid such instances (the best fit with the data using a high value of σ_2), the empirical penalty component (as discussed in 4.4.1) is used in the 4-D inversion scheme. The flow chart of the 4-D inversion approach adopted for estimating the values of seafloor sediment parameters at 33 and 210 kHz is presented in Fig. 4.7b.

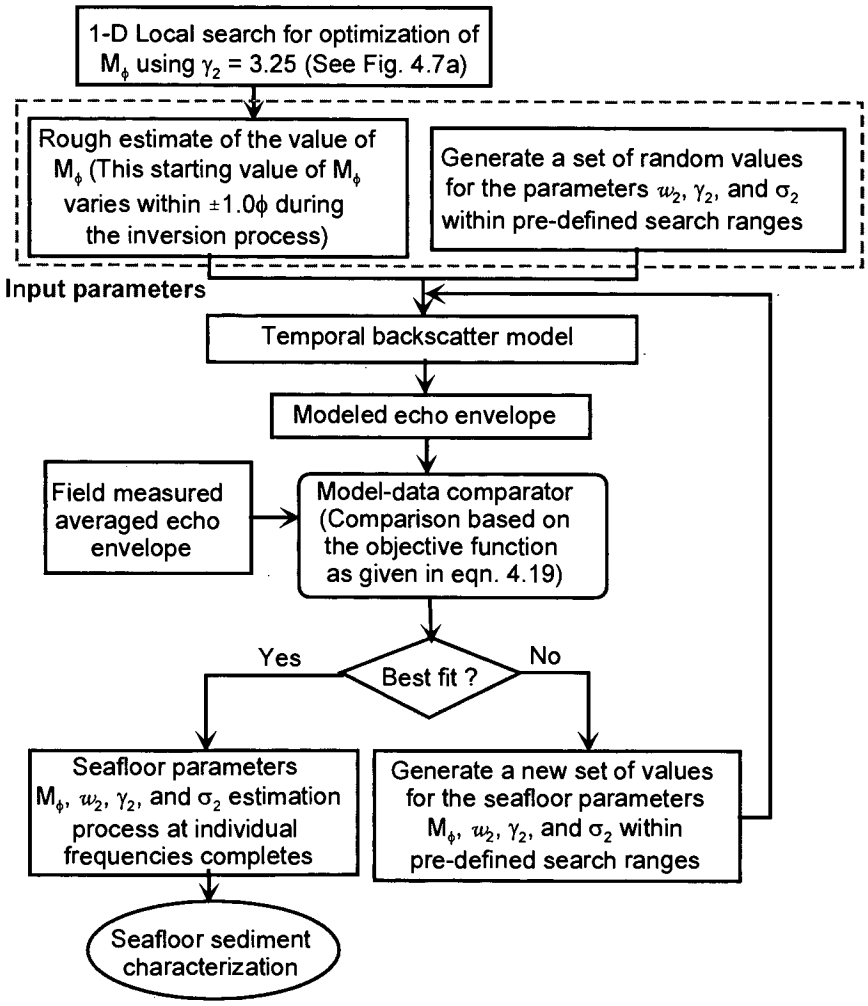

Fig. 4.7b Flow chart of the 4-D inversion procedure for individual single frequencies

Matsumoto et al. (1993) observed that the rate of successful convergence of SADS algorithm is approximately 90% with a single run of the algorithm in their

applications. Press et al. (1992) suggested reinitializing of the downhill simplex algorithm with the optimized values already obtained from the previous run as one of the vertices of the simplex for achieving plausible global minima. In this study, five times of re-initialization of the simplex are done to ensure the global optimization in the 4-D inversion. One of the outputs of this SADS inversion process with an average echo envelope over sandy seafloor is shown in Fig. 4.7c.

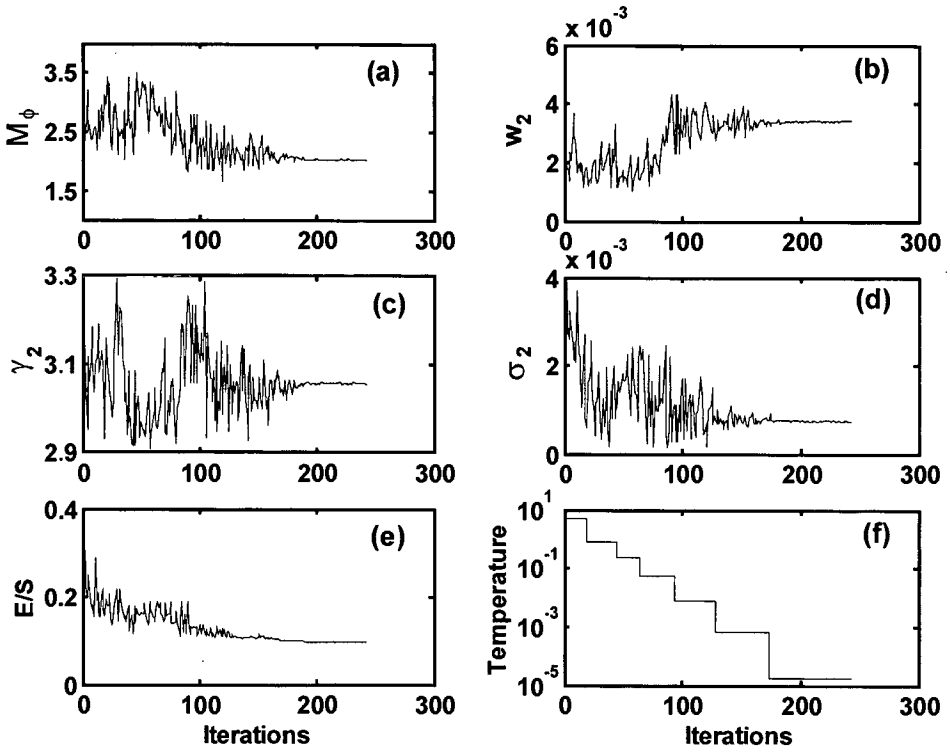

Fig. 4.7c Showing a representative result of 4-D inversion over a sandy seafloor at 33 kHz with the variations of (a) mean grain size, (b) roughness spectrum strength, (c) roughness spectrum exponent, (d) volume scattering parameter, (e) error-to-signal (*E/S*) ratio, and (f) temperature at each iteration

Furthermore, the 2F inversion is performed to investigate the additional advantages of the use of two frequency backscatter data jointly for estimating a single set of seafloor parameters. In this 2F inversion scheme, the summation of the two *E/S*

values, computed at two individual frequencies (33 and 210 kHz), is used as the new objective function to measure the discrepancies between the data and the modeled echo energies (Jackson, 2009). Moreover, a 1-D search is not performed in the 2F inversion. Instead, an average of the two estimates of M_ϕ, obtained from the 1-D search at two individual frequencies, is used as the rough estimate of M_ϕ in the 4-D inversion scheme. This average value of M_ϕ is allowed to vary within $\pm 1.3\phi$ in the 4-D inversion for the 2F approach. A broader search range for M_ϕ is chosen in the 2F inversion scheme because of the differences in the rough estimation of M_ϕ (obtained from the 1-D search at two individual frequencies) for only a few samples. The search ranges for other sediment parameters (i.e., for w_2, γ_2, and σ_2) are kept unchanged from the individual frequency inversions. The flow chart of this 2F inversion approach is shown in Fig. 4.8.

One set of typical model-data matches obtained from 33 and 210 kHz inversions as well as from 2F inversion at different locations (i.e., at different stations) are shown in Fig. 4.9 and Fig. 4.10 respectively. Inversion results are given inside the respective plots and the depth of seafloor at the locations 5, 6, 7, 9, 10, 13, 17, and 18 are 57m, 60m, 63m, 36m, 45m, 40m, 72m, and 85m respectively. For a particular sedimentary environment (i.e., at a particular site), estimations of the values of four parameters (at two individual frequencies as well as 2F inversions) are carried out using the available averaged echo envelopes and subsequently an overall average value is computed from all the estimated values for that particular site. This overall average value (for every individual site) is referred to as the estimated mean value of the sediment parameter (e.g., estimated mean value of M_ϕ, or estimated mean value of w_2,

etc.) in the following text. These estimated mean values of seafloor sediment parameters obtained at individual frequency inversion and 2F inversions are listed in Table 4.1.

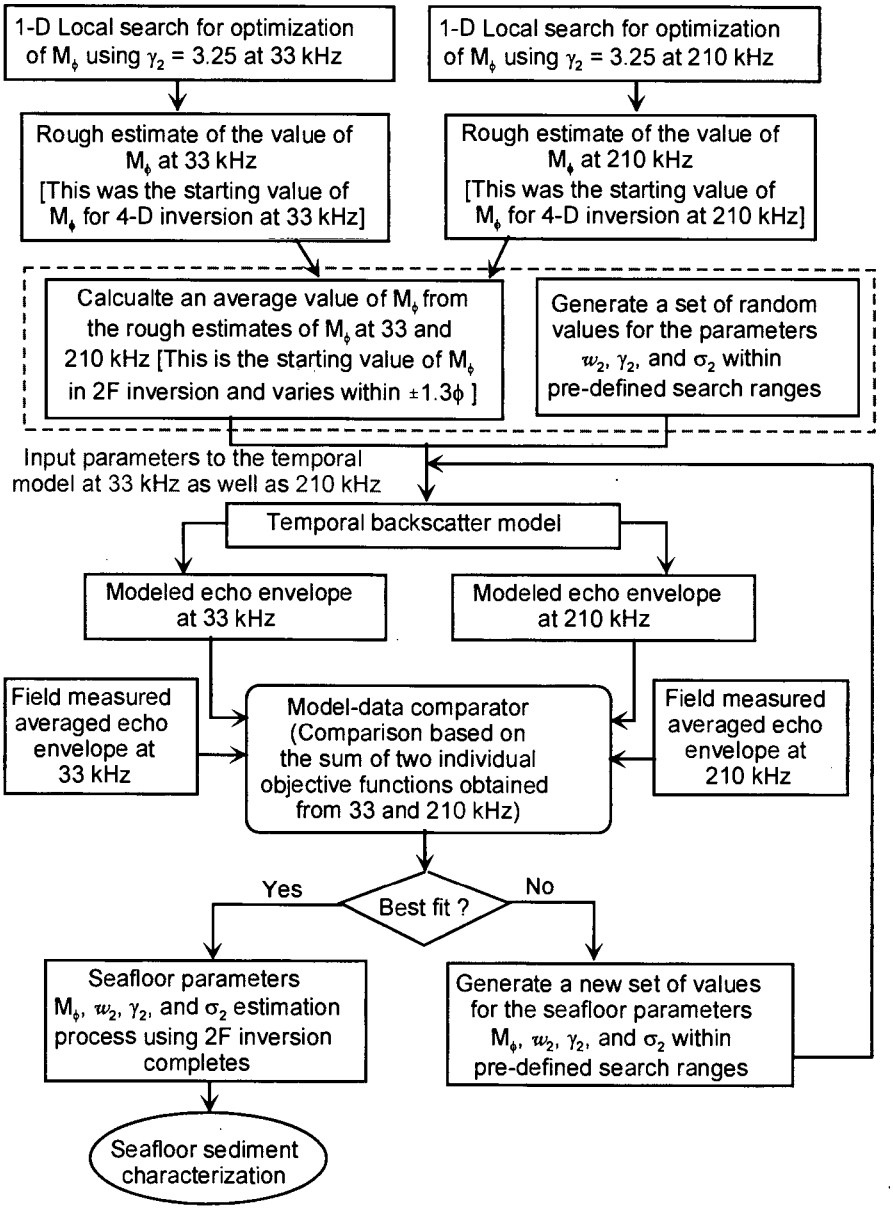

Fig. 4.8 Flow chart of the 2F inversion approach

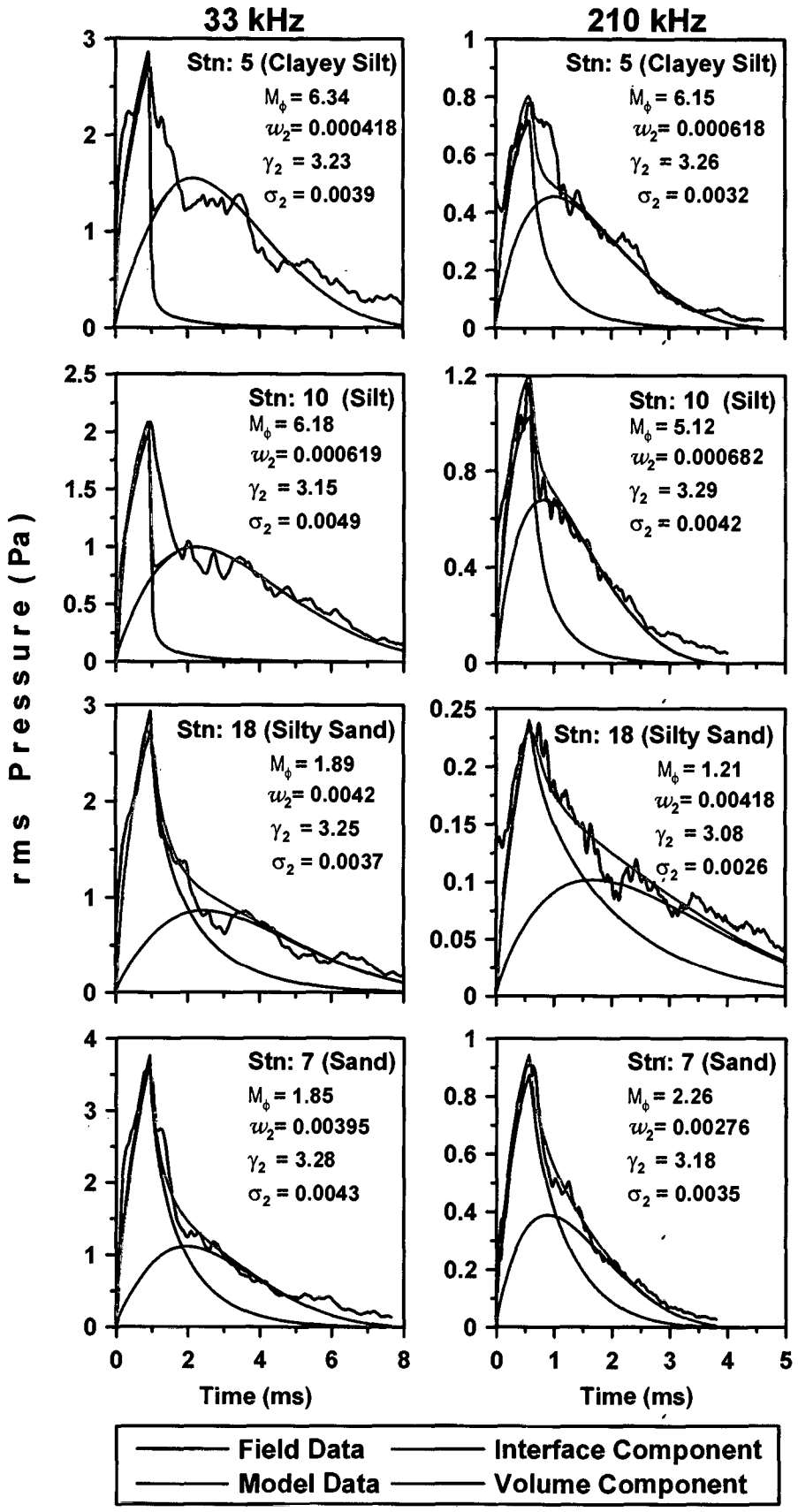

Fig. 4.9 Typical model-data matches obtained from 33 and 210 kHz inversions

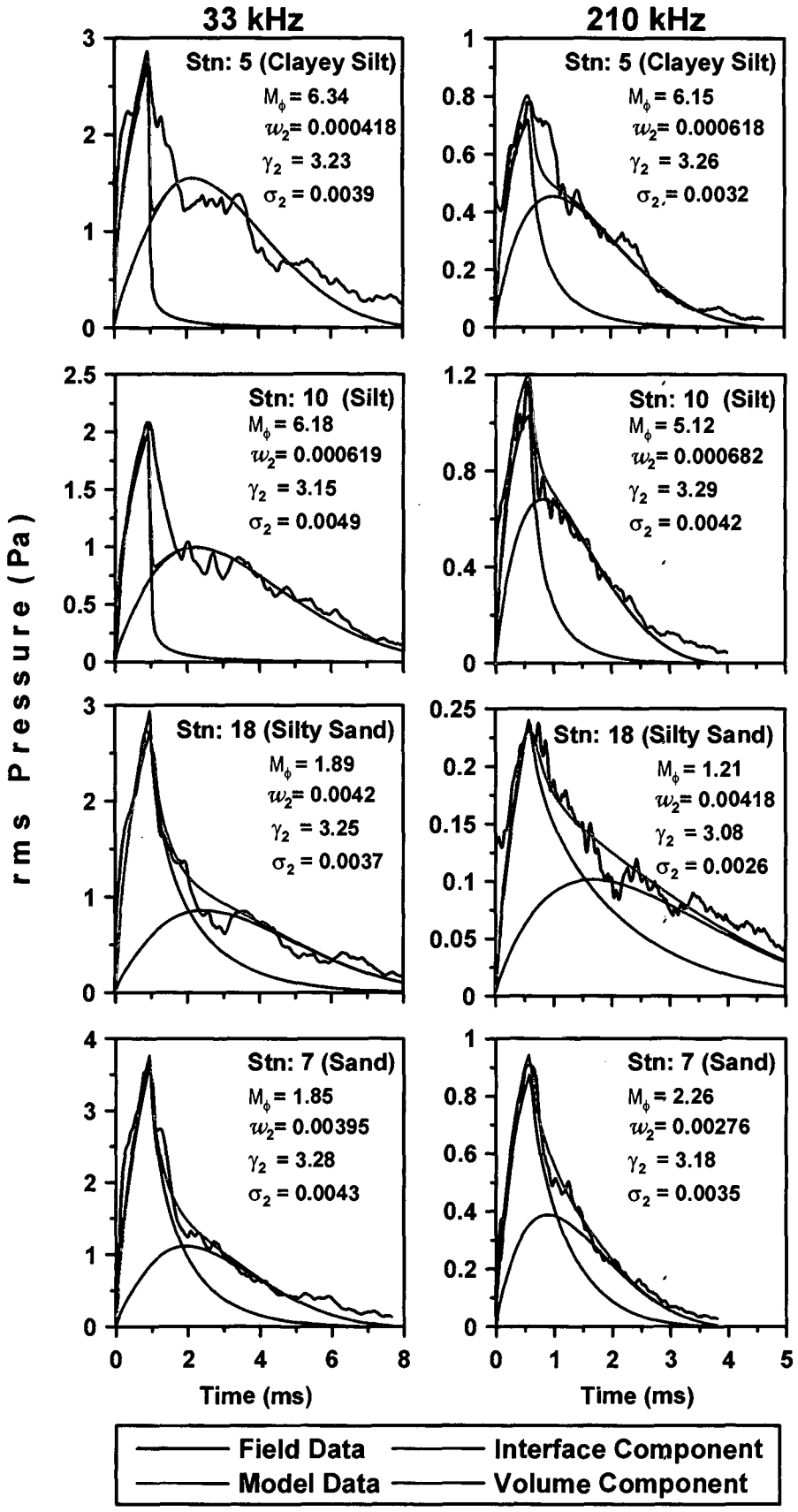

Fig. 4.10 Typical model-data matches obtained from 2F inversions

Table 4.1 Inversion results

Stn. No.	Estimated mean values of M_ϕ (phi units)			Estimated mean values of w_2 (cm^4)			Estimated mean values of σ_2			Estimated mean values of γ_2			Average signal-to-error ratio, *S/E* (dB)		
	33 kHz	210 kHz	2F	33 kHz	210 kHz	2F	33 kHz	210 kHz	2F	33 kHz	210 kHz	2F	33 kHz	210 kHz	2F
1	6.30	5.17	5.28	0.000313	0.000618	0.000498	0.0048	0.0042	0.0047	3.18	3.29	3.30	18	13	14
2	6.95	4.70	5.11	0.000284	0.000663	0.000480	0.0055	0.0044	0.0050	3.14	3.31	3.26	17	15	14
3	5.92	5.68	5.75	0.000476	0.000592	0.000525	0.0053	0.0049	0.0050	3.15	3.35	3.30	12	14	14
4	6.13	5.03	5.24	0.000285	0.000579	0.000544	0.0044	0.0037	0.0039	3.30	3.29	3.30	11	12	16
5	6.26	5.45	5.53	0.000408	0.000592	0.000512	0.0049	0.0040	0.0034	3.23	3.31	3.25	15	12	20
8	6.96	5.00	5.94	0.000527	0.000524	0.000516	0.0037	0.0040	0.0029	3.32	3.22	3.28	18	10	14
13	6.71	5.01	5.83	0.000593	0.000582	0.000516	0.0050	0.0044	0.0034	3.21	3.34	3.30	16	14	15
9	6.59	4.75	5.79	0.000561	0.000625	0.000469	0.0049	0.0040	0.0050	3.29	3.27	3.29	20	12	13
10	6.29	5.02	5.15	0.000643	0.000670	0.000625	0.0049	0.0045	0.0037	3.10	3.29	3.26	16	11	17
14	6.08	4.21	5.22	0.000516	0.000603	0.000479	0.0050	0.0045	0.0043	3.24	3.28	3.25	12	11	13
11	2.79	3.08	3.17	0.00237	0.00153	0.00222	0.0045	0.0041	0.0042	3.29	3.12	3.16	20	14	18
17	2.37	2.05	2.63	0.00366	0.00255	0.00243	0.0043	0.0029	0.0032	3.24	3.11	3.16	22	18	22
18	1.86	1.10	2.37	0.00419	0.00439	0.00293	0.0039	0.0027	0.0024	3.20	3.10	3.19	18	13	23
19	2.33	1.03	2.40	0.00346	0.00452	0.00318	0.0038	0.0032	0.0023	3.19	3.20	3.19	16	13	22
6	1.51	1.10	1.65	0.00355	0.00454	0.00388	0.0049	0.0032	0.0050	3.30	3.20	3.20	17	19	16
7	1.98	2.08	2.49	0.00375	0.00296	0.00294	0.0046	0.0035	0.0037	3.29	3.20	3.21	20	19	20
12	1.80	1.92	2.41	0.00371	0.00344	0.00212	0.0045	0.0035	0.0046	3.27	3.20	3.19	21	17	18
15	1.97	1.40	1.85	0.00343	0.00401	0.00398	0.0046	0.0029	0.0036	3.12	3.10	3.09	23	17	19
16	2.10	1.31	1.91	0.00365	0.00438	0.00235	0.0042	0.0040	0.0028	3.25	3.14	3.12	20	19	19
20	1.75	1.51	1.86	0.00388	0.00424	0.00376	0.0029	0.0028	0.0019	3.10	3.20	3.08	14	15	13

4.5 INVERSION RESULTS AND DISCUSSION

The estimated mean values of M_ϕ obtained from the individual frequency and 2F inversions (given in Table 4.1) are compared with the ground-truth. However, no ground-truth is available on other seafloor parameters (w_2, γ_2, and σ_2) in this study area. In the absence of ground-truth, the estimated mean values of roughness spectrum parameters and the sediment volume scattering parameter are compared with the information available in published literature. In the last three columns of Table 4.1, the average values of *S/E* ratio (in dB) are given for 33 kHz, 210 kHz, and 2F inversions. These values provide useful information on the comparison of model-data matching results, where a higher value represents a better match of the model with the field data. The averaged values of backscatter strength in dB (termed as the mean values of backscatter strength), computed from the available averaged echo envelopes using the echo sounder transceiver characteristics (the computation details are given in Chapter 5), are used for assessing the consistency of the estimated mean values of M_ϕ at both the frequencies. Silty sand and sand sediments will be referred to as coarse sediments (with estimated $M_\phi < 4\phi$); and clayey silt and silt sediments will be referred to as fine sediments (with estimated $M_\phi \geq 4\phi$) in the following discussion.

4.5.1 Mean Grain Size

The peak amplitudes of echo envelopes primarily depend on impedance contrast between water and seafloor sediments. In surficial sediments, the impedance contrast is

often correlated with the mean grain size of sediments (Sternlicht and de Moustier, 2003b). The estimated mean values of M_ϕ of surficial sediments obtained from the inversions of echo envelopes are therefore expected to correlate with the laboratory-measured values of M_ϕ. The linear regression analysis (between the estimated mean values of M_ϕ and the laboratory-measured values of M_ϕ) shows that the correlation coefficients are 0.98, 0.96, and 0.97 respectively for 33 kHz, 210 kHz, and 2F inversions (Fig. 4.11a). For these three correlations, the associated p-values (p <<0.0001) are much smaller than the 5% level of significance (computed using a Student's t-distribution), which indicates that the probability in obtaining these correlation coefficients by chance is close to zero. Since $p < 0.05$, these correlations are statistically significant at 5% level of significance. The 95% confidence limits for the three regression lines are also shown in Fig. 4.11a. The correlations also indicate that the regression models can explain about 92-96% of the variances in the estimation of M_ϕ. Moreover, this result indicates that the least square line obtained from the best fit of the 33 kHz data, gives the best estimation of M_ϕ when compared with the 1:1 straight line (shown as the dotted lines in Fig. 4.11a).

A linear regression analysis reveals that the correlation coefficients between the laboratory-measured values of M_ϕ and the mean values of backscatter strength are 0.75 and 0.69, respectively, at 33 and 210 kHz. It is expected that the estimated mean values of M_ϕ from the inversions should also exhibit similar correlations. Fig. 4.11b shows that the correlation coefficients between the estimated mean values of M_ϕ and the mean values of backscatter strength are 0.78 and 0.68, respectively, for 33 and 210 kHz. The

estimated mean values of M_ϕ from 2F inversions are also correlated with the mean values of backscatter strength at 33 and 210 kHz with the correlation coefficients 0.77 and 0.72 respectively (not shown in figure). Since the p-values associated with these correlation coefficients (r) are less than the 5% level of significance (i.e., $p < 0.05$), all these correlations are statistically significant. The 95% confidence limits are shown in Fig. 4.11b. These regression models (for 33 and 210 kHz) can explain about 46-60% of the variances in the dataset.

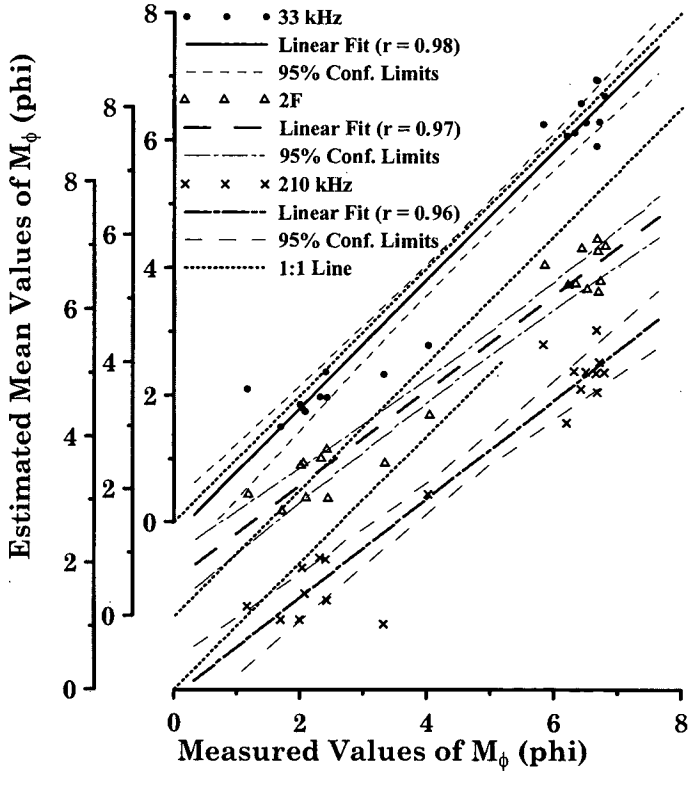

Fig. 4.11a Scatter plot showing the relationship between the laboratory-measured values of M_ϕ(phi) and the estimated mean values of M_ϕ(phi) for the three inversion cases. Diagonal dotted lines indicate the 1:1 lines.

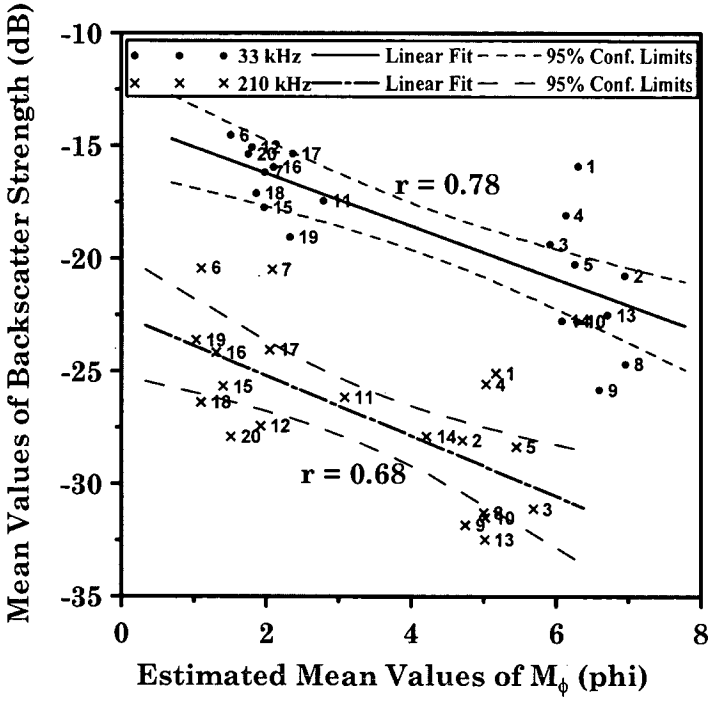

Fig. 4.11b Scatter plot showing the relationship between the estimated mean values of M_ϕ (phi) and the mean values of backscatter strength (in dB) at 33 and 210 kHz. The values of the correlation coefficients (r) are indicated in the plot. The labels against the symbols indicate the station locations.

As pointed out earlier, the backscatter strength from the sea floor is primarily controlled by the acoustic frequency, the contrast in acoustic impedances between water and sediment, and the contributions from seafloor interface roughness as well as sediment volume inhomogeneity. Scattering due to seafloor interface roughness is relatively more important at higher acoustic frequencies, while scattering due to volume inhomogeneity below the water-sediment interface is relatively more significant at lower acoustic frequencies. In soft sediments, the acoustic energy penetrates into the sediment and likely to be scattered from the buried inhomogeneities such as coarse sand particles, shell hash, mollusk shells, buried layers of coarse materials, etc. The intensity of the scattered energy depends on the sizes of these buried inhomogeneities relative to

the impinging acoustic wavelength. This phenomenon might be responsible for the few outlying values of backscatter strength, observed especially in fine-grained sediments. The station locations are used as labels against the symbols in Fig. 4.11b. The effect of the fluctuations of backscatter strength on the correlation coefficient is examined by removing only two higher and outlying values of backscatter strength measured at stations 1 and 4 from the dataset. It was observed that the values of the correlation coefficient increased to 0.90 and 0.79 respectively, for 33 and 210 kHz. The p-values ($p < 0.05$) associated with these correlation coefficients indicate that these correlations are also statistically significant at 5% level of significance. This indicates that if the fluctuations of the backscatter data at two stations are removed, the regression models (at 33 and 210 kHz) can explain about 62-81% variances in the dataset. Similar significant (statistically) enhancement in the correlation coefficients is also observed for the estimated mean values of M_ϕ obtained from 2F inversion, if the values of the backscatter strength at stations 1 and 4 are ignored.

It is mentioned earlier that acoustic impedance contrast is one of the factors, which controls the seafloor backscatter strength. The acoustic impedance is the product of density and sound speed in sediment. The finer sediments with high porosity (that have low values of density and sound speed, i.e., small impedance contrast between water and sediment) are expected to exhibit low backscatter strengths. The coarser sediments with low porosity (that have higher values of density and sound speed, i.e., high impedance contrast between water and sediment) are expected to have higher backscatter strengths. These theoretical expectations are well supported by the field measurements (Davis et al., 1996; Collier and Brown, 2005; Ferrini and Flood, 2006; Goff et al., 2000). In this study, the statistically significant linear correlations (with 95%

confidence level) between the estimated mean values of M_ϕ and the measured backscatter strength support these observations. Furthermore, the statistically significant linear correlations (with 95% confidence level) between the laboratory-measured values and the estimated mean values of sediment mean grain size (as shown in Fig. 4.11a) primarily support these estimations from inversions.

4.5.2 Roughness Spectrum Parameters

The estimated mean values of roughness spectrum parameters (w_2 and γ_2) of the seafloor relief and the estimated mean values of M_ϕ are plotted in a scatter diagram to understand their relationships. The scatter diagram (Fig. 4.12a) between the estimated mean values of M_ϕ and w_2 revealed that the values of w_2 are less than 0.001 cm^4 for fine sediments and are confined within 0.002 to 0.005 cm^4 (except one value for a silty sand sample at 210 kHz inversion) for coarse sediments. In addition, the scatter diagram (Fig. 4.12b) between the estimated mean values of M_ϕ and γ_2 shows that the values of γ_2 are confined within 3.21 to 3.4 for fine sediments and within 3.0 to 3.21 for coarse sediments at 210 kHz and 2F inversions. In contrast, the estimated mean values of γ_2 at 33 kHz inversions do not exhibit any clear trend distinguishing between fine and coarse sediments.

It is observed (Fig. 4.12a) that the estimated mean values of w_2 are clustered with less fluctuation for fine sediments for all the three inversion cases. For coarse sediments, the estimated mean values of w_2 are relatively scattered. In addition, the estimated mean values of γ_2 are relatively more clustered for 2F inversions than the

individual frequency inversions. For coarse sediments, the overall average estimates of γ_2 (from 10 coarse sediment samples) are 3.23 ± 0.071, 3.16 ± 0.047, and 3.16 ± 0.047, respectively, at 33 kHz, 210 kHz, and 2F inversions. For fine sediments, the overall average estimates of γ_2 (from 10 fine sediment samples) are 3.22 ± 0.074, 3.30 ± 0.037, and 3.28 ± 0.022, respectively, at 33 kHz, 210 kHz, and 2F inversions. Moreover, it is observed that higher values of w_2 and lower values of γ_2 are associated with coarse sediments. In contrast, lower values of w_2 and higher values of γ_2 are associated with fine sediments.

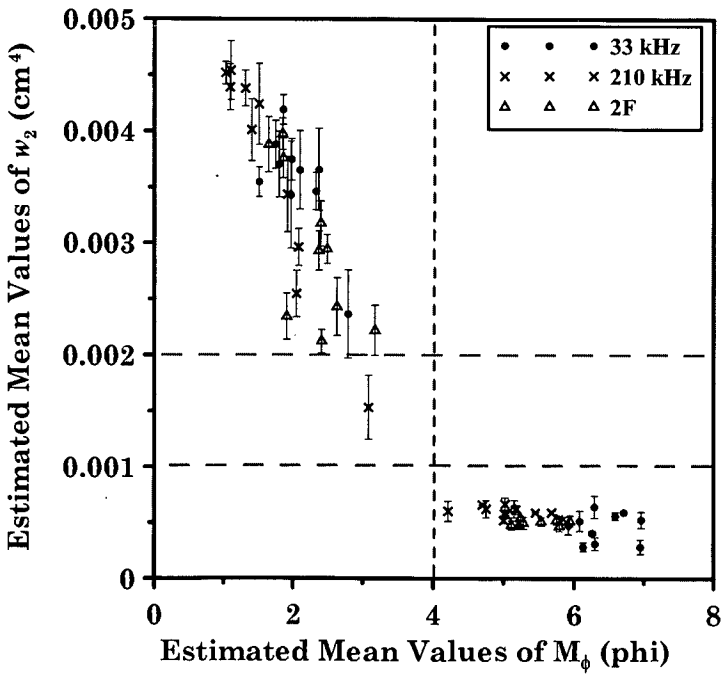

Fig. 4.12a Scatter diagram between the estimated mean values of M_ϕ (phi) and w_2 (cm^4). The vertical dashed line at $M_\phi = 4\phi$ demarcates the fine and the coarse sediments. The two horizontal dashed lines at $w_2 = 0.001$ cm^4 and $w_2 = 0.002$ cm^4 demarcate the maximum and minimum limits of w_2 for fine and coarse sediments respectively. The error bars indicate one standard deviation in either direction.

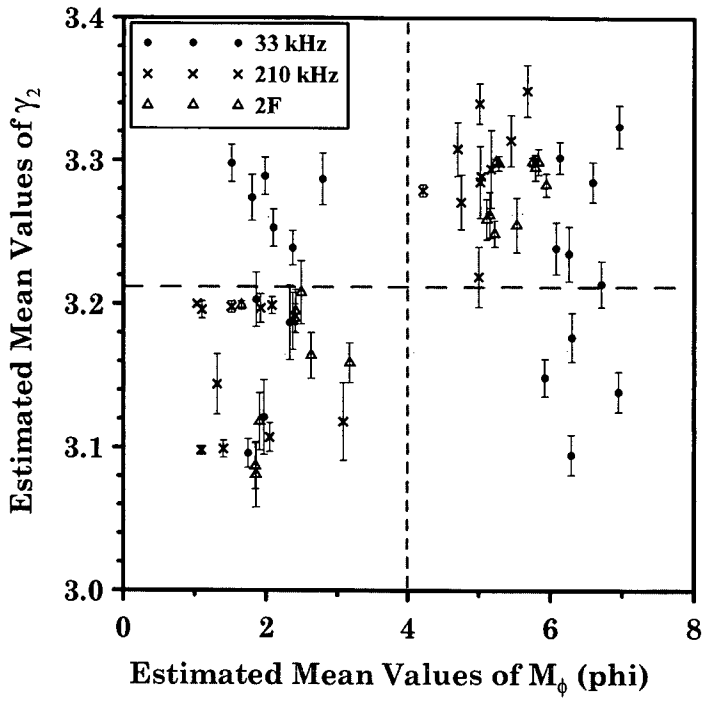

Fig. 4.12b Scatter diagram between the estimated mean values of M_ϕ (phi) and γ_2. The vertical dashed line at $M_\phi = 4\phi$ demarcates the fine and the coarse sediments. The horizontal dashed line at $\gamma_2 = 3.21$ indicates the separation between fine and coarse sediments. The error bars indicate one standard deviation in either direction.

The roughness spectrum parameters are usually calculated from the slope and intercept of the averaged 1-D spectrum through a linear regression and then converted to two-dimensional (2-D) roughness spectrum parameters (w_2 and γ_2) under the assumption of isotropic sea bottom roughness (Briggs, 1989). A wide range of 2-D roughness spectrum parameters (which are computed from the 1-D-averaged spectrum as well as from the 2-D digital elevation measurements) is thus available in the literature (Briggs, 1989; Stanic et al., 1989; Briggs et al., 2005; Jackson et al., 1996). The data on seafloor roughness spectrum parameters and sediment grain size obtained from the

various field experiments (Jackson et al., 1986b; Briggs, 1989; Stanic et al., 1989; Briggs et al., 2005; Jackson et al., 1996) revealed that the majority of the values of w_2 are greater than 0.002 cm^4 for coarser sediments and confined within 0.0 to 0.003 cm^4 for finer sediments (Sternlicht and de Moustier, 2003a). In addition, these measured data indicated that the majority (after ignoring the outliers and redundant observations) of the values of γ_2 are confined within 2.9 to 3.3 for coarse sediments and within 3.2 to 3.5 for fine sediments (Sternlicht and de Moustier, 2003a). In this study, the estimated mean values of w_2 and γ_2 (Fig. 4.12a and Fig. 4.12b) are in general agreement with these published data.

Briggs et al. (2005) attempted to construct regressions between the sediment grain size and the seafloor roughness spectrum parameters. The study by Briggs et al. (2005) revealed that there is no unique empirical relationship between sediment grain size and roughness spectrum strength or sediment grain size and roughness spectrum exponent. However, Briggs et al. (2005) and Jackson and Richardson (2007) reported that the values of roughness spectrum strength and roughness spectrum exponent appear to cluster according to the sediment type with separate trends for sand and mud. This apparent clustering of roughness spectrum parameters according to fine-grained and coarse-grained sediments is also evident in Fig. 4.12a and Fig. 4.12b. This cluster nature is more prominent for the 2F inversion data. However, further assessment of this 2F inversion approach in conjunction with ground-truth data may be required (probably in the frequency range 20-150 kHz, the reason for choosing this frequency range is discussed in section 4.6).

Briggs (1989) reported that the roughness parameters derived from a power spectrum vary with the sediment type. Seafloor characterized by coarse sediments has

less-steep decay (i.e., lower value of γ_2) in the power-law relationship (Briggs, 1989). One of the possibilities for a power spectrum to have less-steep decay (i.e., less-steep slope of the regression line) is that the intercept energy of the spectrum at a unit spatial frequency is higher (i.e., higher value of w_2). Thus, in general, coarse sediments are associated with higher values of w_2 and lower values of γ_2. On the contrary, fine sediments are associated with comparatively lower values of w_2 and higher values of γ_2. This is also evident in the study area (Fig. 4.12a and Fig. 4.12b).

Gaussian distribution of relief height deviations about a mean surface is used in the model for describing the interface relief statistics (Jackson et al., 1986a; Sternlicht and de Moustier, 2003a). Since a pure power-law relief spectrum is assumed in the scattering model, the height difference between two points on the surface separated by a fixed horizontal distance (r_f) can be used for computation of relief statistics. The structure function provides a measure of roughness, which is easier to interpret than the power spectrum (Jackson et al., 1986a). The structure function for the pure power-law spectrum has the form $D(r) = C_h^2 r_f^{2\alpha}$, where the square of the 'structure constant (C_h)' is related to the parameters of the power-law spectrum through an expression $C_h^2 = [2\pi w_2 \Gamma(2-\alpha)2^{-2\alpha}]/[\alpha(1-\alpha)\Gamma(1+\alpha)]$. Here, Γ is the gamma function and the exponent α is related to the roughness spectrum exponent γ_2 as follows $\alpha = (\gamma_2/2) - 1$. The constant C_h is used in this study to compute the rms height difference ($C_h r_f^{\alpha}$) for the points separated by 100 cm (i.e., r_f = 100 cm, chosen arbitrarily for comparison). The values of rms height difference, computed using the

estimated mean values of roughness spectrum parameters (w_2 and γ_2) for all the three inversion cases, are plotted in Fig. 4.13 against the estimated mean values of M_ϕ.

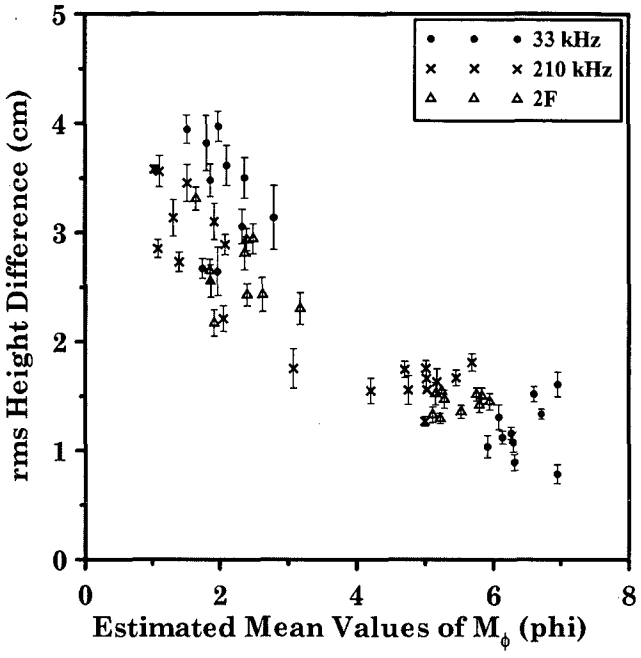

Fig. 4.13 Scatter diagram showing the relationship between the estimated mean values of M_ϕ (phi) and the computed rms height difference in cm (for the points separated by 100 cm). The error bars indicate one standard deviation in either direction.

The rms height difference statistic, in general, does not provide any information on the sediment grain size or the spacing of seafloor roughness features (Briggs et al., 2005). However, Briggs et al. (2005) reported a general decrease in the relative height variations as the sediment grains become finer. In addition, Jackson and Richardson (2007) observed that there is no predictive relationship between rms height difference and sediment grain size. In this study area, the decrease in the relative rms height variation with reference to the sediment type is also evident (Fig. 4.13).

All these observations, which are in general agreement with the theoretical expectations as well as with the published information, indirectly support the estimations on seafloor roughness spectrum parameters (in the absence of ground truth from digital photographic records).

4.5.3 Sediment Volume Scattering Parameter

The sediment volume scattering parameter (σ_2) is dimensionless and is used as a free parameter in the model-data match (Jackson et al., 1986a). For fine sediments, the overall averages of the estimated mean values of σ_2 are 0.0048 ± 0.0005, 0.0043 ± 0.0003, and 0.0041 ± 0.0008, respectively, for 33 kHz, 210 kHz, and 2F inversions (Table 4.1). For coarse sediments, the overall average values of the estimated mean values of σ_2 are 0.0042 ± 0.0006, 0.0033 ± 0.0005, and 0.0034 ± 0.001, respectively, for 33 kHz, 210 kHz and 2F inversions. The overall average of the estimated mean value of σ_2 is higher than 0.004 (but less than 0.005) for fine as well coarse sediments at 33 kHz. Only two individual fine samples have values slightly higher than 0.005 at 33 kHz. However, the overall average estimates of σ_2 are more than 0.004 (but less than 0.005) for fine sediments only at 210 kHz and 2F inversion. It is also noticed (Table 4.1) that the individual estimations of σ_2 are slightly higher at 33 kHz compared to 210 kHz and 2F estimations at all the sample locations. In addition, no definite relationship between the estimated mean values of σ_2 and the mean grain size is found in the study area.

Because the inhomogeneities within the sediment volume are difficult to measure, Jackson and Briggs (1992) suggested that the sediment volume scattering

parameter can be considered as a free parameter in the backscatter model and could be reasonably estimated by means of model-data fit. Jackson and Briggs (1992) also reported that the contributions of the volume scattering component are significant for 'soft' sediments. Though low values of σ_2 are generally used for fine-grained sediments (Jackson et al., 1986a), the experiments by Jackson and Briggs (1992) and Briggs (1989) revealed that the predicted data matches the observed data well in some experimental area if relatively large values for σ_2 (in the range 0.004 to 0.006) are used for the 'soft' sediments. As mentioned earlier, coarser inhomogeneities if embedded within the finer particle matrix, can act as strong volume scatterers. Thus, larger value of σ_2 may be required for best model-data fit in 'soft' sediments (Briggs, 1989). In this study area, the low values of σ_2 (<0.004) produced low values of *S/E* ratio in model-data matching process. By increasing the value of this free parameter σ_2, the level of the predicted backscatter strength was increased to that of the observed data. The larger coarse particles embedded in fine sediment matrix may be the reason for higher backscatter strength in this study area and thus the higher values of σ_2 is obtained for 33 kHz.

Jackson et al. (1986a) stated that the single-scattering assumption in their composite roughness model might be violated if the numerical value of σ_2 exceeds 0.004. The value 0.005 lies on the borderline between single and multiple scattering domains (Jackson and Briggs, 1992). Though the estimations of σ_2 in the study area broadly fall within the limits of single scattering mechanism, the assessment on the correctness of these values is difficult in the absence of ground-truth data.

4.6 DISCUSSION ON ROUGHNESS SPECTRUM PARAMETERS

It is mentioned earlier that the interface roughness is modeled by a single power-law relief energy (based on the assumption of isotropic Gaussian distribution of surface relief). Thus the values of the roughness spectrum parameters are not expected to vary with the acoustic frequency. However, it is observed that the roughness spectrum parameters obtained from the inversions at 33 and 210 kHz have different values in the present experimental area. The magnitudes of the differences vary with the sediment types (i.e., with M_ϕ). The temporal backscatter model (of Sternlicht and de Moustier, 2003a) utilizes the Helmholtz-Kirchhoff theory for computation of interface roughness and the model is not valid for extremely rough surfaces as well as for very high frequencies, where the Kirchhoff's criterion fails (Jackson et al., 1986a; Sternlicht and de Moustier, 2003a). However, the Kirchhoff's criterion computed with the estimated values of w_2 and γ_2 indicates that the condition is satisfied at all the experimental sites in the study area for 210 kHz.

It appears that the failure in obtaining the same values on roughness spectrum parameters at 33 and 210 kHz may be due to the fact that a single power-law relief (which is assumed in the scattering model) is too simple to describe seafloor roughness over a wide range of scales (Jackson and Richardson, 2007). Williams et al. (2009) compare the high frequency (20-500 kHz) backscatter data and model predictions utilizing the measurements from two experiments SAX99 and SAX04. Earlier, the investigation by Williams et al. (2002) revealed that the physics behind the backscattering mechanism appeared to be changing in the critical region of the

frequency range from 150 to 300 kHz. Recently, Williams et al. (2009) concluded that above 200 kHz, a new scattering mechanism is coming into play for the backscatter data obtained from both SAX99 and SAX04 experiments. At lower frequencies (20-150 kHz), the backscattering was dominated by roughness scattering during SAX99 experiments, whereas volume scattering was dominated at higher frequencies (>150 kHz) during SAX04 experiments (Williams et al., 2009). This dominant volume scattering in SAX04 experiments was explained by the scattering from the embedded shells (Ivakin, 2010). At high frequencies (150 kHz to 2 MHz), a revealing difference in scattering strength from the surrounded medium and the embedded coarse material is also observed in controlled laboratory experiments (Ivakin and Sessarego, 2007). Ivakin (2010) reported that at higher frequencies (above 200 kHz), even a small portion of embedded shell fragments (without affecting the mean grain size of sediments) could significantly change the scattering characteristics of the seafloor. This possible changing mechanism in the seafloor scattering in the critical region of the frequency range from 150-200 kHz may be responsible for obtaining the different values of the roughness spectrum parameters at 33 and 210 kHz in this study area. In addition, this possible new mechanism in scattering from the seafloor may be the reason for achieving a marginal success with 2F inversion in the frequency range 33-210 kHz.

4.7 CONCLUSIONS

The results presented in this chapter are useful to understand the applicability of the temporal backscatter model over a wide frequency range (33 to 210 kHz) over different types of sediments. The values of sediment mean grain size estimated from the

33 kHz inversions provide relatively improved results over the higher frequency inversion.

Furthermore, in the absence of experimental ground-truth data (e.g., photogrammetric), the estimated values of roughness spectrum parameters and the sediment volume parameter are assessed with reference to the available published information. It seems that the estimated values of roughness spectrum parameters from the 2F inversion are reasonably more consistent with the published data than the estimated values obtained from the individual single frequency inversions.

The estimations of seafloor sediment parameters are discussed in this chapter. The next chapter deals with the seafloor sediment classification using echo features.

Chapter 5

Echo Features Analysis

5.1 OVERVIEW

Classification of seafloor sediments is mainly a criteria based data processing algorithm to segment seafloor sediments in homogeneous groups using the properties such as grain size, density, roughness, benthic habitats etc. Basically, it is a process that involves in extracting a number of characteristic features from the backscatter echo and segments (or partitions) them into relatively homogeneous groups (Simrad and Stepnowski, 2007). Ground-truth supports (such as sediment properties from grab or corer samples; roughness information from stereo photogrammetry as well as laser scanning systems) are essential for proper evaluation of the success of the employed classification technique.

There are two broad categories of classifications for seafloor sediments. The first category is called supervised classification. In supervised classification system, the algorithm is trained with the available ground-truth information. Subsequently, this trained algorithm is used to segment an unknown data into various homogeneous sub-groups.

Another type of classification is called unsupervised classification. The information on sediment classes is not known a-priori in this case. The algorithm itself

differentiates dissimilar subgroups (within a subgroup it is homogenous) in a dataset based on the characteristics of backscatter echo (Simrad and Stepnowski, 2007). The classification with unsupervised approach highly depends on the representative characteristics content within a dataset.

All classification methods use some kind of characteristic features (or attributes), which are extracted from the normalized backscatter echo envelopes (Orlowski, 1984; Klusek et al., 1994). The normalization is essential to make these features independent of echo amplitude (Simrad and Stepnowski, 2007). These echo features are grouped into few categories: features that (a) represent the characteristics of acoustic backscatter energy, (b) describe the shape characteristics and the amplitude variability of echo envelopes, (c) represent the statistical characteristics of echoes, (d) describe the spectral characteristics of echo envelopes, and (e) other features such as fractal, Hausdroff dimension, and wavelet characteristics.

The acoustic backscatter energy computed from an echo envelope is one of the prominent features for classification of the seafloor sediments (Chakraborty et al., 2007a). The energy characteristics of an echo envelope (obtained from a single-beam echo sounder) are extracted from different time spans of the envelope. The backscatter echo from seafloor first attains a maximum amplitude, which represents coherent reflections at normal-incidence. Subsequently, the echo decays down to a minimum level. The rate of decay depends on the beam pattern of the echo sounder and the seafloor properties during the oblique incidence of the acoustic pulse. Various echo shape features (which describe the shape characteristics of an echo envelope) such as peak amplitude, rise time, decay time, echo duration etc. are successfully used for the classification of seafloor sediment (Oroloski, 1984). However, some of these shape features are effective if active pulse length option of an echo sounder is used at the time

of field experiments (Pouliquen, 2004; Lubniewski and Pouliquen, 2004). Statistical echo features, extracted from the backscatter echo envelope, such as time spread, statistical moments (e.g., statistical skewness, statistical kurtosis etc.), probability density function, and cumulative energy function of an echo are used for the classification of seafloor sediments (van Walree et al., 2005). In addition, several spectral moments, which describe the spectral characteristics of an echo envelope, are used in seafloor classification (Tegowski and Lubniewski, 2002; Tegowski et al., 2003). Fractal characteristics and Hausdroff dimensions are some other useful discriminatory features for the classification of seafloor sediments (Lubneiwski and Stepnowski, 1998; Tegowski and Lubniewski, 2000; Chakraborty et al., 2007b). Moreover, if the elementary wavelet is chosen carefully, wavelet transform can also provide useful information on the classification of seafloor (Moszynski et al., 2000; Tegowski and Lubniewski, 2002).

Additional features, such as seafloor roughness spectra (obtained from laser scanning, video and stereo photogrammetric systems) (Briggs, 1989; Moore and Jaffe, 2002; Briggs et al., 2002; Wang and Tang, 2009; Wang et al., 2009), sediment properties (e.g., grain size statistics, density, sound speed, etc. obtained from sediment samples) are also used in supervised classifications of seafloor sediments (Chakraborty et al., 2000, 2003b; Chakraborty and Kodagali, 2004).

The simplest classification is based on a single attribute associated with the seafloor sediment (Simrad and Stepnowski, 2007). Various single attributes are seafloor roughness characteristics, backscatter strength, hardness of sediment, seafloor reflection coefficient, presence of gas or benthic habitat on the seafloor etc. Based on a-priori knowledge from sediment samples (ground-truth), a correlation between particular

attribute and seafloor sediment is first established. Subsequently, attributes of unknown sediments can be classified based on the already established correlation.

If two variables (or attributes) of the seafloor are available, then classification is carried out using scatter plots of the variables in two-dimensional space. This classification is based on the grouping of attributes and different group represents different class based on the a-priori knowledge (Burns et al., 1985; Chivers et al., 1990; Bates and Whitehead, 2001).

If the number of features (attributes) is more than three, then statistical methods are available for the classification of sediments such as principal component analysis and cluster analysis. Principal component analysis provides a new set of orthogonal components, which are utilized for clustering into different classes. However, the decision on the number of principal components required for the classification is an important aspect (Legendre et al., 2002). Every individual group possesses homogeneous properties within a group, but different properties among the groups. The process of segmenting seafloor sediments in different groups is called clustering. There are different methods of clustering. The most common methods of clustering are K-means algorithm and Fuzzy C-means algorithm (Burczynski, 1999; Legendre et al., 2002; Legendre, 2003; De and Chakraborty, 2009).

A variant of multivariate analysis, called Discriminant Analysis (DA), is also used for seafloor sediment classification (Hutin et al., 2005). In this method, the differences among the predefined sediment classes are maximized and the variations within the individual classes are minimized to determine the best linear combination of feature vectors. The unknown feature vectors are then distributed among the predefined classes based on the minimum Mahalnobis distance from the centroids of each class. Another method, called canonical correlation analysis, is also exploited for the

classification of seafloor sediments (Tsemahman et al., 1997; Preston et al., 1999). All these methods use supervised classification approach. Therefore, a large number of representative training datasets are required to improve the robustness of a classification technique.

There are other classification methods, which use the artificial intelligence such as neural networks, decision tree, unsupervised Self Organizing Map (SOM), Learning Vector Quantization (LVQ) (Stepnowski et al., 1999; Dung and Stepnowski, 2000; Moszynski et al., 2000; Chakraborty et al., 2001, 2003a, 2003b), and hybrid methods (Stepnowski et al., 2003; Chakraborty et al., 2004; De and Chakraborty, 2009).

In addition, there are other methods for the classification of seafloor sediments, which do not use any specific feature vectors. Pouliquen and Lurton (1992) suggested a method based on the seafloor backscattering strength templates corresponding to different sediment types. These templates, once correlated with ground-truth sediment types, can be used as references for classification purposes. In another method, Kim et al. (2002) utilized a single variable called 'similarity index' for the classifications of seafloor. This index is computed from the singular value decomposition of adjoining acoustic profiling. De et al. (2005) demonstrated a very simple method to classify the seafloor sediments utilizing seafloor depth fluctuations. The fluctuations of seafloor depth obtained from a single-beam echo sounder at a particular location (in calm weather condition) are used in this method. The authors (De et al., 2005) utilized topographic roughness spectrum (computed from the depth fluctuations) to estimate the percentage composition of sand, silt, and clay in seafloor sediments.

It is reported (Kiesser et al., 2007) that the statistical or phenomenological approaches are commonly used to classify seafloor sediments with calibrated or un-calibrated (but consistent) data. However, data screening is the most essential part to

eliminate the inevitable unwanted artifacts for achieving better success in the classification.

In this chapter, statistical approaches for the classification of seafloor are explored. Background of various echo features; principal component analysis and cluster analysis are presented in the following sections. Later, the results on the classification of seafloor sediment based on principal component analysis and cluster analyses are discussed.

5.2 ECHO FEATURES

In this study, backscatter echo envelopes are averaged using 20 successive envelopes with 95% overlap (i.e., the echoes are averaged in a moving average sense with sequences 1-20, 2-21, 3-22, and so on till the end of the number of consistent echo envelopes available in the dataset). The time adjustment and the power compensation of the echoes are made (Clarke and Hamilton, 1999; Pouliquen, 2004) at a reference seafloor depth of 50 m (an approximate average of all the spot depths). Subsequently, 7 seafloor echo features are extracted from the normalized averaged echo envelopes. These features are: backscatter strength, statistical time-spread, statistical skewness, spectral skewness, spectral width, spectral kurtosis, and Hausdroff dimension.

5.2.1 Backscatter Strength

The backscatter strength (*BS*) in dB is computed from the record of a single-beam echo sounder using the following equation (Chakraborty et al., 2007a),

$$BS = 20\log_{10} < V[n] > -G_{tot} - R_{xs} - SL + 40\log_{10} R + 2\alpha_w R - 10\log_{10} A, \quad (5.1)$$

where $< V[n] >$ is the ensemble average of the voltage sequence of an averaged envelope with n number of samples; G_{tot} is the total gain (system plus operator gain) utilized in the echo sounder during recording; R_{xs} is the receiver sensitivity; SL is the source level; R is the range in meters; A is the area insonified by the acoustic beam.

5.2.2 Statistical Features

Two statistical features are calculated from echo waveforms in time domain (Tegowski and Lubniewski, 2000; Van Walree et al., 2005). These are called statistical time-spread (*TS*) and statistical skewness (*StatSkew*). *TS* and *StatSkew* are calculated using the following equations,

$$TS = \sqrt{\frac{4}{E_c}\int_0^{T_1} I(t)(t - t_c)^2 dt} \quad (5.2)$$

$$StatSkew = \frac{8}{(TS)^3 E_c}\int_0^{T_1} I(t)(t - t_c)^3 dt \quad (5.3)$$

Here $I(t)$ is the echo intensity, which varies quadratically with the recorded voltage, t_c is the echo center of gravity. E_c is the total energy of an echo and is defined as,

$$E_c = \int_0^{T_1} I(t)dt \quad (5.4)$$

The integral is computed over the time duration T_1= 10 ms of the echo waveform. It is important to note that the echo energy E_c does not possess the exact dimension of

energy (Van Walree et al., 2005), because only the relative values of E_c are important here. The term t_c is defined as,

$$t_c = \frac{1}{E_c} \int_0^{T_1} I(t) t dt \tag{5.5}$$

The feature *TS* is a measure of the temporal extent of an echo and it is equivalent to the second central moment in the time-domain. The *StatSkew* is a measure of the echo asymmetry and it is equivalent to the third moment in the time domain. The features *TS* and *StatSkew* are normalized by the echo energy (E_c) of the envelope, and therefore these two parameters are purely shape parameters, independent of echo energies. In addition, *StatSkew* is normalized by the third power of *TS* to ensure that the echo duration has no effect on *StatSkew*. Since the interface and the volume scattering contribution create an asymmetry in the echo envelope, the *StatSkew* feature has a positive value for the seafloor echoes. It is reported (van Walree et al., 2005) that *TS* offers a significant discriminating power even if the time adjustment of an echo envelope is not done.

5.2.3 Spectral Features

The spectral features are calculated from an echo envelope in a frequency domain. These spectral features are used for describing the shape of the echo envelope spectrum. The spectral moments are used for calculating these features. As the order of the moments increases, these moments become more sensitive to the presence of high frequency components. If $S(f)$ is the power spectral density of an echo envelope, then

the spectral moment m_n of the order n is defined as (Tegowski and Lubniewski, 2000, 2002),

$$m_n = \int_0^\infty S(f) f^n df \quad , n = 0, 1, 2, 3, 4 \tag{5.6}$$

The spectral moment m_0 represents the variance of an echo envelope. The spectral moment of the second order describes the concentration of spectral power around the mean frequency of the echo spectrum. The spectral skewness (*SpSkew*) is computed from the second and the third order moments and is defined as,

$$SpSkew = \frac{m_3}{m_2^{3/2}} \tag{5.7}$$

The echo spectral width (*SpWidth*) and the spectral kurtosis (*SpKurt*) are defined as,

$$SpWidth = \sqrt{\left(\frac{m_0 m_2}{m_1^2} - 1\right)} \tag{5.8}$$

$$SpKurt = \frac{m_4}{(m_2^2 - 3)} \tag{5.9}$$

The *SpSkew*, which is a measure of the spectral asymmetry, provides information on seafloor roughness (van Walree et al., 2005). The spectral width is a measure of the spectral power density concentration around the mean frequency. When the echo spectrum is extremely narrow (i.e., the total energy of the backscatter signal is concentrated around the center frequency), the value of *SpWidth* becomes small (i.e., $SpWidth \rightarrow 0$). On the contrary, the value of *SpWidth* increases when the spectral energy is broadly distributed among frequencies. The echo feature *SpKurt*, which is expressed by the higher order spectral moments, is tried in this study for obtaining the additional discrimination between sediments.

5.2.4 Hausdroff Dimension

The fractal feature, called Hausdroff Dimension (*HD*), is one of the echo features used in the present study. A fractal set is defined as a self-similar, scale-invariant geometric object (Mandelbrot, 1982). Again a geometric object is called scale-invariant, if it can be described as a union of rescaled copies of itself. The rescaled copies may not be strictly identical to the larger pieces, but they are statistically similar. There exist many fractal structures in nature such as tree leaves, clouds, or corrugated seafloors. Euclidean geometry is suitable for describing simple and regular figures. However, Euclidean geometry is not adequate for describing an irregular shaped object such as corrugated seafloor. In such cases, fractal dimension is used. The use of Hausdroff dimension to characterize the seafloor backscatter echo is based on an assumption that the echo sounder signal contains the fractal characteristics of a corrugated seafloor (van Walree et al., 2005).

Hausdroff dimension (*HD*) is a measure of the complexity or roughness of the shape of a given object. *HD* is defined as a limit (van Walree et al., 2005; Tegowski and Lubniewski, 2000),

$$HD = \lim_{r_0 \to 0} \frac{-\log N(r_0)}{\log r_0}, \tag{5.10}$$

where $N(r_0)$ represents the smallest number of open balls of radius r_0 needed to cover the object completely. Since, an echo envelope consists of a finite number of samples; the *HD* cannot be calculated, as the limit at radius r_0 tends to zero. Hence, an indirect method is used for the estimation of *HD* based on the autocorrelation function of an echo envelope (Tegowski and Lubniewski, 2000). This indirect method of estimation is briefed in the following paragraphs.

If an echo envelope $S(t)$ is assumed as the collection of rescaled version of itself within a given range of small time lag τ_L, then it obeys the Lipschitz-Hölder condition,

$$|S(t+\tau_L)-S(t)| \approx C_1 \tau_L^{\beta}, \tag{5.11}$$

where C_1 is a constant. The equation is valid within a range of small time lag τ_L, and the exponent β is called Lipschitz exponent. The *HD* of an echo envelope is then defined as,

$$HD = 2-\beta \tag{5.12}$$

The *HD* and the exponent β are treated as the measure of roughness of $S(t)$. When the value of β is close to 1 (i.e., *HD* is close to 1), then it indicates that the echo envelope $S(t)$ is smoother in nature. When β is closer to 0 (i.e., *HD* is close to 2), then it indicates that the seafloor return $S(t)$ is corrugated in nature. The autocorrelation function $R_{SS}(\tau_L)$ of $S(t)$ for a small time lag τ_L is defined as,

$$R_{SS}(\tau_L) = < S(t)S(t+\tau_L) > \tag{5.13}$$

The operator < > indicates ensemble averaging. By squaring and then averaging the above equation (5.11), we get,

$$< S(t)S(t+\tau_L) > = < \frac{S^2(t)+S^2(t+\tau_L)-C_1^2\tau_L^{2\beta}}{2} > \tag{5.14}$$

The statistical properties of $S(t)$ and $< S^2(t) >$ are independent of time. Therefore,

$$< S^2(t) > = < S^2(t+\tau_L) > \tag{5.15}$$

This gives, $$R_{SS}(\tau_L) \approx R_{SS}(0) - C_2\tau_L^{2\beta} \tag{5.16}$$

where $R_{SS}(0) = < S^2(t) >$ and C_2 is another constant.

Normalizing and taking logarithm of both sides of equation (5.16), we get

$$\ln[1-\bar{R}_{SS}(\tau_L)] = 2\beta \ln \tau_L + C_3, \tag{5.17}$$

where C_3 is a constant. $\overline{R}_{SS}(\tau_L)$ is the normalized autocorrelation function and is given by

$$\overline{R}_{SS}(\tau_L) = R_{SS}(\tau_L)/R_{SS}(0) \tag{5.18}$$

Now the exponent β (and *HD*) can be extracted approximately from the slope of a log-log plot of $[1-\overline{R}_{SS}(\tau_L)]$ versus τ_L (a small time lag), using a linear regression algorithm. The assumption on the fractal nature of an echo envelope $S(t)$ is valid when a straight line fits satisfactorily in the log-log plot of $[1-\overline{R}_{SS}(\tau_L)]$ versus τ_L for a range of small time lag.

5.3 BACKGROUND OF PRINCIPAL COMPONENT ANALYSIS

Principal Component Analysis (PCA) is an effective method to generate a new set of orthogonal variables for interpreting a large dataset (Jollife, 1986). These variables are called Principal Components (PCs). In other words, PCA computes compact and optimal description of a large dataset. The main use of PCA is to reduce the dimensionality of a dataset while retaining the information as much as possible. The individual PCs are ranked in an ascending order of the variances explained by the PCs. PCA is generally used as a pre-processor in a cluster method for the classification of seafloor sediments.

As mentioned earlier that principal component analysis generates a new set (*m* numbers) of orthogonal variables (Z_m), known as principal components. These components have a linear combination with the input variables X (the input dataset X contains *n* variables or feature vectors) such as,

$$Z_m = \sum_n a_{m,n} X, \tag{5.19}$$

where the coefficients ($a_{m,n}$) are computed from the variance-covariance matrix of the normalized input parameters X, satisfying the following relation.

$$\sum_n a_{m,n}^2 = 1, \text{ for each } m. \tag{5.20}$$

These coefficients ($a_{m,n}$) are called orthogonal eigenvectors of the variance-covariance matrix derived from the input variables matrix containing n feature vectors. The component Z_1 computed from the equation (5.19) is called the first principal component and it explains the maximum variances in the dataset. The variances of Z_m are arranged in an ascending order such that $\text{var}(Z_1) \geq \text{var}(Z_2) \geq \ldots \geq \text{var}(Z_m)$. The last few components, which explain the least variances, are generally removed from the subsequent analysis without losing any significant information. However, the number of components that can be removed from the analysis depends on the correlation between the input variables (Manly, 1994).

5.4 BACKGROUND OF CLUSTER ANALYSIS

Cluster analysis is a mathematical tool, which attempts to group the feature vectors in such a way that the features within a group are more similar to each other than those belong to different classes. There are two types of clustering: hard clustering and fuzzy clustering. Hard clustering assigns each feature vector to one and only one of the available clusters with a degree of membership equal to one and there exists well-defined boundaries between the clusters. Fuzzy clustering allows each feature vector to belong to more than one cluster at the same time with different degrees of membership (within 0 to 1) and there exists fuzzy boundaries between the clusters. Usually, it is

assumed that the number of cluster centers is known a-priori, but the location of cluster centers are not necessarily known in advance and an initial guess is necessary.

Hard clustering partitions a given dataset into a fixed number of non-overlapping cluster centers (centroids) by minimizing the distances between the data points and the cluster centers. Here the membership function takes the value of either 1 (if a particular data point belongs to a cluster) or 0 (otherwise). The performance of hard clustering mainly depends on the initial positions of the centroids. Therefore, the algorithm does not guarantee an optimal solution.

Fuzzy clustering is generally an objective function based algorithm and an optimal clustering is determined by minimizing the objective function. Each cluster is usually represented by a cluster prototype. This prototype consists of a cluster center with an additional information on size and shape of the cluster. The size and the shape parameters define the extension of a cluster in different directions. The degrees of membership for a given feature vector (or data points) are computed from the distances of data points to various cluster centers. The closer the data point lies to the center of a cluster, the higher is the degree of membership towards this cluster. Therefore, fuzzy clustering algorithm divides a given dataset into different clusters by minimizing the distances of data points to the cluster centers and by maximizing the degrees of membership.

In the present study, the most commonly used fuzzy algorithm, known as Fuzzy C-Means is employed as a supervised method for the classification of seafloor sediments. A brief background on Fuzzy C-Means is given below.

5.4.1 Fuzzy C- Means Cluster Algorithm

Fuzzy C-Means (FCM) algorithm is one of the most widely used methods in fuzzy clustering, initially proposed by Dunn (1973) and later generalized by others (Bezdek, 1981; Hathaway and Bezdek, 1988). It is based on a concept of fuzzy c-partitions, where each data point can belong to all the clusters with a varying degrees of membership value within 0 to 1. FCM is an iterative algorithm with an aim to find the cluster centers (also called centroids) by minimizing an objective function.

Let us assume that $X = \{x_1,...,x_n\}$ is a dataset, where each x_j is the individual data point. The membership matrix (U) is randomly initialized using the following equation

$$\sum_{i=1}^{nc} u_{ij} = 1, \quad \forall j = 1,...,n \tag{5.21}$$

where nc is the number of cluster centers ($2 \le nc < n$), n is the number of data points, and u_{ij} is the i^{th} membership function of the j^{th} data point. The objective function (J_F) is defined as

$$J_F(U, c_1, c_2,..., c_{nc}) = \sum_{i=1}^{nc}\sum_{j=1}^{n} u_{ij}^q \left\| x_j - c_i \right\|^2 = \sum_{i=1}^{nc}\sum_{j=1}^{n} u_{ij}^q d_{ij}^2 \tag{5.22}$$

Here the membership function u_{ij} assumes a value within 0 and 1; d_{ij} is the Euclidian distance between the i^{th} centroid (c_i) and the j^{th} data point x_j, the weighting exponent q (within [1, ∞]) is a constant that influences the membership values; and $[c_1, c_2,..., c_{nc}]$ is a matrix of the unknown cluster centers (prototypes).

The aim of FCM algorithm is to find an optimal fuzzy c-partition by minimizing the objective function J_F in the equation (5.22) (Bezdek, 1981). Initially, the elements

of the matrix of unknown cluster centers and the value of q are chosen. In addition, a random fuzzy c-partition matrix is initialized at the iteration number $p = 0$. For a given membership value $u_{ij}^{(p)}$, the cluster centers $c_i^{(p)}(i = 1,...,nc)$ at p^{th} iteration are calculated by

$$c_i^{(p)} = \frac{\sum_{j=1}^{n} (u_{ij}^{(p)})^q x_j}{\sum_{j=1}^{n} (u_{ij}^{(p)})^q} \tag{5.23}$$

Subsequently, the membership values of $u_{ij}^{(p)}$ are updated at $(p+1)^{th}$ iteration $(u_{ij}^{(p+1)})$ based on the values of cluster centers $c_i^{(p)}$. The iteration process stops when $\left|u_{ij}^{(p+1)} - u_{ij}^{(p)}\right| \leq \varepsilon$, where ε is a small positive constant or a pre-defined number of iterations. By iteratively updating the cluster centers and the membership grades for each data point, FCM iteratively moves the cluster centers to a stable position within a given dataset.

5.5 RESULTS AND DISCUSSION

5.5.1 Principal Component Analysis

It is already mentioned that the data used in this analysis consists of 7 echo features namely *BS*, *TS*, *StatSkew*, *SpSkew*, *SpWidth*, *SpKurt*, and *HD*. The variations in the values of these 7 features for different sediment types are shown in Fig. 5.1a and Fig. 5.1b respectively, for 33 and 210 kHz. Though each echo feature has a varying degree of discriminating power (van Walree, 2005; Tegowski and Lubniewski, 2002) to classify the seafloor sediments, these features have redundant information among them-

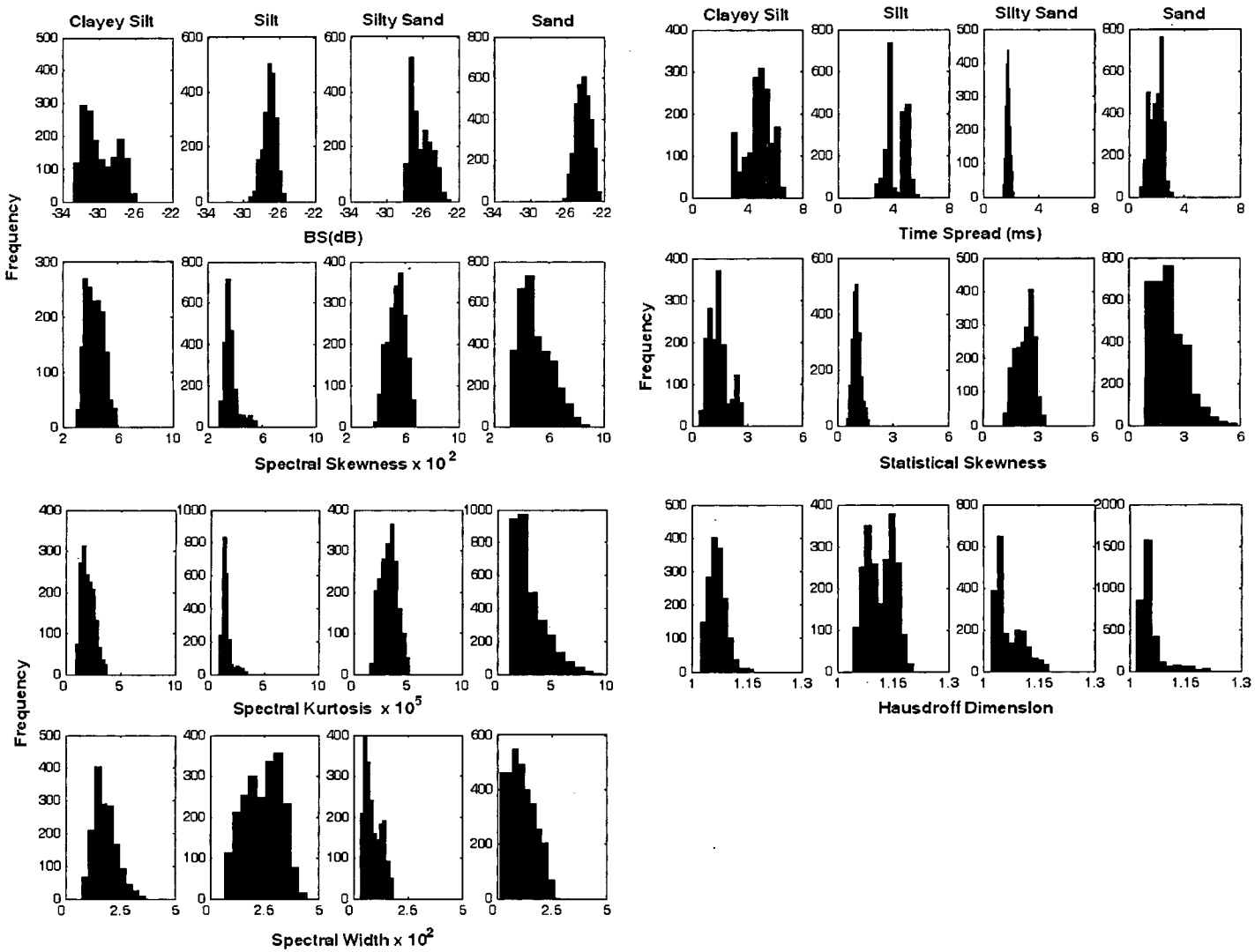

Fig. 5.1a Histograms of the 7 echo features for different sediment types at 33 kHz

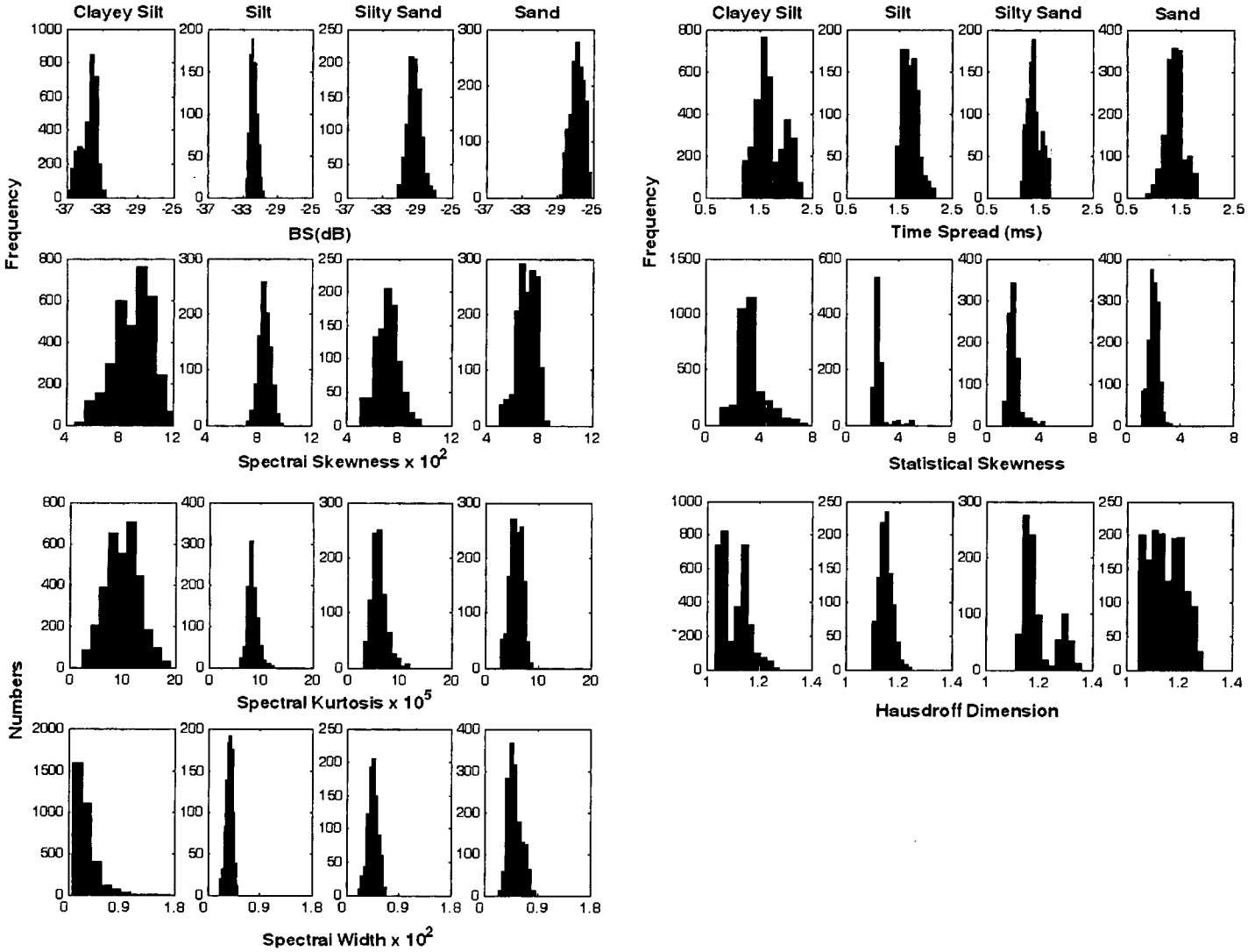

Fig. 5.1b Histograms of the 7 echo features for different sediment types at 210 kHz

-selves. Therefore, principal component analysis is carried out to reduce the dimensionality. Initially, all the echo features are normalized with zero mean and unit standard deviation. This standardization is essential to ensure that all the echo features have equal weights in the analysis. The functions available in the Statistical Toolbox of MATLAB 7.0 (2004) are used for the present analysis. Each principal component is linearly related to the input variables (i.e., 7 echo features) through the eigenvectors or the coefficients (as discussed earlier). The computed eigenvectors ($a_{m,n}$) are given in Table 5.1 (for 33 kHz) and in Table 5.2 (for 210 kHz).

Table 5.1 Orthogonal eigenvectors ($a_{m,n}$) and the percentages of variation accounted for by each principal component for 33 kHz.

Features	Orthogonal eigenvectors						
	$a_{1,n}$	$a_{2,n}$	$a_{3,n}$	$a_{4,n}$	$a_{5,n}$	$a_{6,n}$	$a_{7,n}$
BS ($n = 1$)	0.14	0.82	0.01	0.4	-0.38	0.01	-0.04
SpSkew ($n = 2$)	0.44	-0.19	0.29	0.07	-0.09	0.38	-0.73
SpKurt ($n = 3$)	0.43	-0.18	0.35	0.19	-0.07	0.4	0.68
SpWidth ($n = 4$)	-0.42	0.07	0.25	0.57	0.61	0.23	-0.07
TS ($n = 5$)	-0.37	-0.47	0.02	0.49	-0.62	-0.13	-0.03
StatSkew ($n = 6$)	0.44	-0.1	0.23	0.3	0.23	-0.78	-0.02
HD ($n = 7$)	-0.32	0.16	0.82	-0.37	-0.17	-0.16	0.0
Variance (%)	66.1	18.2	9.4	3.7	1.4	1.0	0.2

Table 5.2 Orthogonal eigenvectors ($a_{m,n}$) and the percentages of variation accounted for by each principal component for 210 kHz

Features	Orthogonal eigenvectors						
	$a_{1,n}$	$a_{2,n}$	$a_{3,n}$	$a_{4,n}$	$a_{5,n}$	$a_{6,n}$	$a_{7,n}$
BS ($n = 1$)	0.34	-0.4	-0.33	-0.73	-0.24	0.11	-0.03
SpSkew ($n = 2$)	-0.46	-0.14	-0.03	-0.11	0.25	0.45	-0.7
SpKurt ($n = 3$)	-0.46	-0.11	-0.14	-0.07	0.07	0.51	0.7
SpWidth ($n = 4$)	0.42	0.01	0.43	0.22	-0.4	0.65	-0.05
TS ($n = 5$)	-0.13	0.81	0.16	-0.53	-0.13	0.07	-0.01
StatSkew ($n = 6$)	-0.42	-0.01	-0.27	0.19	-0.82	-0.13	-0.13
HD ($n = 7$)	0.31	0.38	-0.77	0.28	0.13	0.27	-0.07
Variance (%)	63.2	17.4	8.8	5.4	3.3	1.8	0.1

The results (in Table 5.1) reveal that the first principal component accounts for 66.1% of the variability of the total variance. The rest of the principal components carry 18.2%, 9.4%, 3.7%, 1.4%, 1.0%, and 0.2% of the variability respectively of the total variance. The first three principal components together explain 94% of the total variability of the dataset. Therefore, the rest of the principal components (which explain only 6% of the variability of total variance) can be ignored for further analysis. The relative contributions of four echo features (*SpSkew*, *SpKurt*, *StatSkew*, and *SpWidth*) to the first principal component have comparable magnitudes. The second and the third PCs are highly dominated by *BS* and *HD* respectively.

In case of 210 kHz, the results reveal that the first principal component accounts for 63.2% of the total variability and the rest of the components explain 17.4%, 8.8%, 5.4%, 3.3%, 1.8%, and 0.1% variability of the dataset respectively. The first three principal components together explain 89% of the variability of the total dataset. The remaining 11% of the variability is explained by the other four principal components. The relative contributions from *SpSkew*, *SpKurt*, *SpWidth*, and *StatSkew* are comparable in the first PC, whereas the contributions from *TS* and *HD* are prominent in the second and in the third PCs. Though backscatter strength is considered as one of the prominent echo features in the classification of seafloor sediments, this principal component analysis shows that the contributions from *BS* is prominent only in the fourth PC, which accounts only 5% of the total variance for 210 kHz.

5.5.2 Fuzzy C-Means Cluster Analysis

The number of principal components that can be used for further analysis depends on the contributions of various inputs to the PCs (Manly, 1994) (as stated earlier). The first three PCs, which account for 94% and 89% of the total variance

respectively at 33 and 210 kHz, are used in the cluster analysis using FCM algorithm. The functions available in Fuzzy Logic Toolbox of MATLAB 7.0 (2004) are used for the FCM cluster analysis. The various parameters used in FCM algorithm are: exponent for the membership function matrix - 2.0, maximum iterations - 200, minimum improvement value - 1e-5. The most important input parameter in cluster analysis is the optimum number of cluster centers. As such, there is no specific rule to decide the number of cluster centers for a given dataset (Legendre, 2003; van Walree et al., 2005). Therefore, a priori knowledge on the number of cluster centers is essential for cluster analysis. Four different types of sediments exist in this study area. This ground-truth information is used to decide that the number of available cluster centers is four. The results obtained from FCM analysis using the first three PCs with four cluster centers are given in Table 5.3 for 33 and 210 kHz.

Table 5.3 FCM Results using first three PCs for 33 and 210 kHz (with 4 cluster centers)

Stn. No	Percentage of classification								Sediment type from FCM		True sediment type
	Sand		Silty Sand		Silt		Clayey Silt				
	33 kHz	210 kHz	33 kHz	210 kHz	33 kHz	210 kHz	33 kHz	210 kHz	33 kHz	210 kHz	
1	0	0	0	0	0	48	100	52	CS	CS	CS
2	0	0	0	0	0	1	100	99	CS	CS	CS
3	0	0	0	0	0	1	100	99	CS	CS	CS
4	0	0	0	0	16	97	84	3	CS	Si	CS
5	0	23	0	61	0	16	100	0	CS	SS	CS
8	0	0	0	0	33	100	67	0	CS	Si	CS
13	0	0	0	0	0	100	100	0	CS	Si	CS
9	0	0	0	0	99	100	1	0	Si	Si	Si
10	0	1	0	5	53	94	47	0	Si	Si	Si
14	11	0	1	0	0	96	88	4	CS	Si	Si
11	6	72	94	13	0	12	0	3	SS	Sa	SS
17	10	86	90	14	0	0	0	0	SS	Sa	SS
18	63	0	37	100	0	0	0	0	Sa	SS	SS
19	95	0	0	100	5	0	0	0	Sa	SS	SS
6	100	100	0	0	0	0	0	0	Sa	Sa	Sa
7	86	100	14	0	0	0	0	0	Sa	Sa	Sa
12	62	96	38	4	0	0	0	0	Sa	Sa	Sa
15	2	0	98	100	0	0	0	0	SS	SS	Sa
16	8	42	92	58	0	0	0	0	SS	SS	Sa
20	79	0	0	100	21	0	0	0	Sa	SS	Sa

The results (in Table 5.3) show that clayey silt sediments are well classified (with the overall average 93%) at 33 kHz. However, the overall averages of correct classification for silt, silty sand, and sand sediments are 51%, 55%, and 56% respectively at 33 kHz. For 210 kHz, silt sediments are well classified (with the overall average 97%), whereas clayey silt, silty sand, and sand sediments are poorly classified (with the overall averages 36%, 57%, and 56% respectively). The results reveal that seafloor sediments are well classified at very few locations in the study area. The classification with 33 kHz shows relatively consistent results as compared to 210 kHz. However, the overall successes in classifying the seafloor sediments with PCA-FCM analysis are not encouraging in this study area.

5.6 CONCLUSIONS

The results indicate that the cluster analysis in combination with the principal component analysis did not provide any significant success in the classification in this study area. The information on the optimal number of cluster centers available in a dataset is one of the essential inputs for the cluster analysis. This information is generally obtained a-priori from the ground-truth in the study area. The requirement of a-priori information on the ground-truth in a study area limits the effective use of PCA-FCM analysis for the classification of seafloor sediments in an unknown area.

This chapter discussed the results obtained from seafloor echo features analysis using PCA-FCM method. The next chapter introduces the basic concepts of artificial neural networks and their application for the selection of prominent echo feature subset to classify the seafloor sediments.

Chapter 6

Neural Networks Based Selection of Echo Features

6.1 INTRODUCTION

An Artificial Neural Network (ANN) is a nonlinear information processing system especially useful for mapping input vectors to specific outputs, where no hard and fast rules are applicable. An ANN uses mathematical algorithms to learn the relationships and the patterns in a given dataset.

ANN is an analogy of a biological neuron (Hertz et al., 1991). The schematic diagram of a biological neuron is shown in Fig. 6.1. A human brain is composed of about 10^{11} neurons (nerve cells). Tree like networks of nerve fiber is called dendrites and these are connected to a cell body, which contains nucleus. A single long fiber extending from the cell body is called axon, which eventually branches into strands and sub-strands. The ends of these branches are called synaptic junction or synapses, which transmit signals to the other neurons. The receiving ends of these junctions on other cells may be located on the dendrites as well as on the cell bodies. A few thousand synapses exist on the axon of a typical neuron. The transmission of a signal from one cell to the other through synapses is a complex chemical process. Specific chemicals are released from the sending side of the junction to raise or lower the electrical potential

inside the body of a receiving cell. When this potential reaches a threshold value, a pulse, called action potential, with certain strength and duration is fired through the axon. The pulse moves from one cell to the other through these synapses. After firing, a cell waits for a specific time, called the refractory period, before the next firing.

The aim of an artificial neural network is to imitate neurons in a brain and its ability to adapt to the current situation and the changing circumstances. The performance of a neural network depends heavily on the ability to learn from the past events and apply this information to a future situation. In general, a neuron receives inputs from the outside, performs non-linear operations on them, and then outputs the final results. The fundamental processing element of a neural network is called neuron.

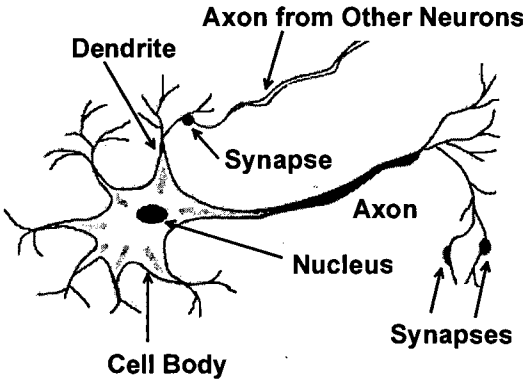

Fig. 6.1 Schematic diagram of a typical biological neuron

In ANN, several neurons (also called nodes) are interconnected according to some topology to perform a specific task. The output of each neuron may be given to several neurons. The amount of output from one neuron received by another neuron depends on the strength of the connection between the neurons and it is called weight (or synaptic weight) of the connection links. At any instant of time, each neuron has a unique activation value and a unique output value. In a typical operation, each neuron of an ANN receives inputs from other interconnected neurons and/or from the external

source. A weighted sum of the inputs and a specific activation value determine the actual output of an ANN. Therefore, an artificial network consists of architecture (i.e., the topology) of a network, training or learning algorithm (of the weights between neurons), and activation function (Beale and Jackson, 1990).

Fundamentals of artificial neural networks are covered in several books (Beale and Jackson, 1990; Hertz et al., 1991; Yegnanarayana, 2001; Sivanandam et al., 2006). However, the basics of neural networks and in particular backpropagation networks are presented of this chapter. Later, an analysis on the relative importance of different subsets of echo features for seafloor classification using multilayer perceptron networks (with backpropagation training) is presented.

6.1.1 ANN Terminologies

6.1.1.1 Weight

It is mentioned that the strength associated with the interconnection between two neurons is termed as weight of that connection. Weight in a neural network is the information used by the network to solve a specific problem. The inputs to a neuron may come from the outputs of other neurons or from external sources. The amount of output of one neuron received by another neuron depends on the strength of the interconnection (or weights) between the neurons.

6.1.1.2 Activation Function

The activation function (also called the transfer function) determines the actual output from a neuron. The activation function may be linear as well as non-linear. Each

input signal (let's say x_i) is multiplied by a weight (let's say w_i) and the product is summed. The summation of the products is called *NET*

$$NET = \sum_i x_i w_i \tag{6.1}$$

An activation function is applied to modify the sum of the weighted input signal (i.e., *NET*) to produce the output signal. The activation function is differentiable at every point. This function does not allow the output to exceed a very low and a very high limit regardless of the value of *NET*, and hence it is also called a squashing function. If the function is linear, then the output is equal to *NET*. A non-linear activation function is generally used to map a non-linear process. In general, a logistic or a squashing function, called a *sigmoid* function (S-shaped function), is used because of its self-limiting nature (Beale and Jackson, 1991; Hertz et al., 1991). The sigmoid function is given by

$$y = F(NET) = \frac{1}{1+e^{-NET}} \tag{6.2}$$

This is also called a log sigmoid (or *logsig*) function. The *logsig* function compresses the inputs into a range within 0 to 1 (Fig. 6.2). Basically, the activation function acts as a nonlinear automatic gain control for an artificial neuron. The magnitude of the gain is the slope of the curve (of the activation function) at a specific excitation level. For a small value of *NET* (near to zero), the gain is very high. This central high gain region of a logistic function is useful to solve the problem of processing small signals, whereas the extreme positive and negative regions with low gain are appropriate for large excitations.

Another activation function is the bipolar sigmoidal function. This function is called a hyperbolic tangent function (Hertz et al., 1991) and is given by

$$y = F(NET) = \tanh(NET) = \frac{e^{NET} - e^{-NET}}{e^{NET} + e^{-NET}} \tag{6.3}$$

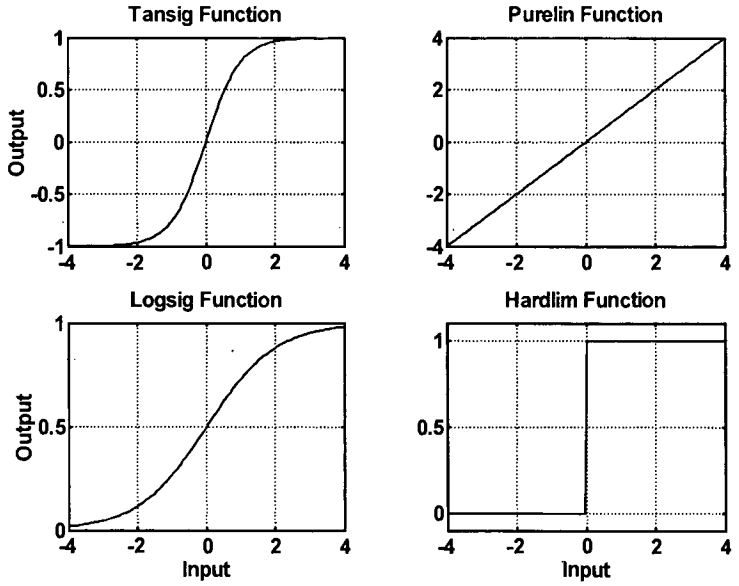

Fig. 6.2 Showing the shapes of four commonly used activation functions

The hyperbolic tangent function is symmetrical about the origin within a range +1 to -1. When the value of *NET* is zero, the output is also zero. This is also called tan sigmoid (or *tansig*) function. Few more transfer functions are also available such as *purelin, hardlim, poslin. Purelin* is a linear function, where inputs and outputs are linearly related. *Hardlim* function has only two outputs either 0 or 1. The output of *poslin* function assumes any positive value, linearly scaled without any restriction of range. The transfer function *poslin* returns the output *n*, if *n* (an integer) is greater than zero and 0 if *n* is less than or equal to zero. The shapes of four activation functions (*tansig, purelin, logsig*, and *hardlim*) are shown in Fig. 6.2.

6.1.1.3 Bias

Bias is a weight, which is always initialized to a value of 1. It is often advantageous to have a bias weight for rapid convergence of a training process. Bias

weight allows a neuron to have an output even if the input is zero. The main purpose of a bias is to shift the origin of an activation function. These weights are trainable just as the other weights. If a bias (b) is present, then the NET is calculated as (Sivanandam et al., 2006),

$$NET = b + \sum_i x_i w_i \tag{6.4}$$

6.1.1.4 Threshold

The threshold is a limiting value of a neuron to produce an output. The weighted sum of inputs must reach or exceeds the threshold value (Hertz et al., 1991) for a neuron to fire (i.e., to get an output). The binary step function is an example of the threshold function. In the presence of threshold (θ_{th}), the equation (6.4) is written as,

$$NET = \left(b + \sum_i x_i w_i \right) - \theta_{th} \tag{6.5}$$

6.1.1.5 Training

Training is a process to modify the weights of interconnection between various layers of a network with an objective to achieve expected output (Sivanandam et al., 2006). The process that takes place inside a network during training is called learning. There are three types of training such as supervised training, unsupervised training, and reinforcement training. Supervised training of a network is the process of learning when the expected target outputs (response vectors) are available. Examples of supervised training algorithms are: Hebb net, backpropagation net etc. If the expected target output is not available, the training method adopted is termed as unsupervised training. In the unsupervised training, the weights of the network are adjusted in such a way that the

similar input vectors are assigned to the same output unit. The reinforcement training is a type of supervised training. The desired output vector is not available in this case, but the condition whether the output is a success or failure is indicated. The network uses this information to improve its performance to learn the input-output mapping through a trial and error process. The supervised backpropagation learning method is discussed in this chapter. Other methods, called Kohonen's competitive unsupervised and supervised learning are discussed in Chapter 7.

6.1.2 Fundamental Model of Artificial Neural Network

McCulloch and Pitts (1943) formulated a synthetic neuron model, based on the concept of a simplified biological model. The input values are connected to neurons either by excitatory (positive) or inhibitory (negative) weights (Fig. 6.3). A neuron fires if the net input to the neuron is greater than a threshold value. Any number of inputs can be added to a neuron. In Fig. 6.3, the inputs x_i, $i = 1, \ldots, n$ are connected to neurons by excitatory weights w_i, and the inputs $x_j, j = n+1, \ldots, n+m$ are connected to neurons by inhibitory weights w_j. The output signal of McCulloch and Pitts model is expressed by the following equations:

$$y = F(NET), \tag{6.6}$$

$$\text{where} \quad NET = (\sum_i w_i x_i + \sum_j w_j x_j) - \theta_{th} \tag{6.7}$$

The function F is called the activation function, θ_{th} is the threshold, and NET is the total net input signal received by the neuron (without bias term).

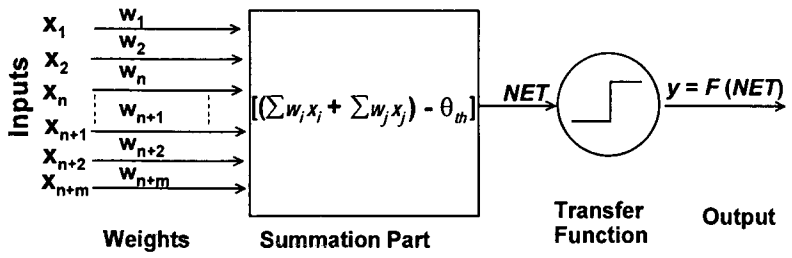

Fig. 6.3 Showing a schematic diagram of McCulloch-Pitts model

The activation function in McCulloch-Pitts is given by (Hertz et al., 1991),

$$F(NET) = \begin{cases} 1, & if \quad NET \geq \theta_{th} \\ 0, & if \quad NET < \theta_{th} \end{cases} \tag{6.8}$$

6.1.3 Perceptrons

Layered feed-forward network is called a perceptron. Rosenblatt (1962) and Minsky and Papert (1969) developed this network. There were three layers in the original perceptron e.g., sensory unit, association unit, and response unit (Fig. 6.4a). The sensory and association units have binary activations. The response unit uses activations of +1, 0, or -1. All the units have their own weights. The association unit performs the predetermined mathematical operations on its inputs. The difference between the McCulloch-Pitts model and the perceptron model is that the learning function (adjustment of weights) is introduced in the perceptron (Fig. 6.4b). The desired or target output (T) is compared with the actual output (y), and the error (δ) is calculated to adjust the weights. The output signal is given by $y = F(NET)$, where $NET = (\sum_i w_i x_i + b) - \theta_{th}$. The error term is calculated as, $\delta = (T - y)$. If the error associated with the input vector x_i is δx_i, then the change in weight (Δw_i) is expressed as, $\Delta w_i = \eta \delta x_i$, where η is called the learning rate parameter (Yegnanarayana, 2001).

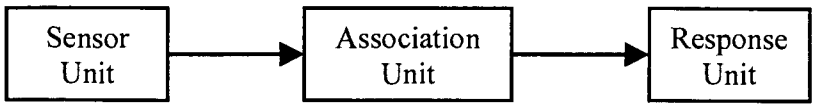

Fig. 6.4a Block diagram of a perceptron

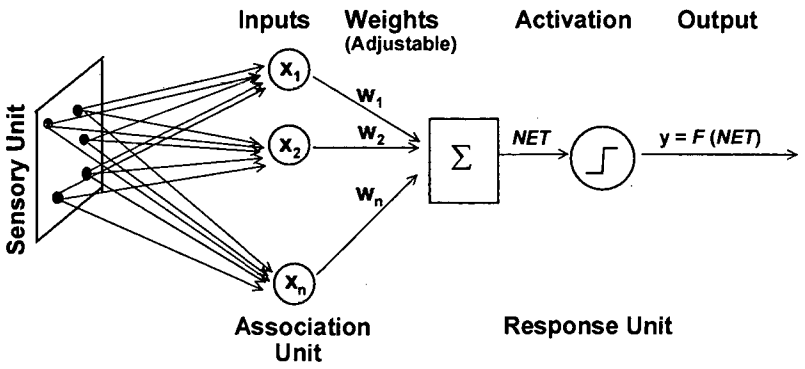

Fig. 6.4b Rosenblatt's perceptron model

A single layer perceptron is the simplest form of a neural network. This type of network model is generally used for the classification of patterns that are linearly separable. There exists another class called MultiLayer Perceptron (MLP). This type of network consists of a set of sensory units with an input layer and one or more hidden layers. These hidden layers are useful for performing complicated tasks, but at the cost of a lengthy learning process. Feed forward network is an example of MLP network.

6.1.4 Network Architectures

The arrangement of neurons into layers and the pattern of connections among the neurons in various layers are termed as neural network architecture (Beale and Jackson, 1990). Schematic diagrams of a simple network and a multilayer network are shown in Fig. 6.5a and Fig. 6.5b respectively. There is no maximum limit to the number

of layers or the number of neurons in a layer. However, computational requirement increases with the increase in the number of neurons (and weights). There are various types of network architectures such as feed forward net, feedback net, competitive net, and recurrent net.

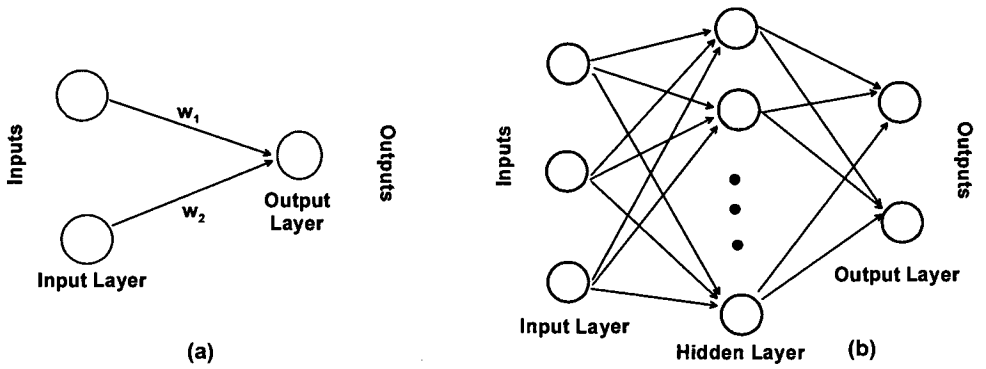

Fig. 6.5 Schematic diagram of **(a)** a simple network **(b)** 3 layers network architectures

In a feed forward network, signal propagates in the forward direction from input layer to output layer i.e., in this network signal travels in only one direction from the input to the output. There are no feedback loops i.e., the output of any layer does not affect the same layer. The feed forward network can be a simple network, where inputs are directly connected to the outputs through only one layer of weighted interconnections. It may also have multiple layers with one or more hidden layers between the input and the output layers. Multilayer network (as shown in Fig. 6.5b) is advantageous over a single layer network to solve complicated problems. Backpropagation network is one of the most important types of feed forward network.

In a feedback network, the signals can travel in both the direction through the network. These networks are dynamic i.e., the state changes continuously till they reach an equilibrium position. A general form of a feedback network consists of a set of processing units, where the output of each unit is fed as input to all the other units

including the same unit. A feedback network does not have any specific structure (Yegnanarayana, 2001). Hopfield network is an example of a feedback network.

A competitive network (Fig. 6.6) is similar to a feed forward network. The difference is that there are connections between the output neurons in a competitive network. Due to these interconnections, the output nodes tend to compete each other to represent an input pattern. The output nodes are connected to each other (or connected to the neighborhood nodes only).

In a fully recurrent network, all the nodes are connected to the rest of the nodes and every node acts as an input as well as an output (Fig. 6.7). For each input pattern, the weights of all the units are modified. The advantage is that if a degraded version of one of the patterns is presented as input, the network tries to reconstruct the true pattern. The examples of recurrent net are the simple recurrent network and the Jordan network.

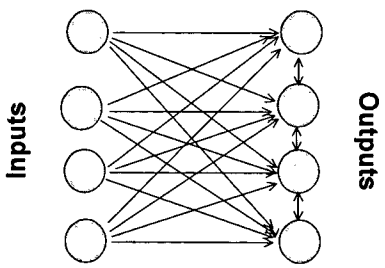

Fig. 6.6 Schematic diagram of a competitive network

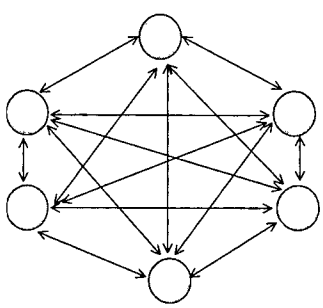

Fig. 6.7 Schematic diagram of a fully recurrent network

6.2 BACKPROPAGATION NETWORK

Backpropagation network is a type of multilayer feed forward network. Rumelhart et al. (1986) first introduced the backpropagation network. Backpropagation network is an efficient supervised learning method to capture the inherent characteristics of a given set of input-output pairs. As the backpropagation method is based on an error-correction learning rule, it is also known as error backpropagation algorithm. It consists of two processes: a forward process and a backward process (Fig. 6.8). In the forward process, a set of outputs is produced through the applications of activation functions to the inputs of a network. During the forward process, fixed synaptic weights are used at different layers of the network. The error signal (deviation of the actual output from the desired response) is propagated backward through the network. The synaptic weights are adjusted (when a signal propagates in the backward direction) based on some form of the error-correction rule (Hertz et al., 1991).

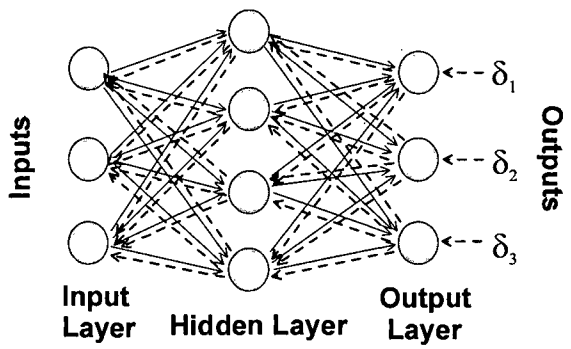

Fig. 6.8 Schematic diagram of a single hidden layer backpropagation network. The solid lines indicate forward propagation of signals and the dashed lines indicate backward propagation of errors (δ_i).

Backpropagation network utilizes the feed forward network with differentiable activation function. The training of a backpropagation network is based on some

algorithm to minimize the total error of the network output. The error function is a measure of the deviation between the desired and the actual output of a network. The mean square error for the m^{th} training pattern is defined (Masters, 1993) as

$$E_m = \frac{1}{N}\sum_{j=1}^{N}(T_{mj} - O_{mj})^2, \tag{6.9}$$

where E_m is the error for the m^{th} training pattern; T_{mj} is the desired (correct) output value of the j^{th} output neuron ; and O_{mj} is the actual output from the j^{th} output neuron; N is the total number of output neurons. Therefore, the total error (E) for all the training patterns is obtained from $E = \sum_m E_m$. By squaring the absolute error (between the desired and the actual output in the equation (6.9)), it is ensured that the distant output from the desired value contributes more strongly in the summation of total error.

6.2.1 Backpropagation Training Algorithms

There are number of training algorithms, which can be used with a backpropagation network. The algorithms namely gradient descent method, variable learning rate backpropagation with momentum, Levenberg-Marquardt backpropagation, and resilient backpropagation methods are commonly used. These methods are introduced in the following sections.

6.2.1.1 Gradient Descent Method

Gradient descent method, also called the steepest descent method, utilizes a negative gradient of an error function with respect to the weights for rapid reduction of

the error function. The gradient (Δw_{ji}) i.e., the change in the weight (w_{ji}) for the i^{th} source neuron in a layer to the j^{th} destination neuron in the next layer is expressed as,

$$\Delta w_{ji} \propto -\frac{\partial E_m}{\partial w_{ji}}, \tag{6.10}$$

where E_m is the error for the m^{th} input training vector. This can be expressed as,

$$\Delta w_{ji} = \eta \delta_{mj} O_{mi} \tag{6.11}$$

Here the constant of proportionality, η is known as the learning rate and it governs the distance moved in the direction of negative gradient at each step. O_{mi} is the output of the i^{th} neuron for the m^{th} training vector. δ_{mj} is the error at the j^{th} output neuron in a layer for the m^{th} training vector and is expressed as,

$$\delta_{mj} = (T_{mj} - O_{mj}) O_{mj} (1 - O_{mj}), \text{ For output neurons} \tag{6.12}$$

$$\delta_{mj} = O_{mj} (1 - O_{mj}) \sum_n \delta_{mn} w_{nj}, \text{ For hidden neurons} \tag{6.13}$$

Here T_{mj} is the desired output value from the j^{th} neuron; O_{mj} is the actual output of the j^{th} neuron; and δ_{mn} is the error signal at the n^{th} neuron in the hidden layer. Finally the change in weights ($\Delta w_{ji}(p+1)$) at $(p+1)^{th}$ iteration are adjusted by utilizing the change in weights ($\Delta w_{ji}(p)$) at p^{th} iteration. This is expressed by the equation,

$$\Delta w_{ji}(p+1) = \eta \delta_{mj} O_{mi} + \alpha_m \Delta w_{ji}(p), \tag{6.14}$$

where α_m is called momentum constant (lies within 0 and 1) and is used for rapid convergence. To speed up the convergence time, the variable learning rate is generally used. A larger learning rate is utilized during training when the neural network model is far from the desired target and a smaller learning rate is used when the neural model approaches towards the desired target.

6.2.1.2 Levenberg-Marquardt Algorithm

Levenberg-Marquardt algorithm minimizes the total error of a network by solving the equation,

$$(J^t J + \mu_L I)\Delta w_{ji} = J^t E_m \tag{6.15}$$

where J is the Jacobian matrix containing first derivatives of the network errors with respect to the weights; J^t is the transpose of J; I is the identity matrix; and μ_L is the Levenberg's damping factor controlling the behavior of the algorithm. The new weights at (p+1) iteration are calculated as,

$$w_{ji}(p+1) = w_{ji}(p) - \Delta w_{ji}(p) = w_{ji}(p) - (J^t J + \mu_L I)^{-1} J^t E_m \tag{6.16}$$

The term $J^t J$ is called Hessian matrix and it is computationally very intensive.

The Levenberg-Marquardt algorithm is very sensitive to the initial weight vectors used for training a network. A network can only be solved with the Levenberg-Marquardt algorithm if the Hessian matrix is not singular.

6.2.1.3 Resilient Backpropagation Algorithm

Sigmoid transfer functions are generally used in the hidden layers of a multilayer network. If the inputs to these functions are large, the slopes of these functions approach to zero. This creates a problem with the gradient approach based algorithms for training a neural network with a sigmoid function. Therefore, a small gradient makes small changes during the adjustment of weights and biases, even if the weights and biases are far from their optimum values.

Resilient backpropagation algorithm eliminates these limitations of partial derivatives based algorithms. In this algorithm, only the sign of the derivative is used to determine the direction of the weights update; and thus the magnitude of the derivative does not play any role in the weights update. The magnitude of the change in weights is controlled by a separate update value. When the derivatives of two successive iterations have the same sign, the update value for each weight and the bias is increased by a separate value. This update is also called the increment in weight change. The update value is decreased (called the decrement in weight change) when the sign of the derivative changes from the previous iteration. If the derivative is zero, then the update value remains unchanged. If the change in weight continues in the same direction for several iterations, then the magnitude of the change in weight is increased. A function '*trainrp*' is available in the Neural Network Toolbox of MATLAB 7.0 (2004), which uses resilient backpropagation algorithm for training a network.

One complete presentation of all the input vectors (i.e., pattern) available in a training set is called the epoch. When the total error of a network reaches or falls below a pre-defined stopping criterion (either based on the maximum number of epoch or the pre-defined acceptable error limit), the network is said to have converged. Several such epochs are necessary to train a network for solving a specific problem.

6.2.2 Performance of a Neural Network

The performance of any neural network is expressed by an error between the predictions of a network and the true value. The Mean Square Error (MSE) is one of the methods to measure this error. A test dataset is generally used for evaluating the performance of a trained network. During the testing, it is assumed that the true values

of outputs (the desired outputs) are known in advance. The MSE is obtained from the difference between the desired target output and the achieved output by a network (as given in the equation (6.9)).

6.3 MLP NETWORKS BASED FEATURES SELECTION

One of the most widely used neural networks in the classification of seafloor sediments is the multilayer perceptron (MLP) with backpropagation (Stewart et al., 1992; Alexandrou and Pantzartzis, 1993; Stewart et al., 1994; Michalopoulou et al., 1995; Chakraborty, 2002; Chakraborty et al., 2003a). As mentioned earlier that most of the neural network based seafloor classification techniques use echo features as inputs, which are usually derived from the seafloor backscatter data. Selection of echo features as input variables to a neural network is an important criterion for achieving the higher success in the classification. Improper selection of the input features leads to difficulties in converging the training of a neural network (thus increasing the computational time). As such there is no general rule for deciding the best features for a given problem (Chakraborty, 2002). It is widely accepted that the selection of input features mainly application oriented and depends on the physical processes under study (Stewart et al., 1994).

In the present analysis, 7 echo features (as discussed in Chapter 5) namely: *BS*, *SpSkew*, *SpKurt*, *SpWidth*, *TS*, *StatSkew*, and *HD* are utilized. The relative importance of different subsets of echo features (among the 7 features) for the classification of seafloor sediments using MLP networks (trained with resilient backpropagation algorithm) is investigated. A set of features chosen out of the 7 echo features is termed as the feature subset in this work. An optimum subset of features with dominant characteristics is

decided on by analyzing the effects of different subsets of echo features on the performance of a given MLP network.

6.3.1 Pre-Processing of Input Data

Preparation of input data is one of the important aspects in neural network analysis. A uniform scaling is essential to equalize the importance of all the variables. The training algorithm uses the total error (from all the outputs) minimization scheme. If the output variables are unequally scaled, the variables with larger variability will be given importance, as these will dominate the total error.

To constrain the range of each input variable, the input data are often rescaled to a new uniform range of values. In this study, the input data are scaled in such a way that all the values lie within an interval -1 and +1 using the relationship (Neural Network Toolbox in MATLAB 7.0, 2004),

$$Xs = 2\left[\frac{(X - MinX)}{(MaxX - MinX)}\right] - 1 \tag{6.17}$$

where, X is the input data, $MinX$ is the minimum value of X, $MaxX$ is the maximum value of X, and Xs is the scaled output of X. Moreover, scaling of data is carried out in such a way that the data used in training are proportional with that used for testing the network.

6.3.2 Methodology

Previous studies indicate that a feed-forward neural network with one hidden layer is sufficient to solve a majority of practical problems (Masters, 1993). Hence, a

three-layer network (i.e., with a single hidden layer) is selected in this study to investigate the relative importance of different subsets of echo features on the performance of a given network for the classification of seafloor sediments. The output layer consists of two neurons. Two neurons are sufficient to classify four types of sediments (such as [00], [01], [10], and [11]). The number of neurons in the hidden layer is safely chosen as 20. The number of neurons in the input layer varies from 2 to 7. Thus, 6 network configurations such as [2-20-2] (i.e., 2 input neurons, 20 hidden neurons, and 2 output neurons), [3-20-2], [4-20-2], [5-20-2], [6-20-2], and [7-20-2] are considered in this study.

Initially, few trials are made to assess the consistencies of the success rates of these 6 network configurations with varying number of hidden neurons ranging from 5 to 30. It is observed that 12 to 14 neurons in the hidden layer are necessary to achieve the optimized result when the number of neurons in the input layer changes from 2 to 4. Similarly, it is also observed that 16 to 20 neurons in the hidden layer are required to achieve the consistency in the success rate using different subsets of echo features when the input neuron number changes from 5 to 7. The increase in the number of neurons in the hidden layer (beyond an optimized value for a given network configuration) does not increase the success rate in the classification, however, the computational time marginally increases. Since the aim of this study is to select an optimum feature subset using MLP networks, the number of neurons in the hidden layer is safely chosen as 20 (which is sufficient to produce consistent results using all the 6 network configurations considered in this study).

Sigmoidal transfer function such as tan sigmoid is used as an activation function in each layer of a three-layer network. Resilient backpropagation algorithm is used as training algorithm of the MLP network. The Neural Network Toolbox available in

MATLAB 7.0 (2004) is used in this study. Various training parameters are: learning rate - 0.05; increment in weight change - 1.2; decrement in weight change - 0.5; initial weight change - 0.07; maximum weight change - 50; and epochs - 6000. A fixed 15% of the total input dataset (consisting of 7 echo features) is optimally used as training dataset and the remaining 85% of the total dataset is used as a validation (or testing) dataset.

It is mentioned that the performance of a neural network for classification of seafloor sediments greatly depends on the training dataset. Significant performance can be achieved if suitable echo features with sufficient discriminating characteristics are chosen optimally for training a neural network. A series of experiments are carried out with different subsets of echo features as inputs to the three-layer MLP network. Different subsets of echo features consist of 2, 3, 4, 5, and 6 features (taken at a time out of the 7 echo features). The overall percentages of success to classify seafloor sediments are evaluated with all these subsets. Accordingly, when a subset with 2 echo features is used as an input, the network configuration [2-20-2] is used. Similarly, [3-20-2], [4-20-2], [5-20-2], and [6-20-2] network configurations are used when the input feature subsets consist of 3, 4, 5, and 6 features. As mentioned earlier, the number of neurons in the hidden layer is kept at a fixed value to assess the performance of a network for different subsets of input features. If 2 or 5 different echo features are selected at a time (without regard to order) out of 7 features, then there exist 21 subsets of inputs (from binomial coefficient). Similarly, there exist 35 subsets of inputs if 3 or 4 different echo features are selected at a time out of 7; and 7 subsets if 6 different echo features are chosen together.

The performance (percentage success of correct classification during testing) of the network [2-20-2] is evaluated with a subset of 2 echo features (for example *BS* and

TS) for all sand, silty sand, silt, and clayey silt sediments at twenty locations. Subsequently, an average percentage of success of the network is computed by taking a mean value of the successes at four sedimentary environments. However, this average percentage of success of the network depends on the initial values of the interconnecting weights (i.e., initialization of the weights during the training of a network). Therefore, the network [2-20-2] is trained and tested 10 times with 10 different sets of initial weights. The number 10 is chosen arbitrarily and it is used to take into account the effect of the variations of initial weights (which are chosen randomly during the training process) on the performances of a network. Subsequently, an overall average percentage of success is obtained by taking the average of these 10 sets of results (for the above-said two features, *BS* and *TS*). Similarly, the same procedure is followed for the rest of the 20 subsets of input features (such as [*BS*, *HD*], [*TS*, *HD*], [*StatSkew*, *HD*] etc.) to compute the overall average percentages of success for the network [2-20-2]. Likewise, the overall average percentages of success are computed for all the 21 subsets of input features using the network [5-20-2]. Similarly, overall average percentages of success are computed for the 35 subsets using the networks [3-20-2] as well as [4-20-2], and 7 subsets for the network [6-20-2].

6.3.3 Results and Discussion

The overall average percentages of success thus obtained from all the 5 networks (i.e., [2-20-2], [3-20-2], [4-20-2], [5-20-2], and [6-20-2]) are first sorted in ascending order (separately for each network) and plotted in Fig. 6.9 for 33 kHz and Fig. 6.10 for 210 kHz. The sequence numbers along the x-axes of Fig. 6.9 and Fig. 6.10 essentially indicate different subsets of echo features. However, a particular sequence number for

[2-20-2] network and for [5-20-2] network does not represent the same feature subset (as [2-20-2] network has 2 input features and [5-20-2] network has 5 input features). These plots clearly indicate how the performances of a network vary with different subsets of input features, if all other parameters remain unchanged. The following observations are obtained from these experiments.

1. The overall average percentage of success in classifying seafloor sediments with a MLP network is reasonably higher for 210 kHz than that for 33 kHz.
2. More numbers of echo features are required for achieving higher success rate at 33 kHz. A subset of two or three echo features as an input to the network could not produce a maximum success rate beyond 89% at 33 kHz. However, subsets of 4, 5, and 6 echo features as inputs to the network produce maximum success rate nearly 92-93% at 33 kHz. On the other hand, the maximum overall average percentages of success lie within 97-98.5% for all subsets of input features at 210 kHz.

   This observation can be explained in terms of penetration of the acoustic energies into the seafloor sediments. The seafloor interface scattering component dominates (compared with the lesser sediment volume scattering component) in the total backscatter strength at 210 kHz because of the weaker penetration of acoustic energies into the sediment volume. On the contrary, 33 kHz penetrates the sediment volume at a relatively greater depth compared to 210 kHz and thus the sediment volume scattering component (in addition to the seafloor interface scattering component) has a significant effect on the total backscatter strength. It indicates that more numbers of echo features are necessary to discriminate different types of surficial seafloor sediments because of the significant contribution of volume scattering component at 33 kHz.

3. It is observed that if all echo features are used as input to a MLP-based classifier (i.e., using [7-20-2] network configuration), the overall percentages of success for seafloor classification are 91.19 ± 1.73 and 95.43 ± 2.39 respectively for 33 and 210 kHz. Therefore, maximum performance of the MLP network degrades marginally with the use of more than optimum number of echo features at both the acoustic frequencies. The neural network configuration [4-20-2] gives highest performance at 33 and 210 kHz. However, the lowest limit of performance for a given network increases with the increase in the number of features as inputs (as shown in Table 6.1).

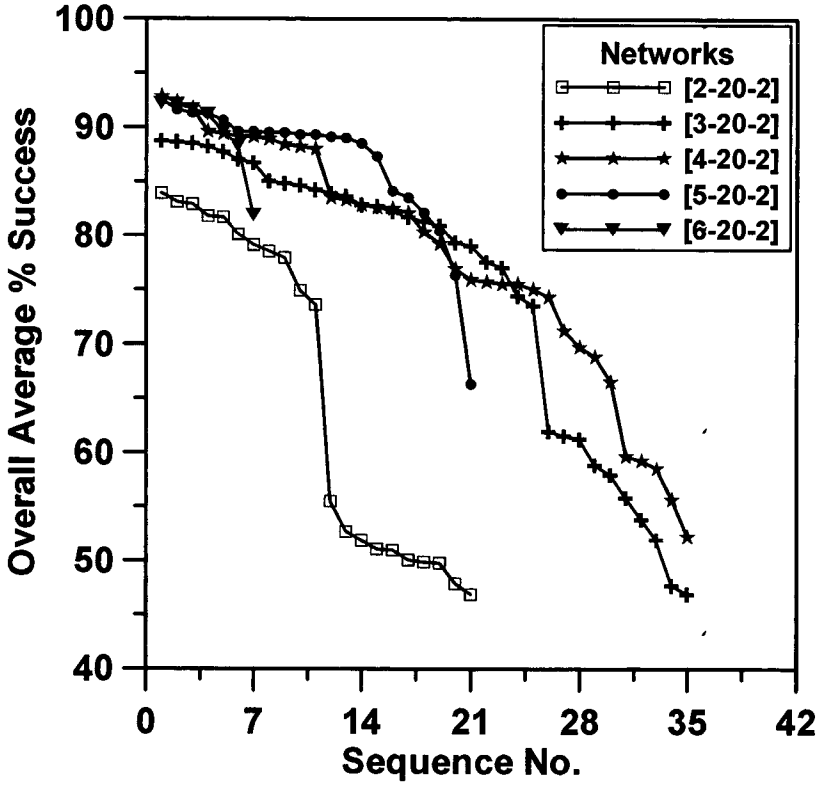

Fig. 6.9 Showing the results of overall average percentage of success obtained with different subsets of input features at 33 kHz. Each sequence number along the x-axis represents different feature subsets.

4. The results show that the highest performance (based on the overall average percentage of success) of the neural network based sediment classifier is achieved with a subset of four features consisting of *BS*, *TS*, *StatSkew*, and *HD*. In addition, the results show that the percentage increase in the success from three-features input subset to four-features input subset is marginal for 210 kHz as compared to 33 kHz. The feature subsets namely [*SpKurt*, *StatSkew*] and [*SpSkew*, *SpKurt*, *StatSkew*] give very low ($\leq 50\%$) success at 33 kHz. In contrast, the feature subsets namely [*SpSkew*, *SpWidth*], [*SpWidth*, *HD*], and [*SpSkew*, *SpKurt*, *SpWidth*] give very low ($\leq 50\%$) success at 210 kHz for seafloor classifications. In addition, it is noticed that training of a neural network does not converge successfully if these feature subsets are used.

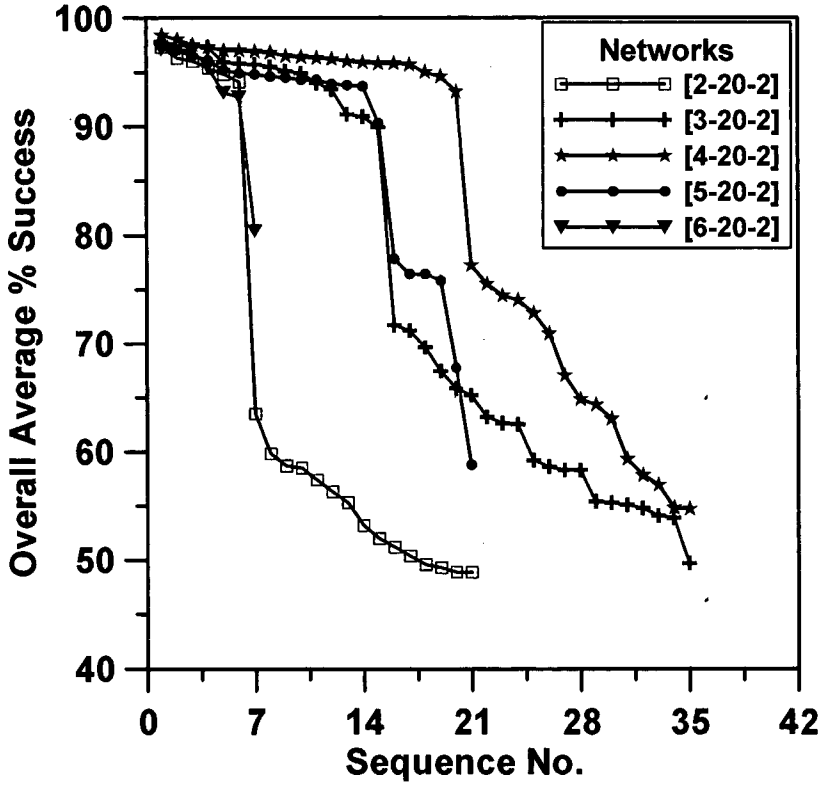

Fig. 6.10 Showing the results of overall average percentage of success obtained with different subsets of input features at 210 kHz. Each sequence number along the x-axis represents different feature subsets.

Table 6.1 Showing the results with highest and lowest overall average percentages of success for seafloor classification with MLP networks. Here F1, F2, ..., F7 represent backscatter strength, spectral skewness, spectral kurtosis, spectral width, statistical time-spread, statistical skewness, and Hausdroff dimension respectively.

Acoustic Freq	Network Configuration	Highest Overall Success			Lowest Overall Success		
		% Success ± STD*	Feature Set	Time (s)# ± STD*	% Success ± STD*	Feature Set	Time (s)# ± STD*
33 kHz	[2-20-2]	83.9 ± 1.9	(F1-F5)	101.2 ± 2.1	46.9 ± 3.8	(F3-F6)	102.8 ± 3.1
	[3-20-2]	88.7 ± 1.1	(F1-F5-F6)	103.3 ± 1.8	46.9 ± 1.7	(F2-F3-F6)	104.3 ± 2.2
	[4-20-2]	92.8 ± 1.3	(F1-F5-F6-F7)	75.0 ± 2.2	52.2 ± 2.9	(F2-F3-F6-F7)	114.4 ± 2.0
	[5-20-2]	92.5 ± 1.5	(F1-F3-F5-F6-F7)	35.7 ± 3.1	66.3 ± 2.6	(F2-F3-F4-F6-F7)	115.3 ± 1.1
	[6-20-2]	92.2 ± 1.1	(F1-F2-F4-F5-F6-F7)	20.4 ± 5.4	81.9 ± 3.6	(F2-F3-F4-F5-F6-F7)	124.8 ± 4.2
210 kHz	[2-20-2]	97.3 ± 1.0	(F1-F7)	9.4 ± 1.6	48.9 ± 2.6	(F2-F4) & (F4-F7)	79.5 ± 2.1
	[3-20-2]	97.8 ± 1.1	(F1-F5-F7)	6.3 ± 0.8	49.7 ± 2.1	(F2-F3-F4)	78.6 ± 1.7
	[4-20-2]	98.4 ± 0.6	(F1-F5-F6-F7)	6.0 ± 0.9	54.7 ± 2.0	(F2-F3-F4-F7)	83.6 ± 1.0
	[5-20-2]	97.6 ± 1.3	(F1-F3-F5-F6-F7)	5.9 ± 1.2	58.8 ± 1.1	(F2-F3-F4-F6-F7)	83.5 ± 1.4
	[6-20-2]	97.1 ± 1.0	(F1-F2-F3-F4-F6-F7)	5.8 ± 1.2	80.4 ± 3.9	(F2-F3-F4-F5-F6-F7)	40.4 ± 5.1

* STD - Standard Deviation values # Computational Time (s)

5. Moreover, the results reveal that the overall average percentage of success decreases drastically (as shown in Fig. 6.9 and Fig. 6.10) after a certain point for all the networks at both the acoustic frequencies 33 and 210 kHz. The results for 33 kHz reveal that if a feature subset contains *BS* or *TS* as one of the inputs, seafloor classification successes are higher than 73%, 73%, 66%, and 76% with [2-20-2], [3-20-2], [4-20-2], and [5-20-2] networks respectively. In addition, if *BS* is one of the input features in a subset, seafloor classification success is higher than 88% for [6-20-2] network at 33 kHz. It is also observed that if the subset of features contains backscatter strength (*BS*), the overall average percentages of success of a network are above 89% for 210 kHz. This interesting aspect is noticed uniformly in all the cases as shown in Fig. 6.9 and Fig. 6.10. The highest and the lowest success rates (with standard deviation i.e., STD values) are listed in Table 6.1 along with the respective feature subsets. This helps in understanding the relative importance of a feature subset for achieving the higher success in seafloor classification. This is to

mention that all the computations are carried out using MATLAB 7.0 (2004), which is installed in a computer having AMD Athlon 64 bit 3000+ processor with 512 MB RAM. The average computational times with standard deviation values are also shown in Table 6.1 for the different network configurations.

6.3.4 Conclusions

This study demonstrates that the improved performance of MLP networks based sediment classifier can be achieved if the input echo features are selected preferentially. The use of more than the optimum number of echo features in a given neural network does not necessarily increase the success rate of a neural classifier. The analysis reveals that backscatter strength, time spread, statistical skewness, and Hausdroff dimension are the most discriminatory echo features (when used as a subset) to MLP neural networks for the classification of seafloor sediments at 33 and 210 kHz. The analyses also reveal that backscatter strength is the most dominant echo feature at both the acoustic frequencies, while time spread is important (in addition to backscatter strength) at 33 kHz only. In addition, the study reveals that 210 kHz is advantageous (in comparison with 33 kHz) for the classification of seafloor sediments. However, the limitation of supervised neural networks based classifier is that these methods require a-priori knowledge (i.e., the ground-truth) on sediment types available in the study area to decide the output target vectors for training such networks.

This chapter has proposed a supervised method to select the prominent echo features using multilayer backpropagation networks. A hybrid approach using Kohonen's self-organizing feature map and Fuzzy C-Means cluster algorithm is proposed in the next chapter.

Chapter 7

Hybrid Approach for Classification of Seafloor Sediments

7.1 INTRODUCTION

The results of previous two chapters reveal that cluster analysis or supervised neural network analysis essentially require a-priori knowledge on the sedimentary environment in a study area for efficient classification of the seafloor sediments. This a-priori information is generally used to decide either the number of cluster centers in cluster analysis or the output target vectors in a neural network based classifier. Therefore, a hybrid scheme is proposed in this chapter for efficient classification of the seafloor sediments without any a-priori knowledge on seafloor sediments in an experimental area. The proposed hybrid scheme is based on Kohonen's unsupervised neural architecture and Fuzzy C-Means (FCM) cluster algorithm.

An introduction on Kohonen's unsupervised and supervised learning methods is given here for easy understanding of the topic. Following this, a method is proposed to estimate the number of cluster centers in a given dataset using Kohonen's unsupervised architecture. Another method is proposed to select three discriminating echo features using FCM algorithm. Finally, results obtained from the proposed hybrid scheme (consisting of the above two methods) are compared with the ground-truth.

7.2 UNSUPERVISED AND SUPERVISED LEARNING METHODS

In Chapter 6, it is mentioned that there are two basic methods of learning namely unsupervised and supervised by which a network learns how to execute a specific task. In addition, there is another learning method called competitive learning. In competitive learning only one neuron in the output unit or only one neuron in a group is the winner and therefore this neuron is often called the winner-take-all neuron (Hertz et al., 1991). The basic aim of such networks is to cluster or categorize the input data based on its inherent characteristics. The unsupervised learning is independent of a target output vector and is based only on the unlabeled input data. The calculation of error (between a desired target and the achieved output) is not required to train such unsupervised networks. The network itself discovers patterns, similar features, and regularities in an input data. Kohonen's Self Organizing Map (SOM) is one such network (Kohonen, 1989, 1990).

On the contrary, when a network learns from labeled sets of input data, it is called supervised learning. The classes are predefined and each training data is tagged with a correct class in a supervised architecture. Learning Vector Quantization (LVQ) network proposed by Kohonen (Kohonen, 1989, 1997) is an example of the competitive supervised learning. SOM and LVQ networks are introduced in the next section.

7.2.1 Self Organizing Map

Kohonen, a Professor of the Faculty of Information Sciences, University of Helsinki, understood self-organizing and adaptive learning features of a brain and

proposed a neural network called Self Organizing Map (SOM) (Kohonen, 1990). Kohonen SOM architecture consists of two layers, an input layer and an output layer. Each neuron in the input layer has feed-forward connections to every neuron in the output layer. Fig. 7.1 illustrates a Kohenen network in two-dimensional grid. Here the neurons are not arranged in layers as in a multilayer perceptron (input, hidden, and output) but rather on a flat grid. The goal of the network is the mapping of *n*-dimensional input vectors into one- or two-dimensional lattice (of the output layer). For a given input vector, one and only one neuron with the maximum value in the output layer is set to a logical one (winner), and all other neurons are set to zero.

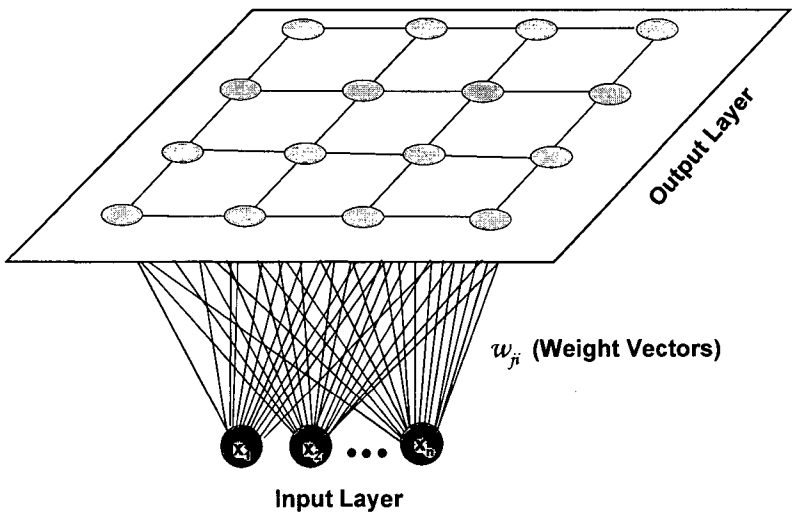

Fig. 7.1 Illustrating a two-dimensional Kohonen network

In general, input data (or input vectors or patterns) are normalized before applying to a Kohonen Network. Normalized input vector is obtained from each component of the input vector by dividing the length of the vector. Randomly initialized weight vectors are also normalized in these networks. Various steps in the training of a SOM network are as follows (Beale and Jackson, 1990).

1. First a normalized input training vector X (with components x_i, $i = 1, 2,..., n$) is applied to the network.
2. The Euclidean distance d_j between the input and each output node j is calculated using an equation given by,

$$d_j = \sqrt{\left[\sum_i (x_i - w_{ji})^2\right]} \tag{7.1}$$

where x_i is the i^{th} component of the input vector X, and w_{ji} is the weight from the i^{th} input neuron to the j^{th} destination neuron.

3. The neuron that has a weight vector closest to X (depending on the minimum distance d_{min}) is declared as the winner. The weight vector associated with the winner becomes a center of a group of weight vectors that lie within a distance d_{min}. The output neuron with the minimum d_{min} is designated as j^*.
4. The weights for the neuron j^* and its neighbors, defined by the neighborhood size $N_{j^*}(p)$ at the p^{th} iteration, are updated using the formula,

$$w_{ji}(p+1) = w_{ji} + \eta(p)[x_i - w_{ji}(p)] \tag{7.2}$$

where $\eta(p)$ is called the learning parameter at the p^{th} iteration and it decreases as the iteration number p increases (adapting nature of weights). The value of $\eta(p)$ starts with 1 and gradually moves to 0.1. The neighborhood $N_{j^*}(p)$ also decreases in size with the iteration number p. The value of $N_{j^*}(p)$ is large at the beginning of iteration and reduces to only one neuron towards the end of a training process.

5. The steps 1 to 4 are repeated till the training cycle reached to a pre-specified maximum number or when no noticeable change in the feature map is observed.

The steps 1 to 5 states that a winning neuron is first located when a new training input pattern is applied to a network. Subsequently, weights near the winning neuron are updated. An epoch is completed when all the input vectors are presented to a network. Several such epochs of training are performed with an updated learning rate to complete the training process in SOM (same as with other neural networks).

7.2.2 Learning Vector Quantization

Kohonen (Kohonen, 1989, 1997) also developed a supervised learning technique to fine-tune the SOM trained feature map to optimize the performance of a network. He described this learning technique as Learning Vector Quantization (LVQ). In LVQ network, the designated categories (into which the input training sets will be classified) are known in advance. This LVQ network is exactly the same as SOM network except the fact that each neuron in the output layer is designated as belonging to one of the available classification classes or categories. This is illustrated schematically in Fig. 7.2. Here few output neurons are assigned to each one of the available classes. Normally these classes are defined by a set of vectors called prototype vectors. The class of a given input is decided from the Euclidean distance nearest to these prototypes. When an input pattern is applied to a network, the neuron with a minimum Euclidean distance is declared as the winner. During the training of a LVQ network, if the winning neuron belongs to a correct category, then it is rewarded by moving the weights closer to the input vector. Conversely, if the winning neuron does not belong to a correct class, it is punished and it is forced to move away from the input vectors. The following rules are used during the training (Beale and Jackson, 1990) of LVQ networks.

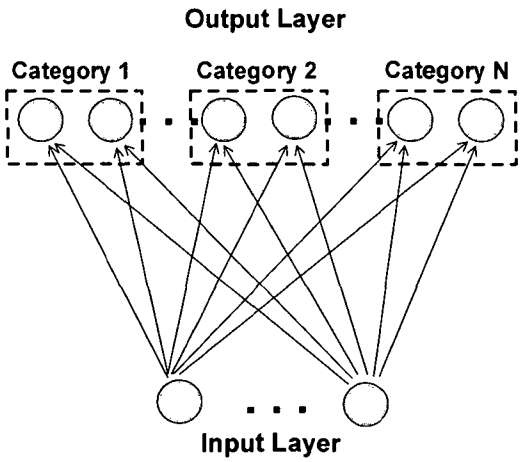

Fig. 7.2 Illustrating the architecture of a LVQ network

$$w_{ji}(p+1) = w_{ji}(p) + \eta(p)(x_i - w_{ji}(p)), \text{ for correct classification} \quad (7.3)$$

$$w_{ji}(p+1) = w_{ji}(p) - \eta(p)(x_i - w_{ji}(p)), \text{ for wrong classification} \quad (7.4)$$

where the learning rate $\eta(p)$ reduces as the iteration number (p) increases (same as SOM).

7.3 PROPOSED HYBRID APPROACH

It is mentioned that the artificial neural networks are suitable for non-linear input-output mapping and hence widely used in the classification of seafloor sediment. Classification of seafloor sediments have been successfully demonstrated earlier with multistage neuro-fuzzy classifier (Dung and Stepnowski, 2000), incremental fuzzy neural network and fuzzy decision trees (Stepnowski et al., 2003) as well as neural networks utilizing simulated reverberation data (Alexandrou and Pantzartzis, 1993), multi-beam backscatter data (Michalopoulou et al., 1995; Zhou and Chen, 2005), and side-scan imagery (Stewart et al., 1992; Stewart et al., 1994; Zerr et al., 1994).

There are two important issues in all model-free techniques for the classification of seafloor sediments: first, the decision on a number of cluster centers (i.e., the number of classes) in a given dataset and second, the selection of most discriminating echo features available in a given dataset. In fact, these are the two most important issues in any pattern recognition problem too.

The classical uses of unsupervised architecture called Self Organizing Map (SOM) are well documented for single-beam (Chakraborty et al., 2001, 2003a, 2004) and multi-beam backscatter data (Alexandrou and Pantzartzis, 1993; Michalopoulou et al., 1995; Chakraborty et al., 2003b; Zhou and Chen, 2005). SOM is used to obtain an approximate idea (Michalopoulou et al., 1995) about the number of classes present in a given dataset, based on the inherent discrimination ability of the input feature vectors. The approximate number of classes obtained from SOM analysis may vary based on the input vector chosen for unsupervised training, which may influence the subsequent analysis with supervised fine-tuning. Therefore, to address the first issue on the maximum number of prevailing seafloor classes plausible in a given dataset without any a-priori information, a SOM based technique is proposed in this work (De and Chakraborty, 2009).

Regarding the second issue, it is already mentioned that there is no general rule to select the best feature vectors for a given dataset and the selection of features is mostly application oriented (Stewart et al., 1992; Pal and Foody, 2010). The performance of any neural network depends on the careful selection of training sets with sufficient information as well as the learning strategy to distinguish the different classes exist in a given dataset (Stewart et al., 1994). Though the use of non-linear techniques and discriminant analysis (Maroni et al., 1997) are available for features selection, Principal Component Analysis (PCA) (Jollife, 1986) is widely used as pre-processors

for features selection (Ghosh et al., 1992; Prager et al., 1995; Legendre et al., 2002; Stepnowski et al., 2003; van Walree et al., 2005). The fuzzy algorithm namely K-means (Legendre et al., 2002; van Walree et al., 2005) and FCM (Burczynski, 1999) have also been in use for the classification of seafloor sediment assuming a pre-decided cluster centers. It is already demonstrated in Chapter 5 that cluster analysis in combination with PCA could not produce encouraging results in the present study area. Moreover, this feature selection issue has already been addressed in Chapter 6 to select an optimal subset of echo features (from seven features) using MLP networks. In this chapter, FCM algorithm based technique is proposed to select the sedimentary environment specific features with dominant discriminating characteristics, using the information on maximum number of cluster centers (obtained from the proposed SOM based method) (De and Chakraborty, 2009).

7.3.1 Estimation of Number of Cluster Centers

A method to estimate the number of classes (or clusters) using a competitive unsupervised SOM classifier is discussed in this section. Here, SOM is applied to the echo feature *BS*, which is observed as one of the most discriminating echo features in the study area (from the analysis presented in Chapter 6).

A random weight matrix (input vectors by output neurons) is initialized within +1 and −1 in SOM architecture. The output neuron number is chosen as 55. The number of training data points (150) is optimized from few trial runs. The normalized input data (within +1 and −1) is segmented successively using 150 data points with 100 points overlap in a moving average sense as 1-150, 51-200, 101-250, and so on till the end of the data (De and Chakraborty, 2009). At each iteration (p), the weights of 5 neurons (2

neighborhood neurons on the either side of a winner) are updated using a learning function $0.4/p^{0.2}$. The neighborhood neuron number is reduced to 1 during the training process. Training stops when the error goal (the Euclidean distance between the input vector and the neuron weights) of 10^{-30} is achieved or the pre-specified maximum iteration number 2000 is reached. Once the training is completed, SOM is tested with the remaining data segments. Similarly, the second segment (51-200 points) is trained and the remaining data segments are tested. The training-testing process continues using the successive segments till the end of data points. The excited neurons obtained during every testing process are plotted with respect to output neurons in a bar diagram (as shown in Fig. 7.3 for 210 kHz for one of the cases). If the testing shows that the wining neuron exists within a range of the trained neuron position, then it is assumed as belong to the same class, where the data was trained earlier. If some other neuron gets activated during the testing, then it is considered as a new class.

The maximum number of classes is estimated from a particular training-testing process by counting the presence of the number of prominent fired neurons (shown as bars in Fig. 7.3). The Fig. 7.3 shows the presence of 4 classes during testing when the network is trained with one of the segments. Here the highest firing of neurons (~ 45%) occurred at position 21. The surrounding neurons with percentage of firing more than 20% of the highest firing (i.e., more than 20% of 45% = 9%) have occurred at positions 6, 16, and 36. Therefore, the maximum number of classes is estimated as 4 (from the prominent firing of neurons at positions 6, 16, 21, and 36) for this particular training-testing process. This 20% selection criterion is optimized from few trial-and-runs.

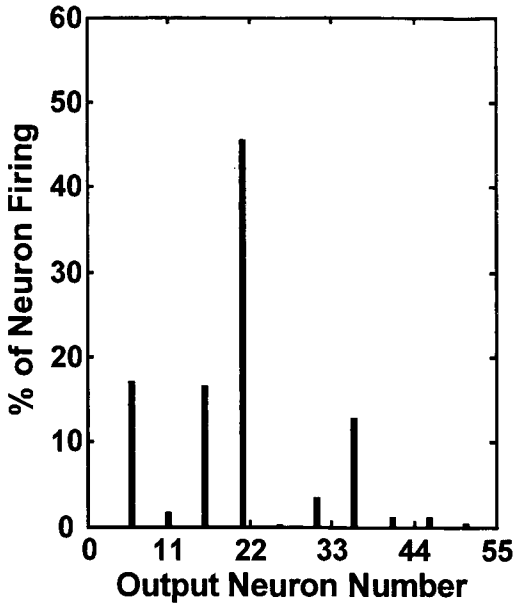

Fig. 7.3 SOM results for one training-testing process (carried out with one of the segments) for 210 kHz, which shows that there are four classes present in this particular testing.

Though Fig. 7.3 shows that there are maximum four classes present, different training-testing processes produce different number of classes. As for example, first training-testing process may show the presence of maximum 4 classes while testing the network, second training-testing process may show the presence of maximum 5 classes; tenth training-testing process may give maximum 3 classes, and so on till the end of training-testing process. All these maximum numbers of classes thus obtained from various training-testing processes are stored and finally plotted in a histogram (Fig. 7.4a for 33 kHz and Fig. 7.4b for 210 kHz). Fig. 7.4a and Fig. 7.4b reveal that four classes are mostly occurred during all such training-testing process in the study area at 33 and 210 kHz. This simple process gives the maximum number of classes (cluster centers) present in any dataset without any prior information.

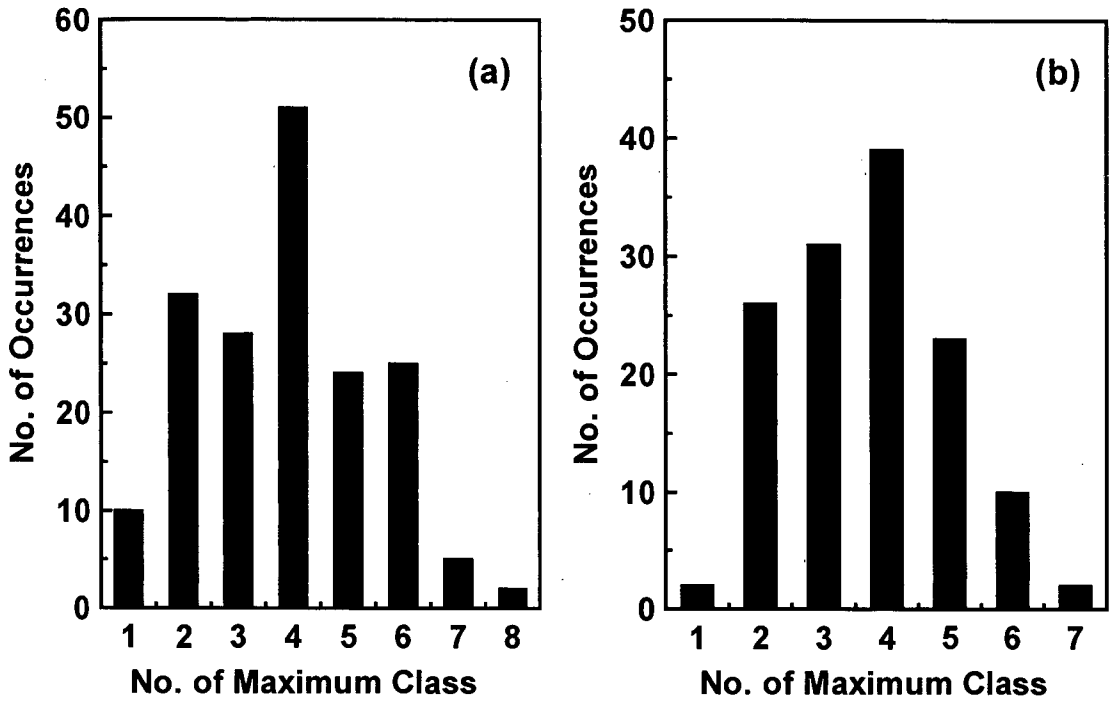

Fig. 7.4 Histogram of the number of occurrences of maximum number of classes obtained from all the training-testing process of SOM analysis (as shown in Fig. 7.3 for one such case) indicates the presence of four classes **(a)** for 33 kHz **(b)** for 210 kHz.

7.3.2 Simulation Study

This proposed method (in section 7.3.1) is tested with simulated data (De and Chakraborty, 2009) for establishing the effectiveness under controlled conditions (Michalopoulou et al., 1995). Though several sediment classification schemes exist to represent a sedimentary environment based on the relative proportions among different particle grain sizes, Wentworth mean grain size grade-scale (Wentworth, 1922) is chosen for its simplicity to simulate echo waveform data. Accordingly, 5 different environments (i.e., 5 sediment classes) comprising of coarse to fine grain sediments are

considered: (a) coarse and medium sand (mean grain size chosen as 1ϕ), (b) fine and very fine sand (3ϕ), (c) coarse and medium silt (5ϕ), (d) fine silt (6.8ϕ) and (e) clay (8.6ϕ).

The echo waveform simulations are performed at 50m depths for 33 and 210 kHz using a theoretical backscatter model (Sternlicht and de Moustier, 2003a) as described in Chapter 4. The pulse duration and 3-dB beam width are assumed as 0.97 ms and 20^0 respectively for 33 kHz and 0.61 ms and 9^0 respectively for 210 kHz. The roughness spectrum strength, roughness spectrum exponent, density ratio, and sound speed ratio are estimated from the published relationships (equation (4.15) to (4.18)) based on the mean grain size (M_ϕ) of sediments (APL Handbook, 1994). Sediment volume scattering coefficient (σ_v) is computed from the sediment volume scattering parameter ($\sigma_2 = 0.003$). In real scenario, for a given sea bottom, echo waveforms can vary from one data ensemble to the other (Sternlicht and de Moustier, 2003a). To incorporate this aspect, the values of M_ϕ, w_2, σ_v are varied within small standard deviations ($\pm 0.1\phi$ for M_ϕ, ± 0.00005 to ± 0.0005 cm^4 for w_2, and ± 0.0002 to ± 0.001 m^{-1} for σ_v) around their mean values. The values of M_ϕ, w_2, σ_v, and γ_2 used in the simulation are listed in Table 7.1.

Five sets of echo waveforms (comprising of 850 echoes in each set) are simulated for these 5 sediment classes at 33 and 210 kHz. Since the calculation of backscatter strength from echo waveforms involves the echo sounder transceiver characteristics (Chakraborty et al., 2007a), echo energies are estimated from the simulated waveforms (for 10 ms duration) (van Walree et al., 2005). These echo energies are used for testing the algorithm. Altogether 4250 echo energy data-points,

extracted from the simulated normalized waveforms, are subjected to the proposed technique (in section 7.4.1) to estimate the maximum number of classes present in a dataset. The output neuron number 55 is sufficient to accommodate at least nine classes with 5 neurons in each class. (In absence of gravel fractions in the seafloor sediments, maximum 9 different types of sediments (Hamilton, 1971b) are possible in real scenario with different combination of sand, silt, and clay).

Table 7.1 Parameters for simulation of echo waveforms at 33 and 210 kHz

Sr. no.	Mean grain size, M_ϕ (phi units)	Spectral strength, w_2 (cm^4)	Spectral exponent, γ_2	Volume scattering coefficient, σ_v (m^{-1})	Number of simulated echoes
1	1.0 ± 0.1	0.005587 ± 0.0005	3.25	0.0475 ± 0.001	850
2	3.0 ± 0.1	0.002070 ± 0.0002	3.25	0.0566 ± 0.001	850
3	5.0 ± 0.1	0.0005175 ± 0.00005	3.25	0.0446 ± 0.001	850
4	6.8 ± 0.1	0.0005175 ± 0.00005	3.25	0.0095 ± 0.0003	850
5	8.6 ± 0.1	0.0005175 ± 0.00005	3.25	0.0053 ± 0.0002	850

Fig. 7.5a shows that different segment of the dataset, when subjected to SOM training and testing processes, produces different number of maximum classes (at 33 kHz). The histogram (Fig. 7.5b) (using the number of maximum classes obtained from different training and testing) shows that maximum 5 classes are available here. This demonstrates that if the maximum number of prevailing classes in a given dataset is estimated from any one of the training segments, the result may not be correct. The five simulated regions in the dataset are indicated by the M_ϕ value at the top of Fig. 7.5a. Similar results are shown in Fig. 7.6 for 210 kHz. This simulation study illustrates that the proposed technique could be extremely useful to estimate the plausible maximum

number of prevailing sediment classes in any experimental site without any a-priori information (De and Chakraborty, 2009).

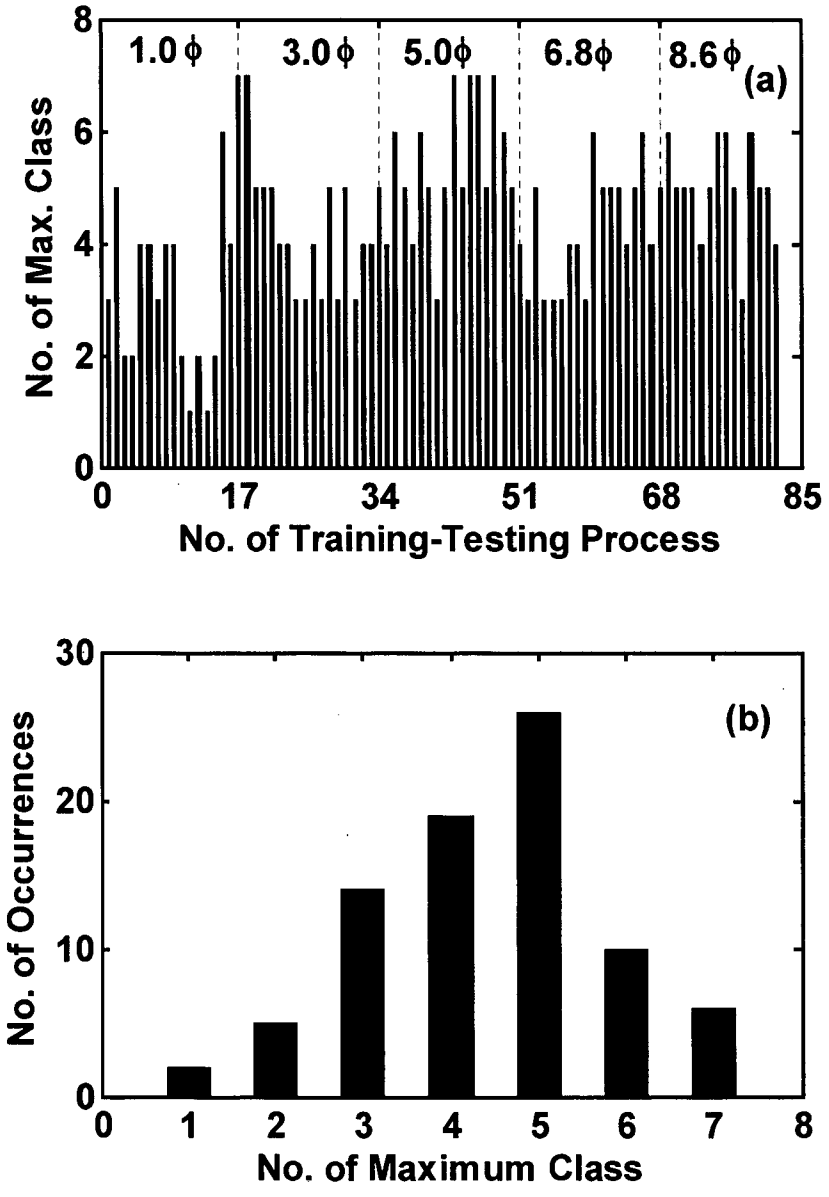

Fig. 7.5 (a) SOM Results for various training-testing processes at 33 kHz using the simulated data. **(b)** Histogram showing the maximum five number of classes obtained from the simulated data at 33 kHz.

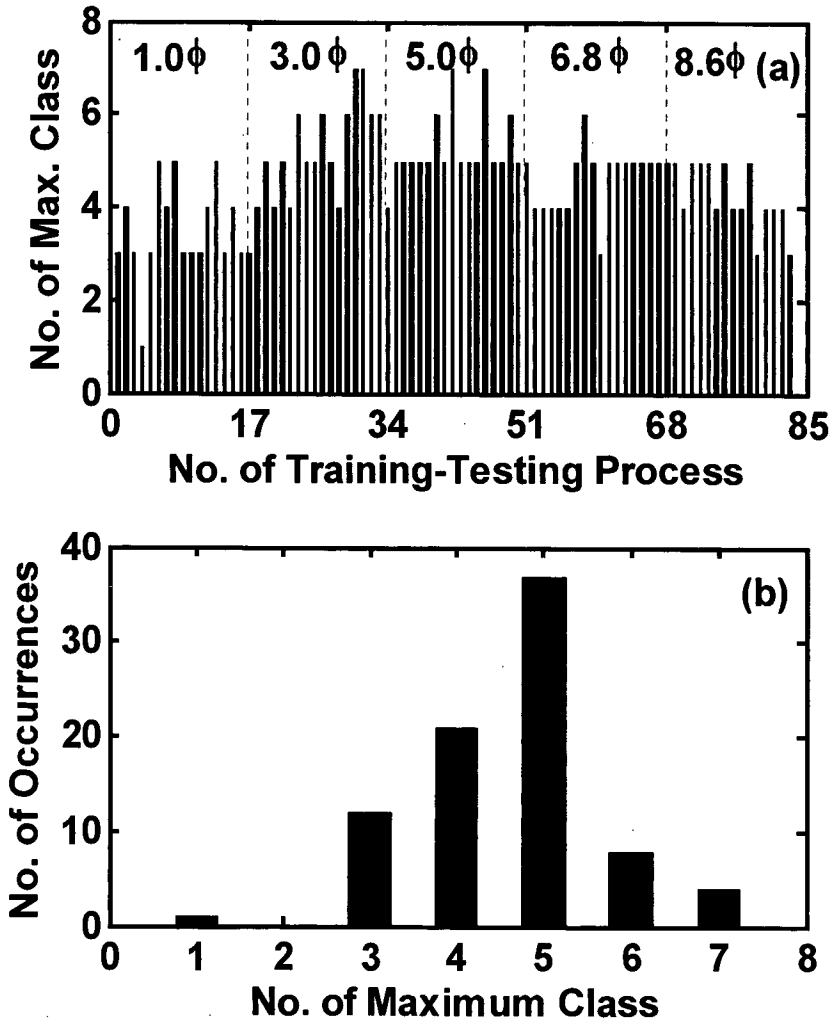

Fig. 7.6 (a) SOM Results for various training-testing processes at 210 kHz using the simulated data. **(b)** Histogram showing the maximum five number of classes obtained from the simulated data at 210 kHz.

7.3.3 FCM Based Selection of Echo Features

The procedure for selection of features has a great importance in wide range of classification problems and can serve as a pre-processor to select a subset of relevant features among the available ones for achieving better results. In this section, a data-

driven approach based on FCM algorithm is proposed to select an optimum subset consists of three dominant features in a given dataset (De and Chakraborty, 2009).

With an aim to classify the seafloor sediments efficiently using three most discriminating echo features, the FCM algorithm (using Fuzzy Logic Toolbox in MATLAB 7.0, 2004) is used. If three echo features are selected at a time, out of seven features (without regard to order), there exist 35 cases (from binomial coefficient) (as discussed in Chapter 6). The FCM algorithm is used for all the 35 cases/subsets with three different echo features at a time. Various parameters used in the FCM algorithm are: exponent for the membership function matrix - 2.0, maximum iterations - 200, minimum improvement value - 1e-5. The number of cluster centers is obtained from the proposed unsupervised method (in section 7.3.1). The FCM algorithm classifies every data point in one of the available classes. To compare the FCM output with the ground-truth, the percentages of data points falling in the available classes are computed. The results for different combination of echo features are shown in Fig. 7.7. These analyses indicate that the success (to classify sediments correctly) is high only for the echo feature subset numbers 13, 14, and 15. These three feature subsets (13, 14, and 15) represent the feature combinations [*BS*, *TS*, *StatSkew*], [*BS*, *HD*, *TS*], and [*BS*, *StatSkew*, *HD*] respectively. The overall average percentages of correct classification for feature subsets 13, 14, and 15 are (86%, 84%, and 78%) and (86%, 91%, and 89%) respectively at 33 and 210 kHz. This reveals that feature subsets 13 and 14 give maximum success at 33 and 210 kHz respectively. The results are given in Table 7.2.

From these trials, it can be inferred that the most dominant discriminating feature *BS*, when used in combination with *TS*, *HD*, and *StatSkew* produces much improved results than any other feature subsets. Moreover, the combination of the features *TS*, *StatSkew*, and *HD* could not show any improvement in the results (De and

Chakraborty, 2009). Although the sediment classification based on echo spectral features showed very good results in other areas (Tegowski and Lubniewski, 2002), these features could not produce good results in this study area.

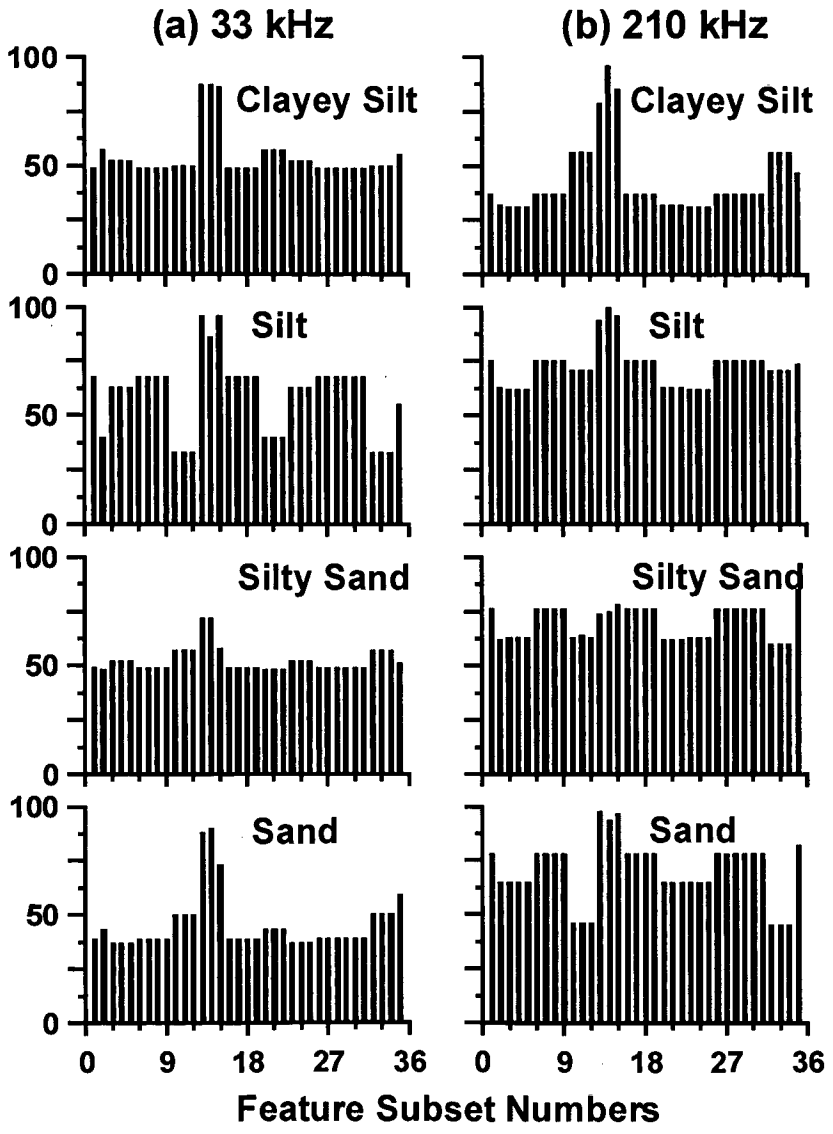

Fig. 7.7 Bar diagram of percentage of correct classification vs. feature subset numbers for (a) 33 kHz and (b) 210 kHz. Here feature subset numbers 1, ... 5, ... 35 indicate [F1, F2, F3], ... [F1, F2, F7], ... [F5, F6, F7] respectively, where the symbols F1, F2, F3, F4, F5, F6, F7 indicate echo features *BS*, *SpSkew*, *SpKurt*, *SpWidth*, *TS*, *StatSkew*, *HD*, respectively.

Table 7.2 FCM results with feature subset numbers 13 (for 33 kHz) and 14 (for 210 kHz)

Stn no.	Percentage of correct classification from FCM class								True sediment type
	Sand		Silty Sand		Silt		Clayey Silt		
	33 kHz	210 kHz	33 kHz	210 kHz	33 kHz	210 kHz	33 kHz	210 kHz	
1	0	0	0	0	0	1	100	99	CS
2	0	0	0	0	0	1	100	99	CS
3	0	0	0	0	0	1	100	99	CS
4	0	0	0	0	0	0	100	100	CS
5	0	0	0	0	0	0	100	100	CS
8	0	0	0	0	93	24	7	76	CS
13	0	0	0	0	0	0	100	100	CS
9	0	0	0	0	100	100	0	0	Si
10	0	0	0	0	100	100	0	0	Si
14	0	0	11	0	89	100	0	0	Si
11	1	0	99	86	0	14	0	0	SS
17	0	0	100	100	0	0	0	0	SS
18	89	21	11	79	0	0	0	0	SS
19	24	0	76	34	0	66	0	0	SS
6	100	100	0	0	0	0	0	0	Sa
7	87	100	13	0	0	0	0	0	Sa
12	100	100	0	0	0	0	0	0	Sa
15	80	98	20	2	0	0	0	0	Sa
16	100	63	0	37	0	0	0	0	Sa
20	61	100	39	0	0	0	0	0	Sa

7.4 COMPARISON OF RESULTS

7.4.1 Comparison with Ground-Truth

The 3-D plots of the results obtained from FCM analysis with the feature subsets 13 and 14 are shown in Fig. 7.8a for 33 kHz and Fig. 7.8b for 210 kHz. The results in Table 7.2 show that clayey silt samples are well classified for both the frequencies except at station 8, where majority of sediments are misclassified as silt at 33 kHz and partly at 210 kHz. For silty samples, both the frequencies show consistent results with the ground-truth. For silty sand samples, the results at stations 11 and 17 are

comparatively consistent than that of stations 18 and 19. For sandy sediments, the agreements with the ground-truth are consistent at all stations, except at stations 16 and 20. At station 20 for 33 kHz and at station 16 for 210 kHz, sediments are partly misclassified as silty sand. The overall results for silt and sand samples are consistent in comparison with clayey silt and silty sand.

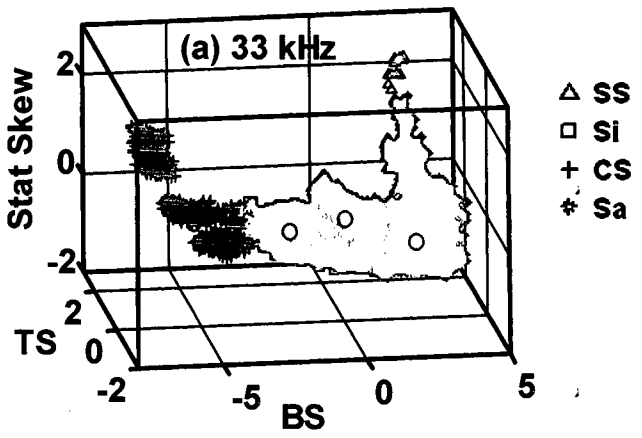

Fig. 7.8a The 3-D plot of the results obtained from FCM analysis with the subset [*BS*, *TS*, *StatSkew*] at 33 kHz. The circles represent the centers of the respective clusters.

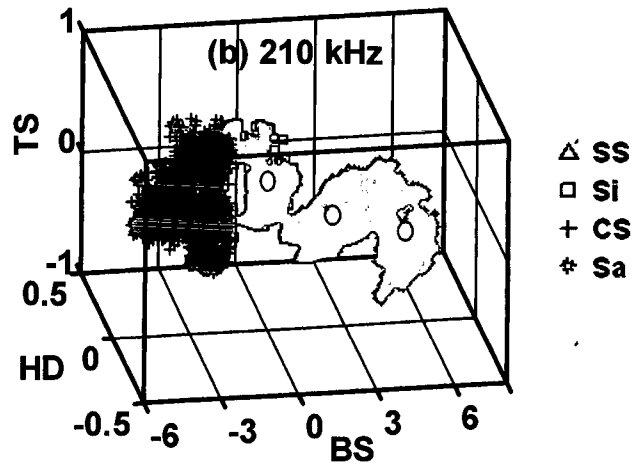

Fig. 7.8b The 3-D plot of the results obtained from FCM analysis with the subset [*BS*, *HD*, *TS*] at 210 kHz. The circles represent the centers of the respective clusters.

In this study, the sediment type (based on Shepard's scheme) is used as ground-truth data. Since this sediment classification scheme does not take into consideration the acoustic characteristics of sediments, the deviations of the results (using the proposed method) from the ground-truth need to be viewed in the light of acoustic seafloor sediment classification.

7.4.2 Comparison with SOM-LVQ1 Hybrid Approach

Echo envelopes obtained from a single-beam echo sounder at three sediment sites in the western continental shelf of India were classified based on SOM architectures with moving average as a pre-processor (Chakraborty et al., 2001). Since this classifier faced few practical difficulties to carry out the moving averages with a smaller dataset, another hybrid classifier tool based on SOM and LVQ was developed (Chakraborty et al., 2004). This hybrid classification scheme (Chakraborty et al., 2004) based on SOM and the first kind of LVQ (called LVQ1) is implemented here for comparison with the proposed hybrid method. The methodology and results are discussed in the following sections.

7.4.2.1 Methodology

The hybrid scheme (following Chakraborty et al., 2004) is applied to echo waveforms data (250 numbers at each of the sample locations) at 33 and 210 kHz. Following the method of Chakraborty et al. (2004), the echo waveforms are divided into 3 segments i.e., 1-70, 71-150 and 151-250 for neural classifier training and testing. For SOM training, three different echo waveform snapshots such as 20^{th}, 80^{th}, and 170^{th} are

chosen, which belong to the above mentioned three segments. Input echo waveforms are normalized within a maximum limit of -1 to +1.

In SOM architecture, a 200x1 input grid (input echo waveforms are re-sampled with 200 points) and 20x1 output grid (sufficient for mapping 4 sediment classes with 3 neurons in each class) are chosen optimally. The weights of the network are initialized randomly within 0.0 to 1.0. For each sediment type, data from two different locations are used for SOM training. Once the training is completed, the classifier is tested with entire dataset (except those used for training). The overall average percentages of the SOM based classifier during testing are calculated from the averages of three segments. To reinforce the correct classifications and for improving the performance of the classifier, supervised architecture LVQ1 is implemented using SOM trained weights. Total 70 waveforms (20 numbers from first two segments and 30 numbers from the last segment) are used for LVQ1 training. Later, LVQ1 classifier is tested with rest of the dataset (De and Chakraborty, 2009).

7.4.2.2 Results and Discussion

The overall average percentages of correct classification obtained from SOM and LVQ1 testing are given in Table 7.3. Asterisks (*) indicate that echo waveforms from these locations are used for training and the remaining waveforms are used for testing. For 33 kHz, the results (after LVQ1) show a mixed response (20% CS, 24% Si, 22% SS, 34% Sa) among the four available classes at location 18. Similarly, the results (after LVQ1) show mixed response for 210 kHz at locations 11 (16% CS, 27% Si, 20% SS, 37% Sa), at 17 (26% CS, 19% Si, 25% SS, 30% Sa), at 7 (22% CS, 22% Si, 23% SS, 33% Sa), and at 12 (24% CS, 21% Si, 22% SS, 33% Sa). Since, the neuron firing

patterns at locations 7, 11, 12, 17, and 18 show mixed response (during the testing of LVQ1) among four available classes, they are denoted by 'Mixed'. After LVQ1, the misclassification percentages for stations 9, 10, 14, 11, and 20 are also shown in the Table. The results obtained from SOM show poor performances for most of the locations (less than 30% success obtained at 13 sites for 33 kHz and at 15 sites for 210 kHz). However, the percentage of correct classification increases significantly by the supervised fine-tuning using LVQ1 for both the acoustic frequencies. The results indicate that the performance with 210 kHz is consistent than that with 33 kHz. The limitation of SOM-LVQ1 hybrid approach is that this also depends on a-priori knowledge on ground-truth for supervised fine-tuning with LVQ1.

Table 7.3 Results using hybrid architecture (SOM and LVQ1) utilizing echo waveforms for 33 and 210 kHz

Stn No.	True sed. type	Percentage classification (SOM)		Percentage classification (LVQ1)		After LVQ1 sediments classified as	
		33 kHz	210 kHz	33 kHz	210 kHz	33 kHz	210 kHz
1	CS	33*	10*	100	95	CS	CS
2	CS	54	7	100	92	CS	CS
3	CS	88	13	100	83	CS	CS
4	CS	58	54	100*	87*	CS	CS
5	CS	56	8	72	76	CS	CS
8	CS	54*	18*	99*	79*	CS	CS
13	CS	23	51	43	72	CS	CS
9	Si	2	73	5*	92*	CS (95%)	Si
10	Si	27*	44*	40*	66*	CS (53%)	Si
14	Si	6*	42*	23	64	CS (74%)	Si
11	SS	42	14	32	20	Sa (65%)	SS (Mixed)
17	SS	16*	5*	43	25*	SS	SS (Mixed)
18	SS	21	20	22*	46*	SS (Mixed)	SS
19	SS	5*	2*	70*	69	SS	SS
6	Sa	23*	10	55	56	Sa	Sa
7	Sa	9	20	59	33	Sa	Sa (Mixed)
12	Sa	6	14*	57	33*	Sa	Sa (Mixed)
15	Sa	7	10	85*	80	Sa	Sa
16	Sa	10*	8*	89*	52*	Sa	Sa
20	Sa	20	4	24	22	SS (54%)	SS (70%)

Though the results obtained from SOM-LVQ1 hybrid scheme show average success in classifying sediments, the applicability of the method is limited in a scenario where ground-truth information is available to carry out a supervised fine-tuning. Therefore, in that scenario (in the absence of ground-truth), the proposed hybrid method (based on SOM and FCM) has great advantages and can be considered as another efficient classification tool. Moreover, SOM based proposed method (in section 7.3.1) can also be used in combination with the supervised MLP-based features selection process (as discussed in Chapter 6) for achieving higher success in the classification of seafloor sediments.

7.4.3 Comparisons with Other Methods

The performance of the proposed hybrid method is also compared with the results obtained from PCA-FCM analysis (presented in Table 5.3 in Chapter 5). The comparison indicates that the data-driven feature selection approach, proposed in this chapter, produces improved accuracy (compared to the use of principal components as the best features).

The results obtained with FCM based feature selection process is compared with that obtained with MLP network based approach. The results in Table 6.1 (of Chapter 6) also revealed that a subset of three features consisting of [*BS*, *TS*, *StatSkew*] and [*BS*, *TS*, *HD*] respectively gives a maximum success with [3-20-2] network at 33 and 210 kHz. However, the echo feature subset [*BS*, *TS*, *StatSkew*, *HD*] produced a highest success at both 33 and 210 kHz using MLP based sediment classifier. To compare this result with FCM based features selection method, the analyses (as discussed in section 7.3.3) are carried out with subsets of four echo features as inputs. However, no improvements in

the success rates are observed with the subsets of four features. This comparison suggests that if FCM based feature selection process is adopted for seafloor classification, the feature subsets [*BS*, *TS*, *StatSkew*] and [*BS*, *TS*, *HD*] respectively are the optimum for achieving the improved success at 33 and 210 kHz, whereas MLP based features selection process revealed that the optimum subset [*BS*, *TS*, *StatSkew*, *HD*] gives a maximum success at both the frequencies.

7.5 CONCLUSIONS

The results show that the proposed hybrid scheme for classification of seafloor sediments gives improved success over the existing hybrid schemes. In addition, the features selection method clearly demonstrates that backscatter strength, time spread, statistical skewness, and Hausdroff dimension are the dominant echo features in this study area. The results also revealed that the use of 210 kHz is advantageous for the classification of seafloor sediments in the study area.

The SOM based unsupervised method essentially reduces the requirement for collecting a large number of sediment samples in an unknown area. This method can be efficiently used in combination with other sediments classifiers. Moreover, the FCM based data-driven features selection process can also be used as a preprocessor with other existing classification methods for improving the success in the classification of seafloor sediments.

Chapter 8

Concluding Remarks

8.1 CONCLUSIONS

This study focused on model-based characterization and model-free classification of seafloor sediments by acoustic methods in the central part of the western continental shelf of India in the Arabian Sea. Normal-incidence, single-beam echo sounder backscatter data, collected at two conventional frequencies (33 and 210 kHz), are utilized and the results are presented in the preceding chapters. This section draws conclusions from the results of this study.

The investigation on the applicability of a temporal backscatter model is presented in this work for estimating the values of seafloor sediment parameters namely, mean grain size of sediment, seafloor roughness spectrum parameters, and sediment volume scattering parameter. These parameters are estimated using a 4-D inversion approach at two acoustic frequencies (33 and 210 kHz). The results revealed that the values of mean grain size of sediments estimated from the 33 kHz inversion are relatively more consistent with the ground-truth data compared to those estimated from the 210 kHz inversion. Furthermore, in the absence of the experimental ground-truth data, the estimated values of the roughness spectrum parameters and the sediment volume scattering parameter are assessed with reference to the available published

information (obtained from several other field experiments). In addition, this study also demonstrated the use of a combined two-frequency inversion scheme for the improved characterization of seafloor sediments. Two echo envelopes (at 33 and 210 kHz) are jointly inverted to estimate a single set of values for seafloor sediment parameters applicable to the backscatter data at both of the acoustic frequencies. The results revealed that the estimated values of seafloor roughness spectrum parameters (using the combined two-frequency inversion scheme) are reasonably more consistent with the available published information than those estimated from the single-frequency inversions.

The studies on seafloor sediment classification using model-free techniques focused on developing a hybrid scheme for achieving improved success in an experimental area without any a-priori information. This hybrid scheme consists of an unsupervised approach for estimating the plausible number of sediment classes available in an unknown area and a method based on either neural network or fuzzy cluster algorithm for selecting an optimal feature subset.

The classification of seafloor sediments with model-free techniques utilized seafloor echo features namely backscatter strength, statistical time-spread, statistical skewness, spectral skewness, spectral width, spectral kurtosis, and Hausdroff dimension. The success in segmenting seafloor sediments primarily depends on a-priori information (i.e., ground-truth data) about the number of sediment classes (or cluster centers) available in an experimental area. This information is obtained either from laboratory analysis or from in-situ analysis of sediment samples. The information on the number of available sediment classes in an unknown area is very important input parameter for classification and it is difficult to obtain this information in the absence of ground-truth. This dissertation presents an unsupervised approach, based on Kohonen's

self-organizing feature mapping technique, for estimating the plausible number of cluster centers corresponding to different unknown seafloor sediment types without any prior information. The applicability and the effectiveness of this proposed unsupervised method in any experimental area is demonstrated with simulated data at two acoustic frequencies.

Selection of echo features is another important task for achieving a higher success in the classification of seafloor sediments in an unknown area. Though principal component analysis is widely used as a pre-processor in seafloor classification, cluster analysis utilizing the first three principal components revealed that this technique did not provide promising results in the study area. In this dissertation, two methods are demonstrated to address the features selection issue. One method is based on multilayer neural network and the other utilizes Fuzzy C-Means algorithm. Both these data-driven features selection methods revealed that the optimum three-features subsets namely [backscatter strength, time spread, statistical skewness] and [backscatter strength, time spread, Hausdroff dimension] give maximum success in the classification of seafloor sediments at 33 and 210 kHz respectively. However, the four-features subset [backscatter strength, time spread, statistical skewness, Hausdroff dimension] gives highest success only with the multilayer neural network based approach for both the acoustic frequencies (33 and 210 kHz). Fuzzy C-Means algorithm based approach did not show any improvement in the success rate with the four-features subset. Moreover, the analyses with neural network based method demonstrated that backscatter strength is the most important feature at both the acoustic frequencies (33 and 210 kHz), while time spread is important (in addition to the backscatter strength) only at 33 kHz. The results from these two methods revealed that the use of 210 kHz is advantageous for the classification of seafloor sediments.

The proposed unsupervised method, to estimate the plausible maximum number of sediment classes corresponding to different unknown seafloor sediment types, practically reduces the requirement for collection of large number of sediment samples in an unknown area. The proposed features selection methods offer a possible use of these approaches as pre-processors to other existing classification tools for improving the success in classification of seafloor sediments.

8.2 PRACTICAL UTILITY

Fine grain sediments in the continental margins often contain free gas bubbles. The presence of gas bubbles, even in small amount, can significantly alter the geo-acoustic characteristics of the seafloor sediments (as mentioned earlier). The contributions from gas-trapped sediments on backscatter response are much stronger compared to the other scatterers. In addition, the features like pockmarks, which are associated the seepage of gases and fluids (in the past or at present), are of considerable interests in the continental margins. Karisiddaiah and Veerayya (2002) reported the presence of pockmarks in sediments in the central western continental margin of India. These seafloor features also change the geo-acoustics characteristics of the sedimentary environment. If the temporal backscatter model is validated against the ground-truth information, model-based estimation of the characteristics of seafloor sediments can give valuable information in this scenario. Additional information from side scan sonar images, video images, and sub-bottom profilers at selected locations in an experimental area can suffice the characterization of seafloor sediments.

Seafloor sediment properties (e.g., mean grain size, sediment type, sound speed in sediment, attenuation in sediment, etc.) are becoming important in the recent years as naval operations shift towards the littoral waters. These properties are very significant for several applications such as the development of sonar performance prediction model and naval mine counter measure operations. An optimum performance of a sonar in any area primarily requires information on the loss of acoustic energy. This loss of energy greatly depends on the characteristics of seafloor sediments and the acoustic frequency of a sonar. Since the type of sediment changes over a distance, estimations of the characteristics of sediments and their classifications using acoustic techniques are advantageous for this purpose. In addition, acoustic backscatter strength is an essential parameter for detection of mines in different types of sediment on the seafloor. If the properties of seafloor sediments are known in advance, fine-tuning of the acoustic frequencies to locate mines in the seafloor sediments becomes effective. Moreover, detail knowledge on the acoustic interaction with seafloor is essential for developing environmentally adaptive acoustic sensors for scientific as well as naval application.

8.3 FUTURE WORK

Scattering from the seafloor is a complex phenomenon and has large variability from region to region. Thus, understanding on the physical processes of seafloor scattering at different acoustic frequencies is important for further development of theoretical models. More experiments are essential to understand the physical processes associated with the seafloor scattering mechanism at different acoustic frequencies. The possibility of utilizing backscatter data obtained from two frequencies of a normal-

incidence, single-beam echo sounder for characterization of the seafloor sediments has been attempted in this work. Though the investigation indicates promising results on the characterization of seafloor sediments using the combined two-frequency inversion approach, well-planned field experiments using multiple acoustic frequencies are essential in future for precise assessment of the temporal backscatter model and its applications in different sedimentary environments. Therefore, the effective discrimination of heterogeneous distribution of seafloor sediments using multiple acoustic frequencies is to be investigated in detail.

Presently, all single-beam echo sounders are fitted with an option to change the transmitted pulse length as the seafloor depth changes. This optional facility of modern echo sounders has to be explored for obtaining the normalized echo waveforms data in field experiments. Echo features computed from these normalized echo waveforms should be explored for effective real-time classification of the seafloor sediments in future.

PUBLICATIONS

1. Chakraborty, B. and De, C. (2008). Seafloor characterization using time-dependent acoustic backscatter: study of Arabian Sea. *Proceedings of IEEE Oceans 2008, Kobe, Japan.* [http://ieeexplore.ieee.org/articleSale/Sarticle.jsp?arnumber=4530999].
2. De, C. and Chakraborty, B. (2009). Acoustic characterization of seafloor sediment employing a hybrid method of neural network architecture and fuzzy algorithm. *IEEE Geoscience and Remote Sensing Letters*, 6(4): 743-747.
3. De, C. and Chakraborty, B. (2010). Preference of echo features for classification of seafloor sediments using neural networks. *Marine Geophysical Researches*, 31(3): 215-221.
4. De, C. and Chakraborty, B. (2011). Model-based acoustic remote sensing of seafloor characteristics. *IEEE Transactions on Geoscience and Remote Sensing*, 49(10): In Press. (DOI: 10.1109/TGRS.2011.2139218)

Bibliography

1. Alexandrou, D. and Pantzartzis, D. (1993). A methodology for acoustic seafloor classification. *IEEE Journal of Oceanic Engineering*, 18(2): 81-86.
2. Anderson, A. L. and Hampton, L. D. (1980a). Acoustics of gas-bearing sediments. I. Background. *Journal of the Acoustical Society of America*, 67(6): 1865–1889.
3. Anderson, A. L. and Hampton, L. D. (1980b). Acoustics of gas-bearing sediments. II. Measurements and models. *Journal of the Acoustical Society of America*, 67(6): 1890–1903.
4. Anderson, J. T., Gregory, R. S., and Collins, W. T. (2002). Acoustic classification of marine habitats in coastal Newfoundland. *ICES Journal of Marine Science*, 59(1): 156-167.
5. Anderson, J. T., Holliday, D. V., Kloser, R., Reid, D. G., and Simrad, Y. (2008). Acoustic seabed classification: current practice and future directions. *ICES Journal of Marine Science*, 65(6): 1004-1011.
6. Anonymous (1999). *NS-420 User Guide*. Reson Navitronics Systems AS, Denmark.
7. APL Handbook (1994). *APL-UW High Frequency Ocean Environmental Acoustic Models Handbook*. Technical Report, APL-UW TR 9407, AEAS 9501, Applied Physics Laboratory, University of Washington, Seattle.
8. Atallah, L., Probert Smith, P. J., and Bates, C. R. (2002). Wavelet analysis of bathymetric sidescan sonar data for the classification of seafloor sediments in Hopvagen Bay - Norway. *Marine Geophysical Researches*, 23(5-6): 431-442.
9. Ballard, M. S., Becker, K. M., and Goff, J. A. (2010). Geoacoustic inversion for the New Jersey shelf: 3-D sediment model. *IEEE Journal of Oceanic Engineering*, 35(1): 28-42.

10. Bates, C. R. and Whitehead, E. J. (2001). *ECHOplus measurements in Hopavagen Bay, Norway*. The Oceanography Society, Biennial Scientific Meeting, April 2001.

11. Beale, R. and Jackson, T. (1990). *Neural computing: An introduction*. Institute of Physics Publishing Ltd., Bristol and Philadelphia.

12. Bezdek, J. C. (1981). *Pattern Recognition with Fuzzy Objective Function Algorithms*. Plenum Press, New York.

13. Biot, M. A. (1957). Reflection on a rough surface from an acoustic point source. *Journal of the Acoustical Society of America*, 29(11): 1193-1200.

14. Biot, M. A. (1968). Generalized boundary condition for multiple scatter in acoustic reflection. *Journal of the Acoustical Society of America*, 44(6): 1616-1622.

15. Boehme, H. and Chotiros, N. P. (1988). Acoustic backscattering at low grazing angles from the ocean bottom. *Journal of the Acoustical Society of America*, 84(3): 1018-1029.

16. Boehme, H., Chotiros, N. P., Rolleigh, L. D., Pitt, S. P., Garcia, A. L., Goldsberry, T. G., and Lamb, R. A. (1985). Acoustic backscattering at low grazing angles from the ocean bottom. Part I. Bottom backscattering strength. *Journal of the Acoustical Society of America*, 77(3): 962-974.

17. Boyle, F. A. and Chotiros, N. P. (1992). Experimental detection of a slow acoustic wave in sediment at shallow grazing angles. *Journal of the Acoustical Society of America*, 91(5): 2615-2619.

18. Boyle, F. A. and Chotiros, N. P. (1995a). A model for high-frequency acoustic backscatter from muddy sediments. *Journal of the Acoustical Society of America*, 98(1): 525–530.

19. Boyle, F. A. and Chotiros, N. P. (1995b). A model for high-frequency acoustic backscatter from gas bubbles in sandy sediments at shallow grazing angles. *Journal of the Acoustical Society of America*, 98(1): 531–541.

20. Brekhovskikh, L. M. and Lysanov, Yu. P. (2003). *Fundamentals of ocean acoustics*. 3rd Edition, Berlin: Springer-Verlag.

21. Briggs, K. B. (1989). Microtopographical roughness of shallow-water continental shelves. *IEEE Journal of Oceanic Engineering*, 14(4): 360-367.

22. Briggs, K. B., Tang, D., and Williams, K. L. (2002). Characterization of interface roughness of rippled sand off Fort Walton beach, Florida. *IEEE Journal of Oceanic Engineering*, 27(3): 505-514.

23. Briggs, K. B., Lyons, A. P., Pouliquen, E., Mayer, L. A., and Richardson, M. D. (2005). Seafloor roughness, sediment grain size, and temporal stability. *Proceedings International Conference Underwater Acoustic Measurements: Technology Results*, Heraklion, Crete, Greece. Eds. J. S. Papadakis and L. Bjørnø, pp. 337-344, July 2005.

24. Burczynski, J. (1999). Bottom Classification. BioSonics Inc., 4027 Leary Way NW, Seattle WA 98107, USA. [http://www.biosonicsinc.com/product_pages/vbt_classifier.htm]

25. Burns, D., Queen, C. B., and Chivers, R. C. (1985). An ultrasonic signal processor for use in underwater acoustics. *Ultrasonics*, 23(4): 189-191.

26. Caughey, D. A. and Kirlin, R. L. (1996). Blind deconvolution of echo sounder envelopes. *Proceedings of IEEE International Conference on Acoustics, Speech and Signal Processing, ICASS-96*, 6: 3149-3152.

27. Chakraborty, B. (1989). Effects of scattering due to seafloor microrelief on a multifrequency sonar seabed profiler. *Journal of the Acoustical Society of America*, 85(4): 1478-1481.

28. Chakraborty, B. and Pathak, D. (1999). Sea bottom backscatter studies in the western continental shelf of India. *Journal of Sound and Vibration*, 219(1): 51-62.

29. Chakraborty, B., Schenke, H. W., Kodagali, V., and Hagen, R. (2000). Sea bottom characterization using multibeam echo sounder angular backscatter: An application of the composite roughness theory. *IEEE Transactions on Geoscience and Remote sensing*, 38(5): 2419-2422.

30. Chakraborty, B., Kaustubha, R., Hegde, A., and Pereira, A. (2001). Acoustic seafloor sediment classification using self-organizing feature maps. *IEEE Transaction on Geoscience and Remote Sensing*, 39(12): 2722-2725.

31. Chakraborty, B. (2002). A neural network based seafloor classification using acoustic backscatter. In *Advances in soft computing AFSS 2002*. Ed. by N. R. Pal and M. Sugeno, Springer-Verlag Berlin, Heidelberg, pp. 245-250.

32. Chakraborty, B., Lourenco, E., Kodagali, V., and Baracho, J. (2003a). Application of artificial neural networks to segmentation and classification of topographic profiles of ridge-flank seafloor. *Current Science*, 85(3): 306-312.

33. Chakraborty, B., Kodagali, V., and Bracho, J. (2003b). Seafloor classification using multi-beam echo sounding angular backscatter data: A real-time approach employing hybrid neural network architecture. *IEEE Journal of Oceanic Engineering*, 28(1): 121-128.

34. Chakraborty, B. and Kodagali, V. (2004). Characterizing Indian Ocean manganese nodule-bearing seafloor using multi-beam angular backscatter. *Geo-Marine Letters*, 24(1): 8-13.

35. Chakraborty, B., Mahale, V., de Sousa, C., and Das, P. (2004). Seafloor classification using echo-waveforms: A method employing hybrid neural network architecture. *IEEE Geoscience and Remote Sensing Letters*, 1(3): 196-200.

36. Chakraborty, B., Navelkar, G. S., and Rao, B. R. (2005). *Cruise report*. National Institute of Oceanography, Goa, India, Sagar Purvi cruise rep. SR 03/05, 2005.

37. Chakraborty, B., Mahale, V., Navelkar, G., Rao, B. R., Prabhudesai, R. G., Ingole, B., and Janakiraman, G. (2007a). Acoustic characterization of seafloor habitats on the western continental shelf of India. *ICES Journal of Marine Science*, 64(3): 551-558.

38. Chakraborty, B., Mahale, V., Shashikumar, K., and Srinivas, K. (2007b). Quantitative characteristics of the Indian Ocean relief using fractal dimension. *Indian Journal of Marine Sciences*, 36(2): 152-161.

39. Chakraborty, B. and De, C. (2008). Seafloor characterization using time-dependent acoustic backscatter: study of Arabian Sea. *Proceedings of IEEE Oceans* 08, *Kobe, Japan.* [http://ieeexplore.ieee.org/articleSale/Sarticle.jsp?arnumber=4530999].

40. Chivers, R. C., Emerson, N., and Burns, D. R. (1990). New acoustic processing for underway surveying. *The Hydrographic Journal*, 56: 9-17.

41. Chotiros, N. P. (1989). High frequency acoustic bottom penetration: Theory and experiment. *Proceedings of IEEE Oceans '89*, 4: 1158-1161.

42. Chotiros, N. P. (1994). Reflection and reverberation in normal incidence echo sounding. *Journal of the Acoustical Society of America,* 96(5): 2921-2929.

43. Chotiros, N. P. (1995). Biot model of sound propagation in water-saturated sand. *Journal of the Acoustical Society of America*, 97(1): 199-214.

44. Clarke, P. A. and Hamilton, L. J. (1999). *The ABCS program for the analysis of echo sounder returns for acoustic bottom classification.* DSTO Aeronautical and Maritime Research Laboratory, Melbourne, Australia, Report No. DSTO-GD-0215.

45. Clay, C. S. and Leong, W. K. (1974). Acoustic estimates of the topography and roughness spectrum of the sea floor southwest of the Iberian Peninsula. In *Physics of sound in marine sediments*. Ed. by L. Hampton. Plenum Press, New York, NY.

46. Clay, C. S., Medwin, H., and Wright, W. M. (1973). Specularly scattered sound and the probability density function of a rough surface. *Journal of the Acoustical Society of America,* 53(6): 1677–1682.

47. Collier, J. S. and Brown, C. J. (2005). Correlation of side scan backscatter with grain size distribution of surficial seabed sediments. *Marine Geology*, 214(4): 431-449.

48. Collins, W. T. (1996). Echo sounders used for seabed classification. *International Dredging Review*, 15(6): 10-11.

49. Collins, W. T. and McConnaughey, R. A. (1998). Acoustic classification of the seafloor to address essential fish-habitat and marine-protected area requirements. *Proceedings of the Canadian Hydrographic Conference '98*, pp. 369-377.

50. Collins, W. T. and Preston, J. M. (2002). Multibeam seabed classification. *International Ocean Systems*, 6(4): 12-15.

51. Collins, W. T., Gregory, R., and Anderson, J. (1996). A digital approach to seabed classification. *Sea Technology*, 37(8): 83-87.

52. Crowther, P. A. (1983). Some statistics of the seabed and acoustic scattering therefrom. In *Acoustics and the Sea-Bed.* Ed. by N. G. Pace, Bath Univ., Bath, England, pp.147-155.

53. Cuff, A., Anderson, J., and Devillers, R. (2009). Improving seabed classification through the use of multiple acoustic frequencies. *Proceedings of Spatial Knowledge and Information Conference*, Fernie (BC), Canada.

54. Davis, K. S., Slowey, N. C., Stender, I. H., Fiedler, H., Bryant, W. R., and Fechner, G. (1996). Acoustic backscatter and sediment textural properties of inner shelf sands, northeastern Gulf of Mexico. *Geo-Marine Letters*, 16(3): 273-278.

55. de Moustier, C. and Alexandrou, D. (1991). Angular dependence of 12kHz seafloor acoustic backscatter. *Journal of the Acoustical Society of America*, 90(1): 522-531.

56. de Moustier, C. and Matsumoto, H. (1993). Seafloor acoustic remote sensing with multibeam echo-sounders and bathymetric sidescan sonar systems. *Marine Geophysical Researches*, 15(1): 27-42.

57. De, C., Murty, G. R. K., and Uthaman, C. P. (2005). Seafloor characterization by inversion of roughness spectrum. *Acta Acoustica*, 91(5): 817-821.

58. De, C. and Chakraborty, B. (2009). Acoustic characterization of seafloor sediment employing a hybrid method of neural network architecture and fuzzy algorithm. *IEEE Geoscience and Remote Sensing Letters*, 6(4): 743-747.

59. Dung, T. V. and Stepnowski, A. (2000). Sea bottom recognition using multistage fuzzy neural network operating on multi-frequency data. *Acta Acustica*, 86(5): 830-837.

60. Dunn, J. (1973). A fuzzy relative of the isodata process and its use in detecting compact, well-separated clusters. *Journal of Cybernetics*, 3(3): 32–57.

61. Eckart, C. (1953). Scattering of sound from the sea surface. *Journal of the Acoustical Society of America*, 25(3): 566-570.

62. Essen, H.-H. (1994). Scattering from a rough sedimental seafloor containing shear and layering. *Journal of the Acoustical Society of America*, 95(3): 1299-1310.

63. Ewing, W. M., Jardetzky, W. S., and Press, F. (1957). *Elastic waves in Layered media*. McGraw-Hill, New York.

64. Ferrini, V. L. and Flood, R. D. (2006). The effects of fine-scale surface roughness and grain size on 300 kHz multibeam backscatter intensity in sandy marine sedimentary environments. *Marine Geology*, 228(1-4): 153-172.

65. Folk, R. L. (1954). The distinction between grain size and mineral composition in sedimentary rock nomenclature. *Journal of Geology*, 62(4): 344-359.

66. Folk, R. L. (1974). *Petrology of sedimentary rocks*. Hemphill Publishing Co., Austin, TX.

67. Fonseca, L., Mayer, L., Orange, D., and Driscoll, N. (2002). The high-frequency backscattering angular response of gassy sediments: Model/data comparison from the Eel River Margin, California. *Journal of the Acoustical Society of America*, 111(6): 26121-2631.

68. Francois, R. E. and Garrison, G. R. (1982a). Sound absorption based on ocean measurements. Part I: Pure water and magnesium sulphate contributions. *Journal of the Acoustical Society of America*, 72(3): 896-907.

69. Francois, R. E. and Garrison, G. R. (1982b). Sound absorption based on ocean measurements. Part II: Boric acid contribution and equation for total absorption. *Journal of the Acoustical Society of America*, 72(6): 1879-1890.

70. Freitas, R., Rodrigues, A. M., Morris, E., Perez-Llorens, J. L., and Quintino, V. (2008). Single-beam acoustic ground discrimination of shallow water habitats: 50 kHz or 200 kHz frequency survey. *Estuarine, Coastal and Shelf Science*, 78(4): 613-622.

71. Ghosh, J., Deuser, L. M., and Beck, S. D. (1992). A neural network based hybrid system for detection, characterization, and classification of short-duration oceanic signals. *IEEE Journal of Oceanic Engineering*, 17(4): 351-363.

72. Goff, J. A., Olson, H. C., and Duncan, C. S. (2000). Correlation of side-scan backscatter intensity with grain-size distribution of shelf sediments, New Jersey margin. *Geo-Marine Letters*, 20(1): 43-49.

73. Gott, R. M. and Martinez, A. B. (1993). Estimation of the composite roughness model parameters. *Proceedings of IEEE Oceans '93*, I: I444-I449.

74. Greenlaw, C. W., Holliday, D. V., and McGehee, D. E. (2004). High-frequency scattering from saturated sand sediments. *Journal of the Acoustical Society of America*, 115(6): 2818-2823.

75. Greenstreet, S. P. R., Tuck, I. D., Grewar, G. N., Armstrong, E., Reid, D. G., and Wright, P. J. (1997). An assessment of the acoustic survey technique, RoxAnn, as a means of mapping seabed habitat. *ICES Journal of Marine Science*, 54(5): 939-959.

76. Hamilton, E. L. (1971a). Predictions of *in situ* acoustic and elastic properties of marine sediments. *Geophysics*, 36(2): 266-284.

77. Hamilton, E. L. (1971b). Elastic properties of marine sediments. *Journal of Geophysical Research*, 76: 579-604.

78. Hamilton, E. L. (1972). Compressional-wave attenuation in marine sediments. *Geophysics*, 37(4): 620-646.

79. Hamilton, E. L. (1980). Geoacoustic modelling of the seafloor. *Journal of the Acoustical Society of America*, 68(5): 1313-1340.

80. Hamilton, E. L. and Bachman, R. T. (1982). Sound velocity and related properties of marine sediments. *Journal of the Acoustical Society of America*, 72(6): 1891-1904.

81. Hamilton, L. J. (2001). *Acoustic seabed classification systems*. Aeronautical and Maritime Research Laboratory, Report No. DSTO-TN-0401.

82. Hamilton, L. J., Mulhearn, P. J., and Poeckert, R. (1999). Comparison of RoxAnn and QTC-View acoustic bottom classification system performance for the Cairns area, Great Barrier Reef, Australia. *Continental Shelf Research*, 19(12): 1577-1597.

83. Hathaway, R. J. and Bezdek, J. C. (1988). Recent convergence results for the fuzzy c-means clustering algorithms. *Journal of Classification*, 5(2): 237–247.

84. Hertz, J., Krogh, A., and Palmer, R. G. (1991). *Introduction to the theory of neural computation*. Lecture Notes Volume I, Addison-Wesley Publishing Co., The Advance Book Program, USA.

85. Hines, P. C. (1990). Theoretical model of acoustic backscatter from a smooth seabed. *Journal of the Acoustical Society of America*, 88(1): 324-334.

86. Holland, C. W. and Neumann, P. (1998). Sub-bottom scattering: A modeling approach. *Journal of the Acoustical Society of America*, 104(3), Pt. I: 1363-1373.

87. Holliday, D. V. (2007). Theory of sound scattering from the seabed. In *Acoustic seabed classification of marine physical and biological landscapes*. Ed. by J. T. Anderson. ICES Cooperative Research Report, No. 286, pp. 7-28.

88. Hutin, E., Simrad, Y., and Archambault, P. (2005). Acoustic detection of a scallop bed from a single-beam echo sounder in the St. Lawrence. *ICES Journal of Marine Science*, 62(5): 966-983.

89. Ivakin, A. N. and Lysanov, Yu. P. (1981a). Theory of underwater sound scattering by random inhomogeneiries of the bottom. *Soviet Physical Acoustics*, 27(1): 61-64.

90. Ivakin, A. N. and Lysanov, Yu. P. (1981b). Underwater sound scattering by volume inhomogeneities of a bottom medium bounded by a rough surface. *Soviet Physical Acoustics*, 27(3): 212-215.

91. Ivakin, A. N. (1986). Sound scattering by random inhomogeneities of stratified ocean sediments. *Soviet Physical Acoustics*, 32(6): 492-496.

92. Ivakin, A. N. and Sessarego, J.-P. (2007). High frequency broad band scattering from water-saturated granular sediments: Scaling effects. *Journal of the Acoustical Society of America*, 122(5): EL 165 - EL 171.

93. Ivakin, A. N. (2010). Scattering from inclusions in marine sediments: SAX04 data/model comparisons. Submitted to *IEEE Journal of Oceanic Engineering*.

94. Jackson, D. R., Winebrenner, D. P., and Ishimaru, A. (1986a). Application of the composite roughness model to high-frequency bottom backscattering. *Journal of the Acoustical Society of America*, 79(5): 1410-1422.

95. Jackson, D. R., Baird, A. M., Crisp, J. J., and Thomson, P. A. G. (1986b). High-frequency bottom backscattering measurements in shallow water. *Journal Acoustical Society of America*, 80(4): 1188-1199.

96. Jackson, D. R. and Briggs, K. B. (1992). High-frequency bottom backscattering: Roughness versus sediment volume scattering. *Journal of the Acoustical Society of America*, 92(2), Pt. 1: 962-977.

97. Jackson, D. R., Briggs, K. B., Williams, K. L., and Richardson, M. D. (1996). Test of models for high-frequency seafloor backscatter. *IEEE Journal of Oceanic Engineering*, 21(4): 458-470.

98. Jackson, D. R. and Richardson, M. D. (2007). *High-frequency seafloor acoustics*, Springer, USA.

99. Jackson, D. R. (2009). Private communication with Dr. Bishwajit Chakraborty, National Institute of Oceanography, Goa. February 2009. *Subject*: Combined two-frequency inversion.

100. Jiang, Y-M., Chapman, N. R., and Gerstoft, P. (2010). Estimation of geoacoustic properties of marine sediment using a hybrid differential evolution inversion method. *IEEE Journal of Oceanic Engineering*, 35(1): 59-69.

101. Jollife, I. T. (1986). *Principal Component Analysis*. Springer-Verlag, New York.

102. Karisiddaiah, S. M. and Veerayya, M. (2002). Occurrence of pockmarks and gas seepages along the central western continental margin of India. *Current Science*, 82(1): 52-57.

103. Kieser, R., Preston, J., Orlowski, A., and Chapman, R. (2007). Acquiring and preparing acoustic data. In *Acoustic seabed classification of marine physical and biological landscapes*. Ed. by J. T. Anderson. ICES Cooperative Research Report, No. 286, pp. 29-44.

104. Kim, H-J., Chang, J-K., Jou, H-T., Park, G-T., Suk, B-C., and Kim, K. Y. (2002). Seabed classification from acoustic profiling data using the similarity index. *Journal of the Acoustical Society of America*, 111(2): 794-799.

105. Kloser, R. J., Bax, N. J., Ryan, T., Williams, A., and Baker, B. A. (2001). Remote sensing of seabed types in the Australian South East Fishery - development and application of normal incident acoustic techniques and associated 'ground truthing'. *Marine Freshwater Research*, 52(4): 475-489.

106. Kloser, R. (2007). Seabed backscatter, data collection, and quality overview. In *Acoustic seabed classification of marine physical and biological landscapes*. Ed. by J. T. Anderson. ICES Cooperative Research Report, No. 286, pp. 47-48.

107. Klusek, Z., Tegowski, J., and Szczucka, J. (1994). Characteristic properties of bottom backscattering in the southern Baltic Sea at ultrasound frequencies. *Oceanologia*, 36(1): 81-102.

108. Kohonen, T. (1989). *Self-organization and associative memory*. 3rd Edition, Springer-Verlag, Berlin.

109. Kohonen, T. (1990). Self-organizing map. *Proceedings of IEEE*, 78(9): 1464-1480.

110. Kohonen, T. (1997). *Self-organizing maps*. Springer-Verlag, Berlin, 2nd Edition.

111. Korneliussen, R. J., Diner, N., Ona, E., Berger, L., and Fernandes, P. G. (2008). Proposals for the collection of multifrequency acoustic data. *ICES Journal of Marine Science*, 65(6): 982-994.

112. Kostylev, V. E., Todd, B. J., Gordon, B. J. F., Courtney, R. C., Gordon, D. M. C., and Pickrill, R. A. (2001). Benthic habitat mapping on the Scotian Shelf based on multibeam bathymetry, surficial geology and sea floor photographs. *Marine Ecology Progress Series*, 219: 121-137.

113. Kuo, E. Y. (1964). Wave scattering and transmission at irregular surfaces. *Journal of the Acoustical Society of America*, 36(11): 2135-2142.

114. LeBlanc, L. R., Mayer, L., Rufino, M., Schock, S. G., and King, J. (1992). Marine sediment classification using the chirp sonar. *Journal Acoustical Society of America*, 91(1): 107-115.

115. Legendre, P., Ellingsen, K. E., Bjornbom, E., and Casgrain, P. (2002). Acoustic seabed classification: Improved statistical method. *Canadian Journal of Fisheries and Aquatic Science*, 59: 1085-1089.

116. Legendre, P. (2003). Reply to the comment by Preston and Kirlin on "Acoustic seabed classification: improved statistical method". *Canadian Journal of Fisheries and Aquatic Science*, 60: 1301-1305.

117. Lubniewski, Z. and Pouliquen, E. (2004). Sensitivity of echo parameters to seafloor properties and depth variability. *Proceedings of Seventh European Conference on Underwater Acoustics*, ECUA 2004, Delft, The Netherlands.

118. Lubniewski, Z. and Stepnowski, A. (1998). Application of the fractal analysis in the sea bottom recognition. *Archives of Acoustics*, 23(4): 499-511.

119. Lurton, X. (2002). *An introduction to underwater acoustics: Principles and applications*. Springer, Praxis Publishing, UK.

120. Lyons, A. P. and Orsi, T. H. (1998). The effect of a layer of varying density on high-frequency reflection, forward loss, and backscatter. *IEEE Journal of Oceanic Engineering*, 23(4): 411-422.

121. Lyons, A. P., Anderson, A. L., and Dwan, F. S. (1994). Acoustic scattering from the seafloor: Modeling and data comparison. *Journal of the Acoustical Society of America*, 95(5): 2441-2451.

122. Lyons, A. P., Fox, W. L. J., Hasiotis, T., and Pouliquen, E. (2002). Characterization of the two-dimensional roughness of wave-rippled sea floors using digital photogrammetry. *IEEE Journal Oceanic Engineering*, 27(3): 515-524.

123. Mackenzie, K. V. (1961). Bottom reverberation for 530- and 1030- cps sound in deep water. *Journal of the Acoustical Society of America*, 33(11): 1498-1504.

124. Mandelbrot, B. B. (1982). *The fractal geometry of nature*. Freeman, San Fancisco.

125. Manly, B. F. J. (1994). *Multivariate statistical methods*. Chapman & Hall, London.

126. Maroni, C. –S., Quinquis, A., and Radoi, E. (1997). A methodology for neural network based classification of marine sediments using a subbottom profiler. *IEEE Proceedings of Oceans '97*, 2:1370-1375.

127. Masters, T. (1993). *Practical neural network recipes in C++*. Academic Press, Inc., London.

128. MATLAB 7.0 (2004). The Math Works, Inc., Natick.

129. Matsumoto, H., Dziak, R. P., and Fox, C. G. (1993). Estimation of seafloor microtopographic roughness through modeling of acoustic backscatter data recorded by multibeam sonar systems. *Journal of the Acoustical Society of America*, 94(5): 2776-2787.

130. McCulloch, W. S. and Pitts, W. (1943). A logical calculus of ideas immanent in nervous activity. *Bulletin of Mathematical Biophysics*, 5: 115-133.

131. McKinney, C. M. and Anderson, C. D. (1964). Measurements of backscattering of sound from the ocean bottom. *Journal of the Acoustical Society of America*, 36(1): 158-163.

132. Medwin, H. and Clay, C. S. (1998). *Fundamentals of acoustical oceanography*. Academic Press, Boston.

133. Metropolis, N., Rosenbluth, A., Rosenbluth, M., Teller, A., and Teller, E. (1953). Equation of state calculations by fast computing machines. *The Journal of Chemical Physics*, 21(6): 1087-1092.

134. Michalopoulou, Z. -H., Alexandrou, D., and de Moustier, C. (1994). Application of a maximum likelihood processor to acoustic backscatter for the estimation of seafloor roughness parameters. *Journal of the Acoustical Society of America*, 95(5) Pt. 1: 2467-2477.

135. Michalopoulou, Z. -H., Alexandrou, D., and de Moustier, C. (1995). Application of neural and statistical classifiers to the problem of seafloor characterization. *IEEE Journal Oceanic Engineering*, 20(3): 190-197.

136. Michalopoulou, Z.-H. and Alexandrou, D. (1996). Bayesian modeling of acoustic signals for seafloor identification. *Journal of the Acoustical Society of America*, 99(1): 223-233.

137. Minsky, M. L. and Papert, S. A. (1969). *Perceptrons*. MIT Press, Cambridge, MA.

138. Moore, K. D. and Jaffe, J. S. (2002). Time-evolution of high-resolution topographic measurements of the sea floor using a 3-D Laser Line Scan mapping system. *IEEE Journal of Oceanic Engineering*, 27(4): 525-545.

139. Morse, P. M. (1948). *Vibration and Sound*. McGraw Hill, New York.

140. Moszynski, M., Dung, T. V., and Stepnowski, A. (2000). Analysis of the influence of wavelet coefficients and other backscattered echo parameters on the performance of seabed neuro-fuzzy classifiers. *Proceedings of the Fifth European Conference on Underwater Acoustics*, ECUA 2000, pp. 301-306.

141. Mourad, P. D. and Jackson, D. R. (1989). High frequency sonar equation models for bottom backscatter and forward loss. *Proceedings of IEEE Oceans '89*, 4: 1168-1175.

142. Mourad, P. D. and Jackson, D. R. (1993). A model/data comparison for low-frequency bottom backscatter. *Journal of the Acoustical Society of America*, 94(1): 344-358.

143. Navelkar, G. S. and Mahale, V. (2005). *Cruise report*. National Institute of Oceanography, Goa, India, Sagar Purvi cruise rep. SR 16/05, 2005.

144. Navelkar, G. S., Prabhudesai, R. G., and Chakraborty, B. (2005). Dual frequency echo data acquisition system for seafloor classification. *Proceedings of SYMPOL*, CUSAT, 40-46.

145. Nelder, J. A. and Mead, R. (1965). A simplex method for function minimization. *Computer Journal*, 7(4): 308-313.

146. Nolle, A. W., Hoyer, W. A., Mifsud, J. F., Runyan, W. R., and Ward, M. B. (1963). Acoustical properties of water-filled sands. *Journal of the Acoustical Society of America*, 35(9): 1394-1408.

147. Novarini, J. C. and Caruthers, J. W. (1998). A simplified approach to backscattering from a rough seafloor with sediment inhomogeneities. *IEEE Journal Oceanic Engineering*, 23(3): 157-166.

148. Orlowski, A. (1984). Application of multiple echoes energy measurement for evaluation of sea bottom type. *Oceanologia*, 19: 61-78.

149. Orlowski, A. (2007). Acoustic seabed classification applied to Baltic benthic habitat studies: a new approach. *Oceanologia*, 49(2); 229-243.

150. Pace, N. G. and Gao, H. (1988). Swathe Seabed Classification. *IEEE Journal of Oceanic Engineering*, 13(2): 83-90.

151. Pal, M. and Foody, G. M. (2010). Feature selection for classification of hyperspectral data by SVM. *IEEE Transactions on Geoscience and Remote Sensing*, 48(5): 2297-2307.

152. Pandian, P. K., Ruscoe, J. P., Shields, M., Side, J. C., Harris, R. E., Kerr, S. A., and Bullen, C. R. (2009). Seabed habitat mapping techniques: an overview of the performance of various systems. *Mediterranean Marine Science*, 10(2): 29-43.

153. Penrose, J. D., Siwabessy, P. J. W., Gavrilov, A., Parnum, I., Hamilton, L. J., Bickers, A., Brooke, B., Ryan, D. A., and Kennedy, P. (2005). *Acoustic techniques for seabed classification*. Cooperative Research Centre for Coastal Zone Estuary and Waterway Management, Technical Report 32.

154. Pouliquen, E. (2004). Depth dependence correction for normal incidence echo sounding. *Proceedings of Seventh European Conference on Underwater Acoustics*, ECUA 2004, Delft, The Netherlands.

155. Pouliquen, E. and Lurton, X. (1992). Seabed identification using echo-sounder signals. *Proceedings of the European Conference on Underwater Acoustics.* Elsevier Applied Science. London and New York. September 1992, pp. 535-539.

156. Prager, B. T., Caughey, D. A., and Poeckert, R. H. (1995). Bottom classification: Operational results from QTC view. *Proceedings of IEEE Oceans '95*, 3: 1827-1835.

157. Press, W. H., Teukolsky, S. A., Vetterling, W. T., and Flannery, B. P. (1992). *Numerical Recipes in FORTRAN: The art of scientific computing*. Second edition. Cambridge University Press, Cambridge.

158. Preston, J. M., Collins, W. T., Mosher, D. C., Poeckert, R. H., and Kuwahara, R. H. (1999). The strength of correlations between geotechnical variables and acoustic classifications. *Proceedings of MTS/IEEE Oceans'99*, 3: 1123-1128.

159. Preston, J. M. and Kirlin, T. L. (2003). Comment on "Acoustic seabed classification: improved statistical method". *Canadian Journal of Fisheries and Aquatic Science*, 60: 1299-1300.

160. Quintino, V., Freitas, R., Mamede, R., Ricardo, F., Rodrigues, A. M., Mota, J., Pérez-Ruzafa, Á., and Marcos, C. (2010). Remote sensing of underwater vegetation using single-beam acoustics. *ICES Journal of Marine Science*, 67(3): 594–605.

161. Reid, D. (2007). Accounting for spatial and temporal scales and interpolation in acoustic seabed classification surveys. In *Acoustic seabed classification of marine physical and biological landscapes*, Ed. by J. T. Anderson. ICES Cooperative Research Report, No. 286, pp. 73-93.

162. Richardson, M. D. and Davis, A. M. (1998). Modeling methane-rich sediments of Eckernforde Bay. *Continental Shelf Research*, 18(14-15): 1671-1688.

163. Richardson, M. D., Briggs, K. B., Bibee, L. D., Jumars, P. A., Sawyer, W. B., Albert, D. B., Bennett, R. H., Berger, T. K., Buckingham, M. J., Chotiros, N. P., Dahl, P. H., Dewitt, N. T., Fleischer, P., Flood, R., Greenlaw, C. F., Holliday, D. V., Hulbert, M. H., Hutnak, M. P., Jackson, P. D., Jaffe, J. S., Johnson, H. P., Lavoie, D. L., Lyons, A. P., Martens, C. S., McGehee, D. E., Moore, K. D., Orsi, T. H., Piper, J. N., Ray, R. I., Reed, A. H., Self, R. F. L., Schmidt, J. L., Schock, S. G., Simonet, F., Stoll, R. D., Tang, D., Thistle, D. E., Thorsos, E. I., Walter, D. J., and Wheatcroft, R. A. (2001). An overview of SAX99: Environmental considerations. *IEEE Journal of Oceanic Engineering*, 26(1): 26-54.

164. Rosenblatt, F. (1962). *Principles of neurodynamics*. New York, Spartan.

165. Rumelhart, D. E., Hinton, G. E., and Williams, R. J. (1986). Learning representations by back-propagating errors. *Nature*, 323(9): 533-536.

166. Schlagintweit, G. E. O. (1993). Real-time acoustic bottom classification for hydrography - a field evaluation of RoxAnn. *Proceedings of IEEE Oceans '93*, III: 214-219.

167. Schock, S. G., LeBlanc, L. R., and Mayer, L. A. (1989). Chirp sub-bottom profiler for quantitative sediment analysis. *Geophysics*, 54(4): 445-450.

168. Schock, S. G. (2004a). A method for estimating the physical and acoustic properties of the seabed using chirp sonar data. *IEEE Journal of Oceanic Engineering*, 29(4): 1200-1217.

169. Schock, S. G. (2004b). Remote prediction of physical and acoustic sediment properties in South China Sea using chirp sonar. *IEEE Journal of Oceanic Engineering*, 29(4): 1218-1230.

170. Shepard, F. P. (1954). Nomenclature based on sand-silt-clay ratios. *Journal of Sedimentary Petrology*, 24(3): 151-158.

171. Simrad, Y. and Stepnowski, A. (2007). Classification methods and criteria. In *Acoustic seabed classification of marine physical and biological landscapes*. Ed. by J. T. Anderson. ICES Cooperative Research Report, No. 286, pp. 61-70.

172. Sivanandam, S. N., Sumathi, S., and Deepa, S. N. (2006). *Introduction to neural networks using MATLAB 6.0*. Tata McGraw-Hill Publishing Co. Ltd., New Delhi.

173. Siwabessy, P. J. W. (2001). *An investigation of the relationship between seabed type and benthic and bentho-pelagic biota using acoustic techniques*. Ph.D. Thesis, School of Applied Science, The Curtin University of Technology.

174. Smith, G. F., Bruce, D. G., and Roach, E. B. (2001). Remote acoustic habitat assessment techniques used to characterize the quality and extent of Oyster bottom in the Chesapeake Bay. *Marine Geodesy*, 24(3): 171-189.

175. Srinivasan, D., Murty, K. R. G. K., and Murty, G. R. K. (1982). Underwater sound scattering model of the topographic features of the seafloor. *Defence Science Journal*, 32(1): 1-8.

176. Stanic, S., Briggs, K. B., Fleischer, P., Ray, R. I., and Sawyer, W. B. (1988). Shallow-water high frequency bottom scattering off Panama City, Florida. *Journal of the Acoustical Society of America*, 83(6): 2134-2144.

177. Stanic, S., Briggs, K. B., Fleischer, P., Sawyer, W. B., and Ray, R. I. (1989). High-frequency acoustic backscattering from a coarse shell ocean bottom. *Journal of the Acoustical Society of America*, 85(1): 125-136.

178. Stanton, T. K. (1984). Sonar estimates of seafloor micro-roughness. *Journal of the Acoustical Society of America,* 75(3): 809–818.

179. Stanton, T. K. (1985). Echo fluctuations from the rough seafloor: Predictions based on acoustically measured microrelief properties. *Journal of the Acoustical Society of America,* 78(2): 715–721.

180. Stanton, T. K. and Clay, C.S. (1986). Sonar echo statistics as a remote-sensing tool: Volume and seafloor. *IEEE Journal of Oceanic Engineering*, OE-11(1): 79-96.

181. Stanton, T. K., Chu, D., Wiebe, P. H., Eastwood, R. L., and Warren, J. D. (2000). Acoustic scattering by benthic and planktonic-shelled animals. *Journal of the Acoustical Society of America*, 108(2): 535-550.

182. Stanton, T. K. and Chu, D. (2004). On the acoustic diffraction by the edges of benthic shells. *Journal of the Acoustical Society of America*, 116(1): 239-244.

183. Stepnowski, A., Maciolowska, J., and Dung, T. V. (1999). Bottom type identification using combined neuro-fuzzy classifier operating on multi-frequency data. *Archives of Acoustics*, 24(3): 365-378.

184. Stepnowski, A., Moszynski, M., and Dung, T. V. (2003). Adaptive neuro-fuzzy and fuzzy decision tree classifiers as applied to seafloor characterization. *Acoustical Physics*, 49(2): 193–202.

185. Sternlicht, D. D. and de Moustier, C. (1997). Ttemporal modeling of high frequency (30-100 kHz) acoustic seafloor backscatter: Shallow water results. *Proceedings of High Frequency Acoustics in Shallow Water Conference.*

186. Sternlicht, D. D. and de Moustier, C. P. (2003a). Time dependent seafloor acoustic backscatter (10-100 kHz). *Journal of the Acoustical Society of America*, 114(5): 2709-2725.

187. Sternlicht, D. D. and de Moustier, C. P. (2003b). Remote sensing of sediment characteristics by optimized echo-envelope matching. *Journal of the Acoustical Society of America*, 114(5): 2727-2743.

188. Stewart, R. A. and Chotiros, N. P. (1992). Estimation of sediment volume scattering cross section and absorption loss coefficient. *Journal of the Acoustical Society of America*, 91(6): 3242-3247.

189. Stewart, W. K., Marra, M., and Jiang, M. (1992). A hierarchical approach to seafloor classification using neural networks. *Proceeding of IEEE Oceans '92,* I: 109-113.

190. Stewart, W. K., Jiang, M., and Marra, M. (1994). A neural network approach to classification of side scan sonar imagery from a Midocean Ridge area. *IEEE Journal of Oceanic Engineering*, 19(2): 214-224.

191. Stockhausen, J. H. (1963). *Scattering from the volume of an inhomogeneous half-space*. Technical Report 63/9, Naval Research Establishment, Canada.

192. Storti, F. and Balsamo, F. (2009). Particle size distributions by laser diffraction: sensitivity of granular matter strength to analytical operating procedures. *Solid Earth*, 1(1): 25-48.

193. Tang, D. and Frisk, G. V. (1991). Plane-wave reflection from a random fluid half-space. *Journal of the Acoustical Society of America*, 90(5): 2751-2756.

194. Tang, D. and Frisk, G. V. (1992). Spectral parameterization of scattering from a random ocean bottom. *Journal of the Acoustical Society of America*, 92(5): 2792-2799.

195. Tang, D. and Frisk, G. V. (1995). Spatial correlation of acoustic wave scattered from a random ocean bottom. *Journal of the Acoustical Society of America*, 97(5): 2783-2803.

196. Tegowski, J. and Lubniewski, Z. (2000). The use of fractal properties of echo signals for acoustical classification of bottom sediments. *Acta Acustica*, 86(2): 276-282.

197. Tegowski, J. and Lubniewski, Z. (2002). Seabed characterization using spectral moments of the echo signal. *Acta Acoustica*, 88(5): 623-626.

198. Tegowski, J., Gorska, N., and Klusek, Z. (2003). Statistical analysis of acoustic echoes from underwater meadows in the eutrophic Puck Bay (southern Baltic Sea). *Aquatic Living Resources*, 16(3): 215-221.

199. Thorsos, E. I. (1988). The validity of the Kirchhoff approximation for rough surface scattering using a Gaussian roughness spectrum, *Journal of the Acoustical Society of America*, 83(1): 78-92.

200. Thorsos, E. I. and Jackson, D. R. (1989). The validity of the perturbation approximation for rough surface scattering using a Gaussian roughness spectrum. *Journal of the Acoustical Society of America*, 86(1): 261-277.

201. Thorsos, E. I., Williams, K. L., Chotiros, N. P., Christoff, J. T., Commander, K. W., Greenlaw, C. F., Holliday, D. V., Jackson, D. R., Lopes, J. L., McGehee, D. E., Richardson, M. D., Piper, J. E., and Tang, D. (2001). An overview of SAX99: Acoustic measurements. *IEEE Journal of Oceanic Engineering*, 26(1): 4-25.

202. Tolstoy, I. (1982). Coherent sound scatters from a rough interface between arbitrary fluids with particular reference to roughness element shapes and corrugated surfaces. *Journal of the Acoustical Society of America*, 72(3): 960-972.

203. Tolstoy, A. (2010). A deterministic (non-stochastic) low frequency method for geo-acoustic inversion. *Journal of the Acoustical Society of America*, 127(6): 3422-3429.

204. Tsemahman, A. S., Collins, W. T., and Prager, B. T. (1997). Acoustic seabed classification and correlation analysis of sediment properties by QTC view. *Proceedings of MTS/IEEE Oceans'97*, 2: 921-926.

205. Urick, R. J. (1983). *Principles of underwater sound.* McGraw-Hill, 3rd Edition, New York.

206. van Walree, P. A., Tegowski, J., Laban, C., and Simons, D. G. (2005). Acoustic seafloor discrimination with echo shape parameters: A comparison with the ground truth. *Continental Shelf Research*, 25(18): 2273-2293.

207. van Walree, P. A., Ainslie, M. A., and Simons, D. G. (2006). Mean grain size mapping with single-beam echo sounders. *Journal of the Acoustical Society of America*, 120(5): 2555-2566.

208. Wang, C.-C. and Tang, D. (2009). Seafloor roughness measured by a laser line scanner and a conductivity probe. *IEEE Journal of Oceanic Engineering*, 34(4): 459-465.

209. Wang, C.-C., Hefner, B.T., and Tang, D. (2009). Evaluation of laser scanning and stereo photography roughness measurement systems using a realistic model seabed surface. *IEEE Journal of Oceanic Engineering*, 34(4): 466-475.

210. Wentworth, C. K. (1922). A scale of grade and class terms for clastic sediments. *The Journal of Geology*, 30(5): 377-392.

211. Williams, K. L., Jackson, D. R., Thorsos, E. I., Tang, D., and Briggs, K. B. (2002). Acoustic backscattering experiments in a well characterized sand sediment: Data/model comparison using sediment fluid and Biot models. *IEEE Journal of Oceanic Engineering*, 27(3): 376-387.

212. Williams, K. L., Jackson, D. R., Tang, D., Briggs, K. B., and Thorsos, E. I. (2009). Acoustic backscattering from a sand and a sand/mud environment:

experiments and data/model comparisons. *IEEE Journal of Oceanic Engineering*, 34(4): 388-398.

213. Yamamoto, T. (1995). Velocity variabilities and other physical properties of marine sediments measured by cross-well acoustic tomography. *Journal of the Acoustical Society of America*, 98(4): 2235-2248.
214. Yamamoto, T. (1996). Acoustic scattering in the ocean from velocity and density fluctuations in the sediments. *Journal of the Acoustical Society of America*, 99(2): 866-879.
215. Yegnanarayana, B. (2001). *Artificial neural networks*. Prentice-Hall of India Private Limited, New Delhi.
216. Zerr, B., Maillard, E., and Gueriot, D. (1994). Sea-floor classification by neural hybrid system. *Proceedings of IEEE Oceans '94*, 2: 239-243.
217. Zhou, X. and Chen, Y. (2005). Seafloor classification of multi beam sonar data using neural network approach. *Marine Geodesy*, 28(2): 201-206.